UNIVERSITÀ DEGLI STUDI DI PARMA

Dottorato di Ricerca in Tecnologie dell'Informazione

XXIV Ciclo

OPTICAL FIBERS
FOR SENSING APPLICATIONS

Coordinatore:

Chiar.mo Prof. Marco Locatelli

Tutor:

Chiar.mo Prof. Stefano Selleri

Dottorando: *Michele Sozzi*

Gennaio 2012

Dedicated to my family

Science is the tool to forge friendship
between the nations and between individuals
Sune Svanberg - Biophotonics 2011

Outline

List of Figures

List of Tables

Introduction

A biosensor can be defined as an integrated receptor-transducer device which is capable of providing selective quantitative or semi-quantitative analytical information using a biological recognition element [1]. A device that transforms a biological information into an analytically useful signal, and it is composed by two parts: a bio-element, and a sensor element. A specific bio-element, such as an enzyme, antibody, living cell, or tissue, recognizes a specific analyte, and it does not recognizes any other analytes. The sensor element transduces the recognition event into a chemical or physical output measurable signal. There can be different combinations of bio-elements and sensor elements that can constitute different type of biosensors, suitable for different kind of analysis [2].

Biosensors appeared in the scientific litterature since the early 1960s where examples of electrochemical sensors capable of measuring pH, pCO_2, and pO_2 in human blood [3], and detecting the presence of organophosphorus compounds [4], or urea [5]. The sensor proposed in [3] was an electrochemical biosensor, based on enzymatic catalysis of a reaction that produces or consumes electrons, with the aim of measuring glucose concentration in blood. This has nothing to do with the glucose biosensors commercialized nowadays, where you just need a drop of blood to make the analysis. In Fig. 1 it is shown the clear difference in dimension of the sensors presented in [3], and of those now commercially available. Therfore since the 1960s many paces forward have been made in the field of biosensors leading to different kinds of sensing platforms, with different kinds of detection, and also this technology spread to other fields of application different from medical diagnostic.

Figure 1: On the left the glucose sensors proposed by Clark and Lyons [3], while on the right two glucose sensors commercially available nowadays.

From recent market analysis [2] [6] it is possible to recognize four main industry segments where the application of the biosensors technology is growing: medical diagnostics, enviormental monitoring, food, and military. The role of the dominant segment is played by medical applications, with the ninty percent of sales that come from glucose biosensors [6] [7]. The main reason of the penetration of biosensor technolgy in these four segments is basically due to a need for the detection of pathogen agents, for example in the medical industry the infection control is an area where biosensors are needed. Enviromental monitoring is an other field where the employment of pathogen detecting biosensors are useful, for instance the monitoring of water supplies can be very critical because of the exposition to bacteria can affect large inhabited area with contaminated water, so biosensors capable to detect quickly a pathogen agent is very important in this field. The other two segments, military and homeland security, and food industry are the ones which growth is expected to rise more than the other two [6]. In the case of military and homeland security the need to have a reliable, fast, accurate, sensitive, and specific tool to detect pathogen agents in the air, soil etc. comes from the possibility to have terrorist attacks of bacteriological type inside the national territory. So it is very important to have a reliable biosensor

capable to monitor the enviroment and rapidly indentifying contaminated water, air, soil, food and equipment. In the food industry it is obviously fundamental the need to find pathogen agents in food either processed or fresh, to give an example the recent case of E.Coli that broke out in Germany. The detection of pathogen agents it's not the only area in which biosensors can be employed in the food industry but they can be used also for quality control, products traceability, and in order to prevent frauds. On top of this the need of more sensitive, and specific devices comes from the always more strict regulations of the EU about the presence of GMO in food products.
There are different types of biosensors that can be used in the food industry, and other areas of interest. A list of the main kind of biosensors is reported below:

- **Electrochemical biosensors**. Electrochemical biosensors, as stated before, were the first to appear in the scientific litterature in 1962 [3], and they were also the first to be commercialized in 1975 [8]. The principle of operation is an enzymatic chemical reaction that involves the analyte. The sensor is composed by three electrodes, a reference one, an active one and a counting one, the reaction take place on the reference electrode surface. The reaction can produce a flow of current, or a voltage. Sensors that measures a voltage are called potentiometric while the ones which measure current amperometric. The voltage, or the current, that is measured is proportional to the analyte concentration. The amperometric sensor is the most widely reported in the food industry [7].

- **Calorimetric biosensors**. These sensors are based on the detection of the heat that is generated or consumed by a chemical reactions. There are chemical reactions of biochemical interest that absorb or produce heat, and with a sensitive system for detecting temperature it is possible to realize a calorimetric biosensor. In the food industry these kind of sensors are mainly used for detecting metabolites [7].

- **Optical biosensors**. Optical-based biosensor, together with electrochemical sensors, are the most widely reported in literature [7]. These sensors are based on the detection of the change of an optical signal due to the presence of the target analyte. There are different techniques of detection that are based on

well established methods. Examples can be fluorescence, light absorbance, Surface Plasmon Resonance (SPR), or optical fiber devices like Fiber Bragg Gratings (FBGs) and Long Period Gratings (LPGs). These are just some of the features carachterizing the optical-based biosensors more of them will be described later.

- **Acoustic biosensors**. Piezoelectric quarz crystals can be affected by a change of the mass on their surfaces, so if one of the surfaces is properly functionalized with biological recognition elements it is possible to develop a biosensor. The principle is based on the fact that if a piezoelecrtic quarz crystal is placed in an alternating electric field can be subjected to mechanical deformations, and at a particular frequency an acoustic resonance is induced. This acoustic resonance is dependent on the mass of the crystal, hence if the mass is changed because of the binding of analytes on the surface crystal there will be a change in the resonance frequency. Acoustic sensors are mainly used for detecting contaminating microorganisms [7].

- **Immunosensors**. These sensors are carachterized by the interaction between the probe and the analyte, and they are based on the specific binding of antibodies with antigens, known also as immunoassays. For these kind of sensors both electrochemical and optical transduction systems have been used.

- **Whole cell biosensors**. These kind of sensors are based on the activity of a whole cell. Tipically an electrochemical method is used [7], but there are also records of optical sensors, based on SPR or Resonant Waveguide Grating (RWG), that use cell activity for drug discovery purposes [9]. Using and optical system, when the cell is in a rest state there are no change in the shape of the cytoskeleton, that is the membrane surrounding the whole cell and is made out of protein, in this state the optical response gives a steady signal. When an event occurs, due to the interaction of the cell with the analyte, there is a change in the shape of the cytoskeleton. The change always occurs in the bottom part of the cytoskeleton that is bound to the sensing platform and this will induce in

a change of the SPR, or the RWG, signal compared to the resting state of the cell.

- **Sensor arrays**. With all the techniques, and methods, above described it is also possible to perform not only a one-shot analysis, that means measuring only one analyte at once, but also to perform multi-analytes analysis increasing the sensor throughput.

Optical based biosensors offer a number of advantages including speed and reproducibility of the measurements [7], moreover they are immune to electromagnetic interference, can perform remote sensing, and multiplexed detection on the same device. Generally optical biosensors can be divided into two main categories: fluorescence-based and label-free sensors [10]. In Fluorescence-based biosensors the target analytes are labeled with fluorescent tags, such as fluorophores or quantum dots (QDs). When the labeled analyte is excited at a particular wavelength emits light at a different wavelength. Detecting the emitted radiation it is possible to detect the presence of the target analyte. Biosensors that exploits fluoresence can be microarray based sensors for the detection of specific DNA sequences like in [11] and in [12], in both cases the DNA target has been labelled with the Cy5 fluorophore. There are also examples where suspended core microstructured optical fibers (SCMOFs) have been used for the detection of proteins labelling the target analyte with QDs [13]. QDs and fluorophores are both particles that absorb energy at a specific wavelength and emit light at a different particular wavelength. The difference is that a fluorophore is a part of a molecule that makes that molecule fluorescent and it can be covalently bound to an other molecule, as for example DNA. A QD instead is a portion of matter that has intermediate electronic properties between a bulk semiconductor and a single molecule, QDs are said to have an emission spectrum narrower than the one of most organic dyes and this makes their fluorescence to be more easily identified above the background signal [13]. The main advantage of labeled optical biosensor is the very high sensitivity with a detection limit that can go down to just a single molecule [14]. On the other hand fluorescence-based biosensors suffer from a laborious labelling process [10], from artifacts like false positives, false negatives, or autofluorescence.

Hence additional sofware is needed in order to eliminate these artifacts, and this adds complexity to the system. But it is worth saying that the end user is only exposed to this complexity added to the system with just a higher instrumentation pricing [15]. Label-free biosensors, differently from fluorescence-based ones, don't use a label in order to detect the analyte and in this way target molecules are not altered and they are kept in their natural form. Label-free detection is also realatively easy and cheap to perform, and it allows to do quantitative and kinetic analysis of molecular interaction [10]. A list of some label-free methods and platforms is reported below:

- **SPR based biosensor**. The first demonstration of the application of SPR technique for biosensing is in 1983 [16], since then this has become a very powerful tool for biological analysis. This technique rely on the generation of a surface plasmon wave (SPW) that propagates between a dielectric substrate and a metal layer, gold is generally used as the metal layer but also silver can be employed. The excitation of the SPW it's possible if particular resonance conditions are satisfied, and different kinds of configurations and methods can be employed. The most convenient and sensytive configuration is the prism coupling [10]. In this configuration the incident light is totally reflected by the surface of the prism which is covered by the metal layer, the sensing surface. The excitation of the SPW is possible only with a certain angle of the incident light. The SPW has an evanescent field outside the sensing surface, in contact with the sample. The detection of the analyte it is possible because the bonding with the recognition molecules changes the refractive index of the prism surface and then induces a change in the resonance conditions, in terms of resonant angle [17]. Alternative ways to excite the SPW can be also waveguides or optical fibers whose cladding is polished and coated with a metal layer. The detection can be performed monitoring a change in the resonant wavelength [18], or in the resonant intensity [19]. Extending the SPR technique it is possible to detect more than one analyte at once, with the SPR imaging (SPRI) method, very advantageous for high-throughput analysis of multiple analytes [20]. Typically a SPRI sensor is based on prism coupling. The incident light strikes a broad area of the sensing surface, divided into many small sensing spots, every spot

is related to a different analytes, and the reflected light is collected by a CCD camera.

- **Interferometer-based biosensors**. In interferometric sensors the recognition event induces a phase change in the optical signal that is detected as an intensity variation. There are different designs to realize an interferometer, a sensor can be based on Mach-Zender (MZ) [21], Young [22], or Hartmann architecture [23]. In these cases the detection is performed comparing the signal with a reference one. In the MZ achitecture an input waveguide is split by a Y junction in a reference arm and a sensing arm. The output is the recombination of the two arms, the detected signal is then given by the interference of the output of the two arms. The sensing arm is functionalized with biorecognition elements and the capture of the analyte induces a change in refractive index and then a change in phase and this is translated in an intensity change at the output of the sensor. Similarly to the MZ architecture the Young interferometer has a reference arm and a sensing arm, in some cases more than one sensing arm [24]. In this case there is no recombination of the arms and the output is an intereference pattern detected by a CCD camera. A change in phase, due to a change in refractive index at the sensing arm, will induce a change in the interference pattern. The Hartmann architecture is composed by an input grating that couples the light in the sensing region. Integrated optics is placed in proximity of the output to create interference between pairs of functionalized strips. The output signal is sent to the receiver through an other grating. The three architectures previously described rely on the same principle of detection, using two different light paths that are combined to form interference, even if they can differ from the design. A different class of interferometric sensors exploit backscattering interferometry (BI) [25]. In such kind of system a coherent single wavelength laser focused on a small sensing area, and the reflected intensity is analyzed by a detector. The capture of biological elements by the probes on the sensing area will induces a phase change of the reflection signal that will produce a variation of the reflected light intensity at the detector.

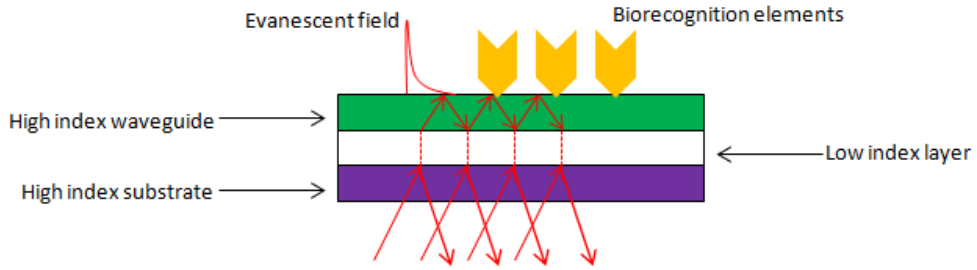

Figure 2: Typical structure of a resonant mirror waveguide. A low refractive index layer is between a high refractive index substrate and a high refractive index waveguide.

- **Optical waveguide based biosensor**. Waveguide based sensors are a family of waveguides desinged in such a way that a leaky mode is present in order to have interaction between the light and the sample. An architecture that has been used over a decade for biosensing is the resonant mirror (RM) [26] [27]. As illustrated in Fig. 2 the structure of a RM is composed by a low refractive index layer that separates two high refractive index layers, the one at the bottom is the substrate and the other is the waveguide in contact with the analyte. The light is delivered through the substrate with a certain angle, when the resonant angle is reached the light is strongly coupled to the high refractive index waveguide layer and it is possible to have a strong reflection at the output. The light coupled with the resonant conditions travels along the waveguide and it has an evanescent field outside the waveguide, in contact with the analyte. A change in the external refractive index, due to a recognition event, induces a change in the resonant angle. Other structures that work in a similar way are possible, like having a metal layer that separates a high refractive index substrate and a low refractive index waveguide, metal clad waveguide [28], or a reverse simmetry waveguide [29].

- **Optical ring resonator based biosensor**. Optical microring resonators are an

emerging technology that has recently been investigated in order to realize biosensors [10]. In these structures the light propagates in the form of whispering gallery modes, or circulating waveguide modes. These modes have the evanescent field at the ring resonator surface, sensitive to molecules binding to the surface. One advantage of the ring resonator is that the interaction length is no longer determined by its physical size but by the number of revolutions of the light that propagates in the ring, while in a waveguide the interaction length is determined by its dimensions. As a result, despite its small dimensions, a ring resonator can have sensing performances comparable or even superior to the ones of a waveguide, with the advantage of occuping less area and using less volume of samples. So far ring resonators have been implemented in three main configurations: chip based ring resonator [30], stand-alone dielectric microsphere [31] [32], and capillary-based opto-fluidic ring resonators.

- **Optical fiber based biosensors**. Optical fibers are very versatile to realize biosensors because they can be relatively inexpensive and provide an efficient and easy signal delivery due to their low signal attenuation. Gratings are in fiber devices that can be exploited to make a sensor. Fiber Bragg gratings (FBGs) are the most popular all fiber-based sensors to analyze load, strain, temperature, vibration, and refractive index [33]. In order to detect a biorecognition event a refractive index measurment is performed but part of the light must be in contact with the analyte. Since a FBG is fabricated inside the core of an optical fiber there is no evanescent field outside the fiber cladding. There are different ways in order to have the evanescent field in contact with the analyte, one is to have a surface grating on a polished fiber side [34], or etching the cladding down to the core of the fiber [35]. There is also a way to couple light out of the cladding without etching or polishing the fiber, by tilting the FBG [36]. Long Period Gratings (LPGs) are fabricated in a similar way to FBGs but they can couple light outside the cladding and then interact with the sample. It is possible to act in order to increase the sensitivity of the grating like etching the cladding [37], or depositing a layer of gold nanoparticles in the grating region [38]. Both devices, FBGs and LPGs, can detect a biorecognition event

because this induces a change in the refractive index of the medium surrounding the grating, they basically work as refrectometers. An other way to have an overlap of the evanescent field with the sample is the possibility to inscribe a FBG or a LPG inside the core of a Photonic Crystal Fiber (PCF) [39] [40]. The first PCF has been drawn in 1995 [41], [42] the cladding of this kind of optical fibers is composed by a lattice of air holes, a fraction of the light that propagates in the core overlaps in the air holes. The overlap between the evanescent field and the sample is possible by infiltrating the air holes. For this reason PCFs are suitable for bio-chemical sensing. Further details on the functioning of these devices, on their fabrication, and possible applications in biosensing will be given in an other section. Apart from FBGs and LPGs there are other fiber based technologies, like nanofiber where an optical fiber is drawn till submicrons dimension [43] with a very large evanescent field outside sensitve to refractive index change, or fiber couplers [44] where two identical optical fibers are fused down to a diameter of 9 μm with a sinusoidal transmission spectrum sensitive to refractive index change.

- **Photonic crystal based biosensors**. A photonic crystal (PC) is a periodic dielectric strucuture, whose periodicity forms a photonic bandgap. The wavelengths that are in the photonic bandgap are reflected by the periodic structure and do not propagate. However it is possible to introduce a defect in the bandgap by introducing a "disturbing" element in the periodic structure leading to the formation of a defect mode. The light in resonance with the defect mode can propagate in the PC structure and it appears as a peak in the transmission spectrum of the device. This peak is very sensitive to the enviromental condition around the defect, then it can be used to track refractive index change due to biorecognition events. The detection of refractive index change can be performed with waveguide [45], microcavity laser configuration [46], and it is possible to adjust the defect mode wavelength by finely tuning the structure parameters.

There are other two techniques that involve optical absorption [47], exploiting the Beer-Lambert law, and Raman [48].
The aim of this work is the investigation of the feasibility of the realization of biosensors using photonics technologies, in particular optical fibers as the sensing platform, used as the sensor itself, or devices based on optical fibers, like LPGs or FBGs. This investigation comes from the need to find new devices for the detection in the biochemical field. These new devices should have better performances in terms of detection limit (DL), i.e. sensitivity, for example in order to satisfy the always stricter regulations of the EU for the presence of Genetically Modified Organisms (GMOs) in food products, or for the detection of pathogen agents. They also should have a detection as simple as possible, and using not cumbersome components in order to have a device as small as possible. An other characteristic should be the realization of a realtively cheap device, then the possibility, for example, of having a mass production of fiber devices, or the re-use of the probes for several, but not infinite, measurements can help to reach this objective.

Chapter 1

Optical fibers

Optical fibers are generally thought to be related to the telecommunications sector for data transmission, but in the last few years they've been also recognized as a valid platform to develop sensors. When people thinks to optical fiber technology they think of something new and of recent discovery, but actually it is quite old. Since the middle of the 19th century the principles that rule the propagation of light in a denser medium were already known [49] and demonstrated [50]. But at that time the only application of this technology was just for amusement with light fountains and special effects in theaters [51]. The first practical applications appeared at the beginning of the the 20th century. In the 1920s the image transmission through glass tubes was demostrated, and the first application was in the medical diagnostic field, they were used for internal examinations. In order to talk about modern optical fibers, for data transmission, we need to wait the invention of the laser and the technology to manufacture optical fibers with a high quality glass matrix in order to have a low signal attenuation. In the 1970s the Corning Corp. was the first manufacturer of an optical fiber suitable for telecom application, the attenuation was first $17 dB/km$ then, after few years, $4 dB/km$, nowadays attenuation is much more lower, $0.2 dB/km$, at the wavelength of $1550 nm$, the minimum that is possible to reach. In 1995 a new kind of optical fiber was manufactured [41], [42] for the first time a PCF was drawn. A PCF is an optical cable that has air holes running all along its length, and the

light guidance is similar to standard optical fiber in a solid core PCF, or in case of a hollow core PCF (HC-PCF) the guidance is possible due to photonic bandgap. For the moment PCFs are not able to substitute standard optical fibers in data transmission systems, they still have a higher attenuation than standard fibers, and attenuation is a very crucial characteristic for data transmission sytems, more attenuation means more optical amplifiers, that means increasing costs. HC-PCFs seem to have the potential to overcome the minimum of attenuation of $0.2dB/km$, but for the moment the best attenuation value recorded is of $13dB/km$ [41]. On the other hand with their flexible design they can be employed in many other applications, like exploiting nonlinearities for supercontinuum generation [52] [53], sensing of gases and liquids by infiltrating the air holes [47] [54], and in the recent years they've been also used for biochemical sensing [40] [55].

1.1 Standard optical fibers

A standard optical fiber is a cilindrical waveguide made of silica glass. The light is guided because of total internal reflection (TIR). When light propagates in two different media, with different refractive index, at the interface of the two media part of the light is reflected and part is refracted. If the incident light is transmitted from the medium which has the higher refractive index for a certain value of the angle of incidence with the interface there will be only reflection, this is the condition of total reflection. Let's consider now a dielectric medium surrounded by an other medium of lower refractive index, if light is propagating inside the dielectric medium will travel through this medium if at the interfaces of the two media the conditions of total reflection will be satisfied. Considering now a rod of glass surrounded by air it will be able to deliver light from its start to its end because of TIR. This can be considered as an optical fiber, but of course not for telecommunications. Fibers used for telecommunication are made of fused silica glass and the inner part of the fiber, called core, is doped usually with germanium, in order to have a higher refractive index than the surrounding part called cladding.

1.1.1 Propagation

The propagation of light inside an optical fiber is well described by the mode theory. The modes that propagate in the core of an optical fiber are the configurations of the electromagnetic field that are able to effectively propagate, for certain solutions of the propagation constant β. The solutions of the modes can be retrieved starting from Maxwell's equation. All the calcultation of the mode theory will not reported here, but they can be found in details here [56].
Consider now an optical fiber with a step index profile. The V-number, or normalized frequency, is an important parameter to understand how many modes are supported by the fiber, and it is defined as:

$$V = ka\sqrt{n_{co}^2 - n_{cl}^2} \tag{1.1}$$

where a is the radius of the core, n_{co} and n_{cl} are the refractive index of the core and the cladding respectively, and k is the wave number defined as: $k = 2\pi/\lambda$, where λ is the propagation wavelength. V can be written as:

$$V = \frac{2\pi a}{\lambda}\sqrt{n_{co}^2 - n_{cl}^2} \tag{1.2}$$

The propagation constants in the core and the cladding can be defined as:

$$\beta_{co}^2 = k^2 n_{co}^2 - \beta^2$$

$$\beta_{cl}^2 = \beta^2 - k^2 n_{cl}^2$$

and with some calculation the eqn. 1.1 can be written as:

$$V^2 = a^2\beta_{co}^2 + a^2\beta_{cl}^2 \tag{1.3}$$

and defining:

$$u^2 = a^2\beta_{co}^2$$

$$v^2 = a^2\beta_{cl}^2$$

eqn. 1.3 can be written in terms of u and v:

$$V^2 = u^2 + v^2 \tag{1.4}$$

The normalized propagation constant b can be defined as:

$$b = \frac{\beta^2 - k^2 n_{cl}^2}{k^2(n_{co}^2 - n_{cl}^2)} \tag{1.5}$$

and it is possible to re-write eqn. 1.5 in terms of u and v:

$$b = \frac{v^2}{u^2 + v^2} \tag{1.6}$$

From eqn. 1.4 and eqn. 1.6 it is then possible to plot V in function of b. In Fig. 1.1 it is represented the graph of V versus b, the labels on the curves are related to the different linearly polarized LP_{nm} modes that can propagate in the fiber, whose solutions are reported in details here [56]. From the graph it is possible to understand how many modes propagate for a certain value of V, but also which value of V it must be taken if a certain numbers of modes can propagate in the fiber. If only one mode can propagate in the fiber V should be taken as $V < 2.405$, and in this case only the LP_{01} mode propagates, called the fundamental mode. If V has a value higher than 2.405 then the fundamental mode and the higher orders modes, how many it depends on the particular value of V. Then once the value of V is set in order to have a single mode fiber (SMF) from eqn. 1.2 the parmeters of the fiber can be set in order to have a SMF. The standard SMF follows the ITU G.652 standard, with a core diameter of 8.2 μm, cladding diameter of 125 μm, and numerical aperture NA of 0.14. The numerical aperture is a parameter that states the cone of acceptance of the light that will propagate inside the fiber and it is defined as: $NA = \sqrt{n_{co}^2 - n_{cl}^2} = nsin\theta$, where n is the refractive index of the medium surrounding the fiber, θ is half of the angle of the acceptance cone, as represented in Fig. 1.2. Multimode mode fibers are also manufactured, they follow the ITU G.651 standard, and they have a 50 μm core diameter, and a 125 μm cladding diameter, with $NA = 0.2$.

1.1.2 Attenuation and dispersion

The light propagation in an optical fiber is affected by two main factors: attenuation and dispersion.

Attenuation is due mainly to the absorption and scattering. Absoprtion is basically

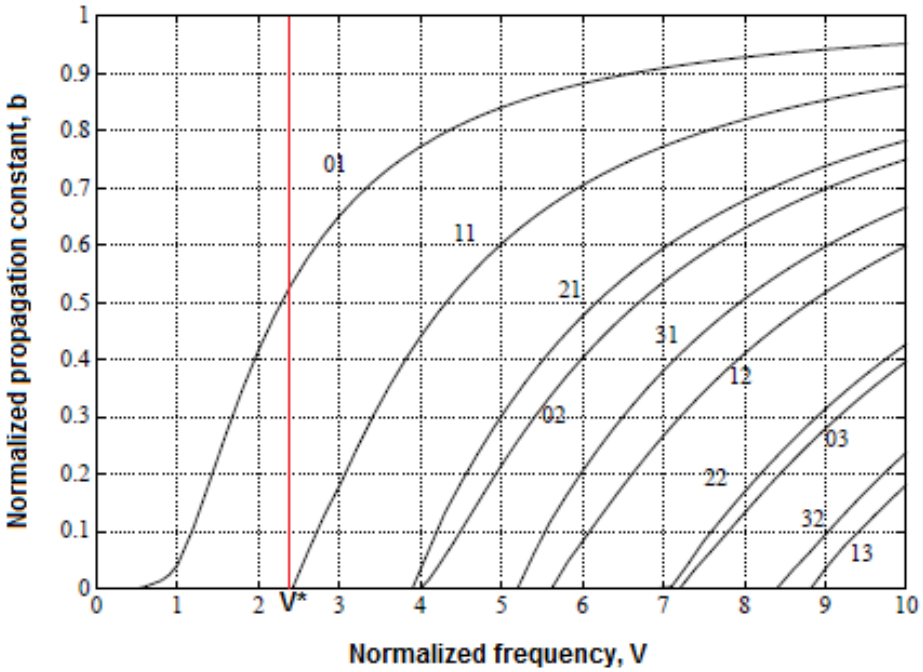

Figure 1.1: Depending on the particular value of V it is possible to understand how many modes propagate in the fiber.

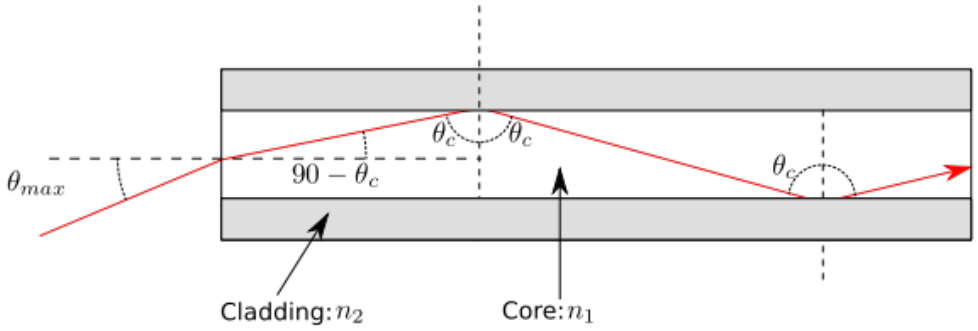

Figure 1.2: θ_{max} is half of the angle of the acceptance cone. It is the maximum angle at which the conditions of TIR are satisfied.

ralted to the material itself, and it can be caused by three factors: presence of impurities, imperfection in the atomic structure of the material, and intrinsic absorption due to the characteristics of the material. While scattering is due to the interaction of the light with density fluctuation inside the fiber. These density changes are produced during the manufacture process. The main scattering factor is due to Rayleigh scattering. In Fig. 1.3 is reported the attenuation profile of an optical fiber. From the graph it is possible to notice that the minimum of attenuation is 0.2 dB/km at 1550 nm, all the telecommunications systems are designed to work in this band. There is also an attenuation peak at 1400 nm, this si due to the absorption of the OH^- ions that are present because of the manufacturing process. Recently Corning Inc. managed to improve the manufacturing process and to almost eliminate the OH^- absoprption peak [57]. Attenuation is then a factor that limits the signal propagation in an optical fiber, after propagating for kilometers the signal needs to be recovered by introducing an optical amplifier in the transmission line.

Dispersion is also a factor that limits the transmission of data. The effect of dispersion is not the loss of optical power, but the broadening of optical pulses, and this is can cause errors at the receiver and the fail of data transmission. In MMFs dispersion is due to the fact that the optical power is divided by different modes that have different propagation constants and then they will arrive at the receiver in different istants of

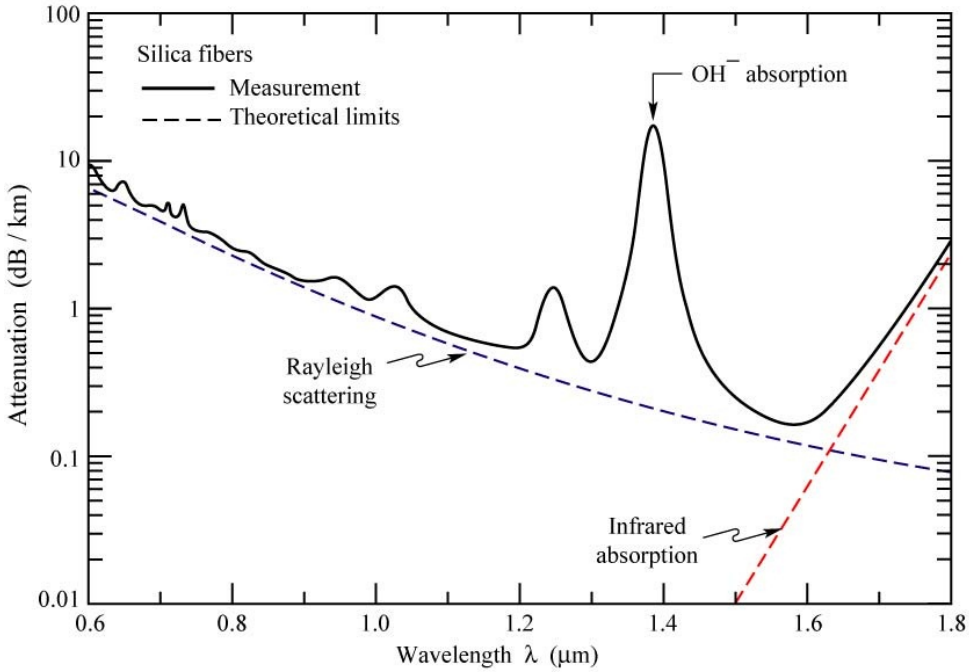

Figure 1.3: This is the experimental attenuation profile of an optical fiber. Theoretical profiles of Rayleigh scattering and infrared absorptio are also reported in the graph.

time, and this will cause the pulse broadening. This kind of dispersion is called modal dispersion. In SMFs of course there is no modal dispersion, but since the effective refractive index depends on the wavelength λ, and the laser pulse is not a perfect Dirac delta but it has a certain bandwidth, this will cause anyway a broadening of the pulse. This kind of dispersion is called cromatic dispersion. Special fibers exists in order to recover the dispersion accumulated along the line. It is worth saying that SMFs don't suffer from cromatic dispertion at the wavelength of 1300 nm, so it would be tempting to built a system working at that wavelength since attenuation is just a little bit higher than the minimum, about 0.3 dB/km. The drawback is that with no dispersion at all there will be the generation of non linear effects that are more disruptive than the dispersion itself.

1.2 PCF

A PCF is an optical cable that differently from standard optical fiber has a pattern of air holes, that goes through all the length of the fiber. PCFs didn't substitute the role of standard fibers in telecommunications transmission systems, due mainly to the fact that attenuation is still higher compared to standard fibers. There are two kinds of PCF, solid core PCF where light propagates in a silica glass core, and hollow core PCF (HC-PCF), where light propagates in an air filled core, in Fig. 4.8 cross sections of solid core PCFs and HC-PCFs are reported.

The advent of this new kind of fibers opened the way to new applications in optical fibers technology. The possibility of re-arrange the pattern of the air holes helps to make a suitable fiber for the particular application. In the first instance the air holes of a PCF can be infiltrated with liquids or gases in order to perform chemical sensing, this also suggests the possibility of biochemical sensing if the surface of the air holes is properly functionalized. In HC-PCFs, since the field is propagating inside the sample filled core, it's easy to have overlap between the two. While with solid core PCF only a small fraction of the field propagates in the air hole, so it is possible to design the fiber in order to have a higher fraction of evanescent field overlapping with the sample [58]. Highly non linear PCFs are produced [59] with a core diameter down

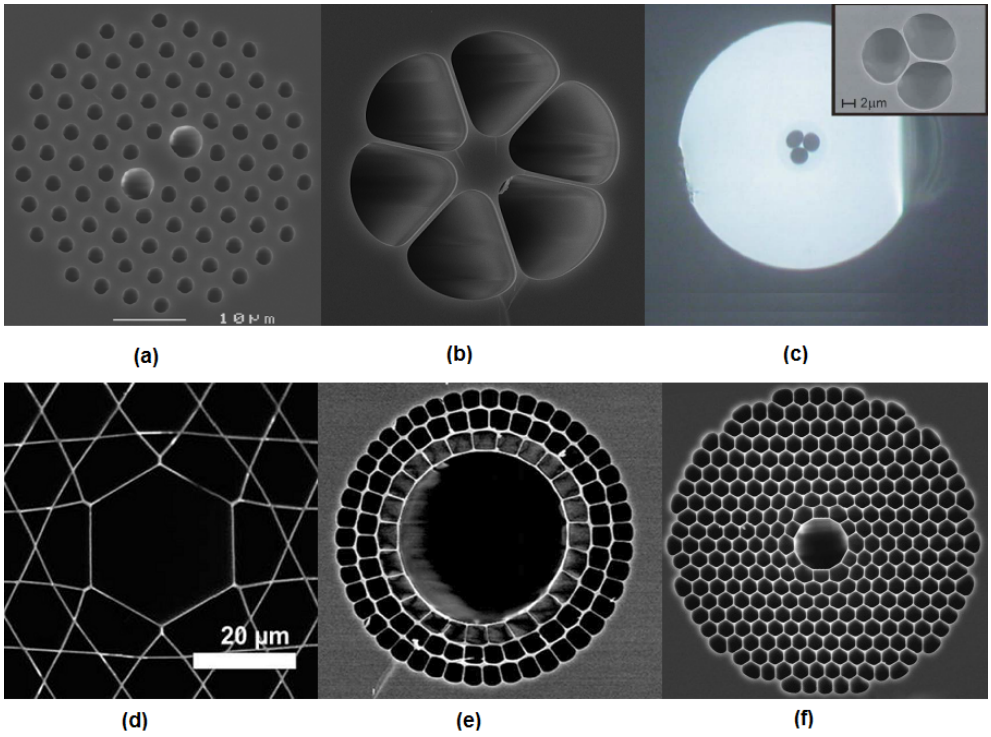

Figure 1.4: Cross sections of solid core (up), and HC-(bottom), PCFs. (a) PM-1550-1, polarizazion mantaining fiber produced by NKT Photonics. (b) HN5 highly non linear fiber, produced by NKT Photonics. (c) Typical design of a suspend core fiber. A 1.17 μm core diameter is surrounded by three holes of 20 μm diameter. (d) Kagome lattice hollow core fiber. (e) Bragg fiber produced by NKT Photonics, now out of production. (f) HC-1060-02 PBG fiber guiding in the 1060 *nm* range, produced by NKT Photonics.

to about 1.5 μm. Having such a small core diameter will enhance non linear effects for the generation of supercontinuum light sources. Double cladding large mode area PCFs are suitable for high power application since they can withstand the delivery of large amount of optical power and at the same time they can be single mode and limiting non-linear effects only by tailoring the design [60]. Some other tantalizing applications are also possible with HC-PCFs thanks to the interaction between gases and light inside the core for the enhancement of non-linear laser-gas interaction. It is then possible the generation of Raman scattering in molecular gases or high hamonic generation.

1.2.1 Propagation

The light guidance in PCFs follows two different principles considering the case of a solid core PCF or a HC-PCF.

Solid core PCF

The cross section of a solid core PCF is represented in Fig. 1.5. In the pictures the air holes are arranged in a periodic triangular lattice, d is defined as the diameter of the air holes, while Λ is the distance between the centers of two neighbourgh air holes.
Solid core PCFs are usually made of pure silica, the air holes in the cladding make the effective refractive index of the cladding lower than the one of the core, so the light can propagate in the core in a similar way as step index fibers, this is called modified TIR (MTIR).
Since the complex strucutre in PCF it's difficult to treat mathematically the solutions for the modes propagation, the Maxwell's equation must be solved numerically. As for standard step-index fibers it is possible to define a V-number for PCF [61]:

$$V_{PCF} = \frac{2\pi\Lambda}{\lambda}\sqrt{n_{co}^2 - n_{cl}^2} \tag{1.7}$$

where n_{co} and n_{cl} are the effective refractive index of the core and the cladding respectively, and the condition single mode regime happens when $V_{PCF} = \pi$. The expression in 1.7 must still be treated numerically in order to design the fiber to be single mode,

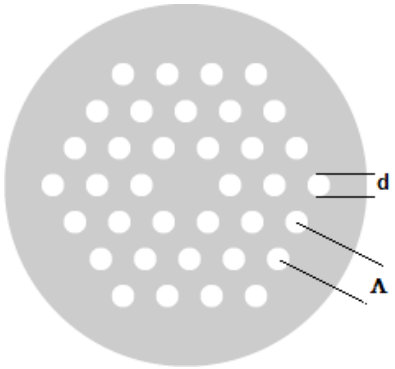

Figure 1.5: This is the cross-section of a solid core PCF with a triangle lattice. d is the hole diameter, while Λ is the distance between two neighbouring holes.

it would be then convenient to have and alternative expression depending only from λ and the parameters of the fiber. A different form of the 1.7 is available as a result of a fit with numerical data [62]:

$$V_{PCF}\left(\frac{\lambda}{\Lambda},\frac{d}{\Lambda}\right)=\frac{A\left(\frac{d}{\Lambda}\right)}{B\left(\frac{d}{\Lambda}\right)exp\left[C\left(\frac{d}{\Lambda}\right)\frac{\lambda}{\Lambda}\right]+1} \tag{1.8}$$

where the expressions of $A\left(\frac{d}{\Lambda}\right)$, $B\left(\frac{d}{\Lambda}\right)$, and $C\left(\frac{d}{\Lambda}\right)$ are reported in [62]. From the 1.8 it is then possible to design the PCF parameters in order to have a single mode regime, and the endlessy single mode (ESM) condition is also demonstrable [62]. That means for a particular value of $\frac{d}{\Lambda}$ the fiber is single mode at every wavelength. This value may be easily obtained from the following:

$$\lim_{\lambda\to 0} V_{PCF}\left(\frac{\lambda}{\Lambda},\frac{d}{\Lambda}\right)=\frac{A\left(\frac{d}{\Lambda}\right)}{B\left(\frac{d}{\Lambda}\right)+1}=\pi \tag{1.9}$$

From eqn. 1.9 it is possible to calculate the value of $\frac{d}{\Lambda}$ for which a PCF can be designed ESM, and it is straighforward that the ESM conditions can be controlled only by the geometry of the design. From calculations the value for this condition is $\frac{d}{\Lambda}\simeq 0.44$.

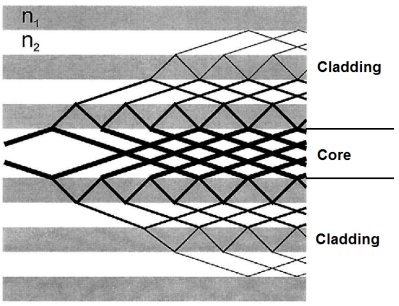

Figure 1.6: n_1 is the refractive index of the core and the air holes, lower than n_2 that is the refractive index of the glass. The light propagates in the core is reflected by the cladding, at the wavelengths that corresponds to the PBG of the PC.

HC-PCF

The cross section of an HC-PCF is composed by a periodic lattice of capillaries forming a 2D photonic crystal (PC), surrounding an air core. In this case since the core has a refractive index lower than the cladding region the light can't propagate through MTIR but through photonic band gap (PBG).
The PBG can be defined as a wavelength range for which a material neither absorbs light nor allows light propagation, this behaviour can be achieved with a periodic dielectric structure as a PC. The periodicity of the PC specifies the particular range of wavelengths that are not allowed to propagate in the structure, a band gap. It is possible to tailor the band gap of a particular structure by changing the periodicity of the PC, and the size of the particular band gap is determined by the difference in refractive index of the material used. Light diffraction is known as the physical mechanism that originates the PBG.
In Fig. 1.6 is represented the schematic of the longitudinal cross-section of a HC-PCF. From the figure it is clear how the light propagates in the core. Because of the PBG it is reflected inside the core. Large air-filling fractions and small inter-hole silica webs are necessary to have propagation in the core, as the core must be sufficiently large [63].

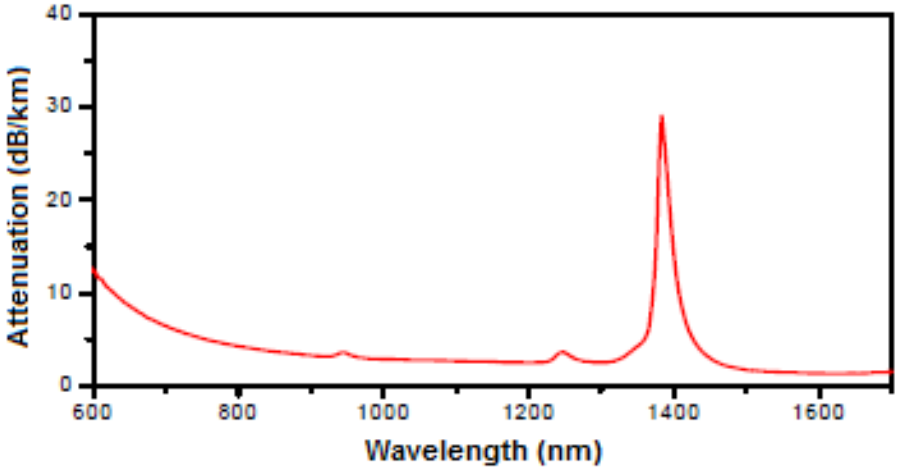

Figure 1.7: Attenuation profile of the LMA10 PCF, produced by NKT Photonics.

1.2.2 Attenuation and dispersion

Light propagation in PCFs, as for SMFs, is affected by attenuation and dispersion. The attenuation mechanisms for PCFs are in part different from SMFs, and they are governed by two main factors the fraction of light in glass and the roughness at the glass-air interface. Solid core PCFs have an attenuation profile similar to the one of an SMF, as shown in Fig. 1.7, since the light propagates in glass. The minimum loss value obtained so far is of 0.28 dB/km at the wavelength of 1550 nm [63], that is slightly higher than the minimum attenuation for a SMF. The fact that the minimum attenuation of SMFs is not reached is mainly due to the roughness at the glass-air interfaces [64].
HC-PCFs have the greatest potential to overcome the 0.2 dB/km minimum attenuation of SMFs since the light propagates in air. Altough the best attenuation achived so far is 1.2 dB/km [65]. The limit in HC-PCFs attenuation comes from the presence of surface roughness, with the formation of ripples on the edge due to the fabrication process. The pure core mode it does not actually feel strongly these ripples, but in

some cases like when phase matching to surface modes happens this cause light to move to the surface and then to experience more scattering. Acting on the core dimensions it is possible to limit the losses due to the resonance of the core mode with the surface ripples. This means that at a given wavelength it is possible to minimize the losses drawing a fiber with a particular core diameter. The optical overlap with the surface roughness scales inversely with the size of the fiber [65]. PCFs suffer less from losses due to the fiber bending. One way of making solid core double cladding PCFs single mode is to bend the fiber of a certain radius enough to make the higher order modes to leak and to have not significant losses of the fundamental mode [66]. An other factor of losses in PCFs is given by confinement losses due to the fact that in a realistic PCF the photonic crystal cladding is finite. In this case for both solid core PCFs and HC-PCFs a certain period of air-holes are needed in order to reduce confinement losses [63].

PCFs as SMFs suffer from dispersion, but what happens in PCFs is that changing the design it's possible to change the zero-dispersion point as well as the dispersion sign. In solid core PCFs if the air holes get larger and the core is more isolated the zero-dispersion point can be shifted down to the visible range. An other characteristics of solid core PCFs is that by arranging the design it is possible to make dispersion almost insensitive to wavelength and the possibility to have almost flat dispersion over a certain wavelength range [63].

Chapter 2

Fiber gratings

Fiber gratings are periodic structures that can be manufactured in the core of an optical fiber. They can be of two types: Fiber Bragg Gratings (FBGs) and Long Period Gratings (LPGs). The difference between the two lies on how the light from the fundamental core mode is coupled to the other modes.
A FBG is a type of distributed Bragg reflector that reflects a particular wavelength and transmits all the others. This is achived by changing periodically the effective refractive index of the fiber core. The period of the grating has the same order of magnitude of the operating wavelength. Because of this the fundamental core mode is coupled to the backscattered core mode, causing the light to be reflected. A LPG is a periodic structure achived, as for FBGs, by changing the effecive refractive index of the core. The periodicity in this case is higher than the operating wavelength. The result is that the propagating core mode si coupled to the co-propagating cladding modes. The transmission spectrum is characterized by attenuation bands centered at different wavelengths, and there is no light reflected.
The periodic change of the refractive index can be achived by exposing the fiber core to ultra violet (UV) laser radiation, exploiting the photosensitivity of the glass composing the fiber core.

2.1 Photosensitivity

Both FBGs and LPGs are obtained by periodically and permanently changing the effective refractive index along the core of an optical fiber. The first observation of refractive index changes in germanosilica fibers was in 1978 [67]. A permanent grating was obtained in the core of an optical fiber by launching an argon laser radiation at the wavelength of 488 *nm*. The purpose of this experiment was to study the nonlinear effects in a specially designed optical fiber, and the authors observed, after a prolonged exposition, the attenuation of the fiber and the backreflected light increased. This new nonlinear photorefractive effect in optical fibers was called fiber photosensitivity. After the first discover of photosensitivity it didn't raised a lot of interest mainly because these *self-induced* gratings were not pratical, and the way of inscription had several limitations [68]. For example the Bragg wavelength was limited to the argon ion laser radiation of 488 *nm*, and the tunabilty was achived only by straining the fiber during the inscription process. This didn't allow to produce grating in the infrared region, the one of interest in the telecommunications sector. An other problem was that the refractive index modulation was very weak and in order to have detectable reflectivities long gratings were required. Almost ten years later, exactly in 1989 [69], a renewed interest raised with the possibility of side writing, and exposing a Ge doped fiber to UV radiation lead to the formation of a grating with a high refractive index change. Germanium doped or germanium-boron co-doped fibers are the ones that experience the largest refractive index modulation compared to photosensitive fibers doped with europium, cerium, or erbium:germanium [68].
The presence in the ideal glass tetrahedral network of defects due to the Ge-Si *wrong bonds* is thought to be the reason of photosensitivity in germania-doped silica fibers. This wrong bond has an absorption band centered at $\approx 240nm$. These defects are caused by the fiber drawing process. On one hand there is always the need to improve the fiber drawing process in order to eliminate these defects as causes of fiber attenuation, on the other hand this can affect the photosensitivity of the fiber and then the grating fabrication. Although the Ge-Si wrong bonds are responsible for triggering the processes for the index change in the glass, this is not the only mechanism

but the most efficent found so far. When a Ge-doped fiber is exposed to UV radiation the wrong bond absorption band is bleached, and new absorption bands are created at the wavelengths of 195, 213, and 281 *nm*.

2.1.1 Refractive index change models

Bragg gratings have been written in many types of optical fibers using different methods, but the mechanisms how the refractive index change happens are not fully understood [68]. Several models have been proposed to explain the photoinduced refractive index change. The only common element in these theories is that the changes are due to the presence of Ge-Si Ge-Ge wrong bonds in the glass matrix. These defects are thought to be directly linked to the change of the refractive index change due to UV exposure, but it is believed that other processes are involved in the dynamics of the grating formation. Below, some of the models that describe the refractive index change are presented.

Color center model

In this model the UV exposure changes the material properties of the glass and introduces new electronic transitions of the defects, the Ge-Si Ge-Ge wrong bonds. These new electronic transitions are called color centers [70]. According to this model the refractive index in a certain point is related only to the number and orientation of defects and is determined by their electronic absorption spectra. It has been also demontrated that heating the fiber the refractive index change can be completely reversed and re-obtain the same result by exposing the fiber again to the same experimental conditions [71].
The bleaching of the wrong bonds absorption bands and the formation of new absorption bands is in agreement with the color center model proposed here [70], and the fact that the refractive index changes reverse with heating the fiber this is consistent with grating formation mechanisms in which the absoprtion changes play a major role.

Dipole model

The dipole model is based on the formation of built-in periodic space-charge electric fields by the photoexcitation of defects. The photoinization of the Ge-Si and Ge-Ge defects creates a positively charged hole centers and free electrons. Free electrons are captured by Ge(1) and Ge(2) neighbouring sites forming negatively $\mathrm{Ge}(1)^-$ and $\mathrm{Ge}(2)^-$ electron traps, with a result in formation of electric dipoles. Each dipoles will produce a static dc polarization field that induce local refractive index changes.
During the Bragg grating writing process the free electrons diffuse till they will be trapped by defects. This redistribution of charges inside the fiber core will form periodic space-charge electric fields that will induce to periodic changes of the refractive index through the Kerr effect.
This mechanism works very well for photorefractive crystals, but it might be diffcult to justify this in the case of photosensitve fibers due to the large density of dipoles needed.

Compaction model

The compaction model is based on density changes induced by laser radiation, which lead to refractive index changes. It has been shown [72] that exposing a thin film of silica to 248 *nm* laser radiation, with an intensity below the damage threshold, induced density variations in the exposed material. In particular a reduction of the thickness of the silica film has been recorded with a change in refractive index at the same time. The compaction disappeared after heating the silica film, and the refractive index change was retrieved by irradiating again the silica film with UV radiation. The compaction model suggests that the refractive index change is a result of an internal structural re-arrangment in the material, that means a change in the density, and not mainly through a process of defects creation.

Stress-relief model

This model is based on the hypothesis that the refractive index change comes from the alleviation of built-in thermoelastic stresses in the core of the fiber. The core of

an optical fiber is under tension due to the difference in the thermal expansion of the core and the cladding during the cooling in the fiber drawing process. It is known that tension reduces the refractive index and through the stress-optic effect a relief of the stress will increase the refractive index. UV irradiation breaks the wrong bonds and promote the relaxation of the glass and then reducing the stresses in the core.
In this model the refractive index change is a consequence of a stress relief in the fiber core. This mechanism is triggered by the breaking of the wrong bonds by UV radiation exposure.

2.1.2 Enhance photosensitivity techniques

Photosensitivity in optical fibers can be then defined as a measure of the amount of change that can be induced in the refractive index in the core of an optical fiber by exposing it to UV laser radiation [68]. At the beginning optical fibers with high germanium dopant levels were fabricated in order to be high photosensitive. Later other techniques have been proposed in order to enhance photosensitivity.

Hydrogen loading/hydrogenation

Hydrogenation or hydrogen loading is a simple technique in order to enhance photosensitivity in germanosilica optical fibers. This is carried out by diffusing hydrogen in the fiber core at high pressure and high temperature conditions. This technique allows the permanent changes of the refractive index, as high as 0.01, after UV exposure, but the enhanced photosensitivity is not permanent. After the hydrogen diffuses out the photosensitivity decreases.
The hydrogenation leads to a broader absoprtion band at the wavelength of 240 *nm*, this means that the reaction of hydrogen molecules with Ge sites generates germanium-oxygen deficiencies, that means Ge-Si and Ge-Ge wrong bonds are responsible for the glass photosensitivity.
The main advantage of hydrogenation is that allows the fabrication of strong Bragg gratings in any germanosilica fibers, even in standard telecommunications fibers that usually have a low level of dopants and then a low photosensitivity. The other advan-

tage of this technique is that the refractive index changes due to hydrogen diffusion are permanent only in the region exposed to UV radiation. In the orther parts the hydrogen slowly diffuses out leaving then negligible losses in the telecommunications window.

Flame brushing

The flame brushing is a simple technique to enhance the photosensitivity in germanosilica fibers [73]. The part of the fiber which is going to be photosensitized is repeatedly brushed by a flame fueled with hydrogen and a small amount of oxygen. This takes place at the temperature of 1700 $^{\circ}C$ for 20 *min*. At this temperature the hydrogen diffuses very quickly inside the fiber and react with the germanosilica glass in order to form oxygen deficiency wrong bonds, creating a stronger absoprtion band at 240 *nm*. This technique follows the same concept of hydrogenation: hydrogen diffusion in order to form more Ge-Si and Ge-Ge wrong bonds is responsible for the photosensitivity. The subsequent UV exposure gives then high refractive index changes. The difference between this technique and hydrogenation is that in this case the increased photosensitivity is permanent and it does not decrease when the hydrogen diffuses out. The main drawback is that the high temperature flame weakens the fiber.

Boron codoping

The codoping of boron [74] in the germanosilica glass leads to a decrease of the refractive index of the core. The boron codoping neither affect the absorption band at 240 *nm*, and it does not generate other absorption bands at different wavelengths. This means that the adding of boron does not generate new defects in the glass matrix. It is then believed that the boron codoping enhances the photosensitivity basically by allowing photoinduced stress relaxation to occur. It seems that the refractive index increases through photoinduced stress relaxation triggered by the breaking of wrong bonds by UV radiation exposure.
Comparing different kinds of germanosilica fibers, with different levels of dopant,

and a boron codoped fiber it is possible to notice that the time for the boron codoped fiber to reach saturation during gratings inscritpion is much lower, 10 *min*, than the other germanosilica fibers, as reported in Table 2.1 [74].

Table 2.1: Photosensitivity of a boron-codoped fiber compared to other kind of fibers.

Fiber design	**Fiber** Δn	**Saturated index modulation**	**Maximum reflectivity for 2** *mm* **Bragg grating**	**Time for reflectivity to reach saturation**
Standard low loss fiber 4 *mol%* germania	0.005	3.5×10^{-5}	1.2 %	2 *h*
High index fiber 20 *mol%* germania	0.03	2.5×10^{-4}	45 %	2 *h*
Reduced fiber 10 *mol%* germania	0.01	5×10^{-4}	78 %	1 *h*
Boron-codoped fiber 15 *mol%* germania	0.003	7×10^{-4}	95 %	10 *min*

ArF excimer vacuum UV radiation

Photosensitivity is associated with the bleaching of an absorption band located at 240 *nm*. It has been demonstrated that it is also possible to fabricate Bragg gratings using an ArF excimer vaccum UV radiation, at the wavelength of 193 *nm* [75]. It appeared that gratings written at this wavelength develop a stronger reflectivity than the ones written with 248 *nm* UV laser radiation, under similar experimental conditions. It is clear that inscription at 193 *nm* provides an efficient mean for writing periodic patterns in Ge-doped fibers.

The main advantage of writing at shorter wavelengths is the possibility of higher

spatial resolution in diffraction limited techniques.

2.2 Theory

A uniform optical waveguide, such as an optical fiber, can propagate a discrete number of modes, whose solutions form an orthonormal base. The modes are orthogonal and then they do not exchange energy between eachother. The energy exchange can be justified only if a perturbation of the waveguide is present, such as a grating, because this induces a lack of uniformity in the waveguide. If the energy is exchanged between a propagating mode and a reflected mode, this is called a counter-propagating mode coupling, this is the case of Bragg gratings. On the contray if the exchange of energy occurs between two modes propagating in the same direction this is called co-propagating mode coupling, this is the case of LPGs.
In order to describe the behaviour of the propagating light in these periodic structures the coupled mode theory is used [76] [77]. Considering the TE propagation for whom the longitudinal components of the electric field is zero as definition, the longitudinal coupling coefficient will be zero as well. Then the coupling coeffcient of the electric field transversal componets, for both co- and counter-propagating coupling, can be expressed in the following way [76]:

$$K^t_{\nu\mu} = \frac{\omega}{4}\int_{-\infty}^{\infty} \Delta\varepsilon(x,z) E_{t\nu} \cdot E^*_{t\mu} dx \tag{2.1}$$

where $E_{t\nu,\mu}$ is the transverse component of the electric field for the ν and μ mode, and $\Delta\varepsilon(x,z)$ is the modulation of the dielectric permittivity, that can be written as:

$$\Delta\varepsilon(x,z) = 2\varepsilon_0 n_{av} \delta n_f cos\left(\frac{2\pi}{\Lambda_G} z\right) \tag{2.2}$$

where n_{av} is the refractive index in the non perturbated region, δn_f is the modulation amplitude of the refractive index, and Λ_G is the period of the grating. This relationship is of course valid only inside the perturbated region. If eqn. 2.2 is substituted in eqn. 2.1 it is possible to write the coupling coefficient in this way:

$$K^t_{\nu\mu} = k_{\nu\mu}\left(e^{j\frac{2\pi}{\Lambda_G}z} + e^{-j\frac{2\pi}{\Lambda_G}z}\right) \tag{2.3}$$

where:

$$k_{\nu\mu} = \frac{\varepsilon_0 \omega n_{av}}{4} \delta n_f \int E_{t\nu} \cdot E^*_{t\mu} dx. \tag{2.4}$$

Substituting equation 2.3 in the coupled-mode equations and doing some calculations, a simplified form is obtained [77].

For the counter-propagating interaction in a Bragg grating the equations have the form:

$$\frac{dA^{co}}{dz} = jk^{co-co}_{01-01}A^{co} + j\frac{m}{2}k^{co-co}_{01-01}B^{co}e^{-j2\delta^{co-co}_{01-01}z} + j\sum_{\nu} k^{cl-co}_{1\nu-01}B^{cl}_{\nu}e^{-j2\delta^{cl-co}_{1\nu-01}z} \tag{2.5}$$

$$\frac{dB^{co}}{dz} = -jk^{co-co}_{01-01}B^{co} - j\frac{m}{2}k^{co-co}_{01-01}A^{co}e^{j2\delta^{co-co}_{01-01}z} \tag{2.6}$$

$$\sum_{\nu}\frac{dB^{cl}_{\nu}}{dz} = -j\sum_{\nu}\frac{m}{2}k^{cl-co}_{1\nu-01}A^{co}e^{j2\delta^{cl-co}_{1\nu-01}z} \tag{2.7}$$

where A^{co} and B^{co} are the amplitude of the core propagating modes, forward and backward respectively, and B^{cl}_{ν} the amplitude of the νth cladding mode. Here the single mode propagation of the fundamental mode LP_{01} is considered and the μ index is substituted with the 01 index. In the equations 2.5-2.7 the δ parameter appears, this is defined as the small detuning or phase matching parameter. For core to core mode coupling can be defined as:

$$\delta^{co-co}_{01-01} = \frac{1}{2}\left(2\beta^{co}_{01} - \frac{2\pi}{\Lambda_G}\right) \tag{2.8}$$

while the following is the detuning parameter for the core to cladding mode coupling:

$$\delta^{cl-co}_{1\nu-01} = \frac{1}{2}\left(\beta^{co}_{01} + \beta^{cl}_{1\nu} - \frac{2\pi}{\Lambda_G}\right). \tag{2.9}$$

The right terms of the equations 2.5-2.7 are neglected when they oscillate too rapidly, on the contrary they can be taken in account when the detuning parmeter δ is equal to or almost zero. The resonant wavelength, or Bragg wavelength can be found considering $\delta^{co-co}_{01-01} = 0$, that means considering the core to core mode counter-propagating coupling:

$$\lambda_B = 2n_{co}\Lambda_G \tag{2.10}$$

where n_{co} is the effective refractive index of the propagating core mode.
The simplified coupled mode equations that describe the co-propagating coupling in a LPG are reported below:

$$\frac{dA^{co}}{dz} = jk_{01-01}^{co-co}A^{co} + j\sum_{\nu} k_{1\nu-01}^{cl-co}A_{\nu}^{cl}e^{-j2\delta_{1\nu-01}^{cl-co}z} \tag{2.11}$$

$$\sum_{\nu}\frac{dA_{\nu}^{cl}}{dz} = -j\sum_{\nu}\frac{m}{2}k_{1\nu-01}^{cl-co}A^{co}e^{j2\delta_{1\nu-01}^{cl-co}z}. \tag{2.12}$$

In this case the small detuning parameter is:

$$\delta_{1\nu-01}^{cl-co} = \frac{1}{2}\left(\beta_{01}^{co} - \beta_{1\nu}^{cl} - \frac{2\pi}{\Lambda_G}\right). \tag{2.13}$$

The same considerations must be done in the same way as for the Bragg grating case, and the oscillating parameters are not neglected if the detuning parameter is equal to or almost zero. Then with this condition is possible to find the resonance wavelength for the LPG:

$$\lambda_{res} = (n_{co} - n_{cl})\Lambda_G \tag{2.14}$$

where n_{co} and n_{cl} are the effective refractive indexes of the propagating core mode and cladding mode, respectively, involved in the energy exchange.
At this point the resonance conditions for FBGs and LPGs have been found, but in order to have a complete understading of the coupling between modes the coupling coefficients must be calculated. The further calculations for the coupling coefficient and the exact solutions of the coupled mode theory are reported here [76] [77] in detail.

2.3 Methods of fabrication

The methods of fabrication of FBGs and LPGs will be reported here. As already stated before the refractive index change is achivable by exposing the fiber to UV laser radiation. For LPGs apart from UV exposure other methods are possible.

2.3.1 FBGs fabrication techniques

Before describing all the techniques that are used to inscribe Bragg gratings a mention of the laser sources requirments will be given. The laser sources must have good temporal and spatial coherence. A light field is called coherent when there is a fixed phase relationship between the electric fields at different locations or at different times. *Spatial coherence* means a strong correlation, i.e. fixed phase relationship, between the electric fields at different locations across the beam profile, that means that at different positions the electric fields oscillate in a totally correlated way. *Temporal coherence* means a strong correlation between the electric fields at one location between different times.
A laser with good spatial and temporal coherence, mainly temporal coherence [68], is very important in writing good quality Bragg gratings because it provides a good contrast ratio for the interfering beams.

Interferometric fabrication technique

This technique was the first to be employed in order to write an external FBG in a photosensitive fiber [69]. The idea is to split the incoming UV beam into two different beams, and then recombine them in order to form an interference pattern, that is going to induce the refractive index modulation inside the fiber core. The fabrication using this technique can be employed by amplitude or wave front splitting interferometer.

a) Amplitude splitting interferometer. In such a kind of interferometer the light is split into two beams of the same intensity, and they are later recombined after they travelled through different optical paths. The FBG period, Λ_G, depends from the irradiating wavelengths, λ_w and ϕ the half angle between the two intersecting UV beams, and it is given by the following equation:

$$\Lambda_G = \frac{\lambda_w}{2sin\phi}, \tag{2.15}$$

The Bragg condition, eqn. 2.10, states that the grating resonant wavelength depends from the core refractive index and the grating period. From the 2.15

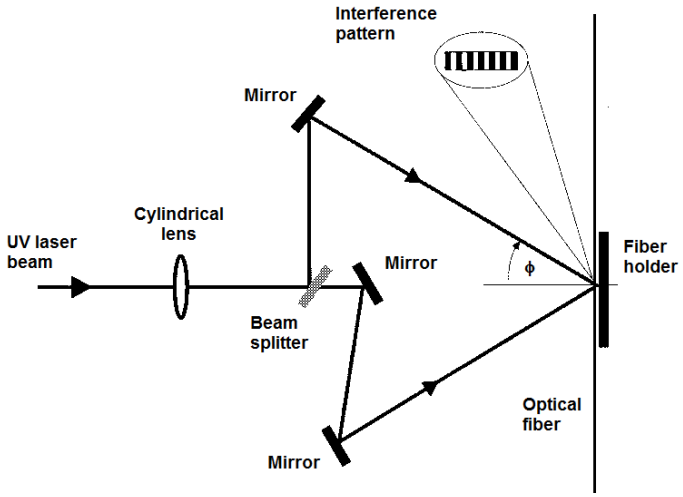

Figure 2.1: A possible set-up for writing a Bragg grating with the amplitude splitting interferometer technique.

it's possible to write λ_B in terms of λ_w and ϕ:

$$\lambda_B = \frac{n\lambda_w}{sin\phi}. \tag{2.16}$$

From eqn. 2.16 it is possible to notice that the Bragg wavelength is tunable by acting on λ_w or the angle ϕ. Of course λ_w is basically fixed due to the photosensitivity region of the fiber, but there is no restriction on the choice of the angle ϕ. The main advantage of this writing technique is the possibility of writing gratings at any wavelengths only by tuning ϕ. A possible set-up is represented in Fig. 2.1, where the angle tuning can be performed by rotating the mirrors. The main disadvantage is that this interferometric technique suffers from mechanical vibrations, and any very small displacement in the position of the optics composing the set-up may result in a drift of the fringe pattern, affecting the grating quality or the inscription. In this kind of interferometer the spatial coherence requirement can be relaxed by making sure that the total amount of reflections are the same for the two optical paths.

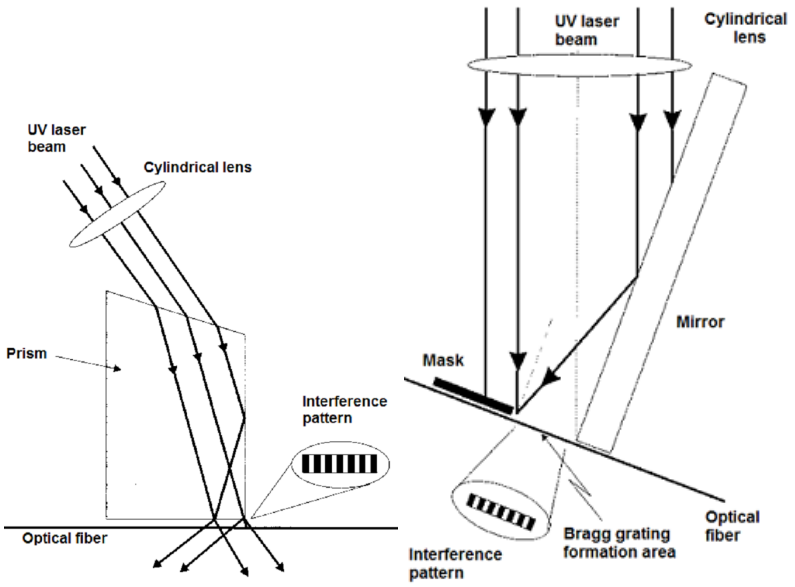

(a) (b)

Figure 2.2: (a) Schematic of the prism interferometer set-up. (b) Schematic of the Lloyd interferometer set-up.

b) Wave front-splitting interferometer. This interferometric technique is not as popular as the one described above but it has some advantages. Two different configurations have been used to inscribe Bragg gratings: prism interferometer [78], and Lloyd's interferometer [68]. The set-up of the two configurations are reported in Fig. 2.2. In the first configuration, Fig. 2.2(a), the UV beam is expanded at the input face of the prism. Inside the prism the two half of the expanded beam have different optical paths and they recombine at the output of the prism forming a fringe pattern.

In the Lloyd's interferometer, Fig. 2.2(b), a dielectric mirror is placed perpendicular to the fiber axis. Half of the UV beam is reflected by the mirror into the fiber, and the other half hits directly the fiber. At the intersection where the two half beams overlap a fringe pattern is generated normal to the fiber axis.

One of the advantage of this technique is that only one optical element is used and the system is less sensitive to mechanical vibrations. The disadvantage of this system comes from the limited grating length possible that is up to half of the beam width. The Bragg wavelength tunability is limited by the physical arrangement of the set-up.

Phase mask technique

One of the most effective methods to inscribe FBGs is the employment of a diffractive optical element, a phase mask [79]. A phase mask is an optical component made by a very high quality silica glass, transparent to UV radiation, on which a surface relief diffraction grating is fabricated. The grating is designed in such a way that when a laser beam hits the structure the zero order diffracted beam is suppressed and the plus and minus first order beams are maximized. A near field fringe pattern is formed by interference of the minus and plus first order beams, and the period is half of the one of the mask grating. The periodic modulation of the refractive index of a photosensitive fiber is possible if it is placed in contact with the phase mask, or in its close proximity. A scheme of the set-up is represented in Fig. 2.3

The use of a single phase mask has some advantages. First of all the inscription system complexity is reduced. Then the fact of using only one optical element makes the grating inscription highly reproducible [68]. Moreover the fact of placing the fiber in the proximity or in contact with the phase mask makes the system less sensitive to mechanical vibrations, even if a set-up with an anti vibrational system is always preferred. Temporal coherence is also minimized due to the geometry of the problem, since the distance of the fiber from the phase mask is identical for the two interfering beams. The separation of the fiber from the phase mask can affect the writing of a high quality grating, if the fiber is positioned far from the phase mask the result will be a low refractive index modulation and poor reflectivity. Then the fiber should be placed in contact with the phase mask to maximize the grating modulation, this is required to the poor spatial coherence of the UV laser source used for the inscription, usually KrF excimer lasers are used, these lasers typically have low spatial and temporal coherence. The placement of the fiber in contact with the corrugated grating of the

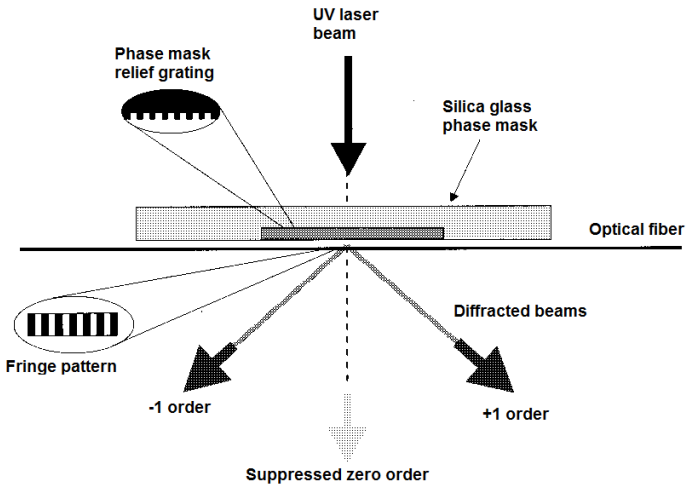

Figure 2.3: A possible set-up for writing a Bragg grating using a phase mask.

phase mask can lead to damage to the phase mask itself, so if the spatial coherence of the laser is improved the constraint of placing the fiber in contact with the phase mask can be relaxed. If there is possibility to place the fiber not in contact with the phase mask there is possibility of fabricate blazed gratings by tilting the fiber.

Double phase mask interferometer. The employment of two phase masks can be used to form a double phase mask interferometer. In this case the phase mask technique is used to form an amplitude interferometer, see Fig. 2.4. The first phase mask separates the UV beam into two different beams, the two beams are the plus and minus first order beams generated by the diffractive grating. It is possible to talk about amplitude interferometer because the phase mask is designed to minimize the zero order diffracted beam, and maximize the minus and plus first order beams. The incident beam intensity is then split in equal part to the minus and plus first order beam respectively. The two beams are recombined by the second phase mask and they form a fringe pattern behind it, even few centimeters far. This permits to position the fiber far from the phase mask and allows a tight focusing on the fiber without having high energy

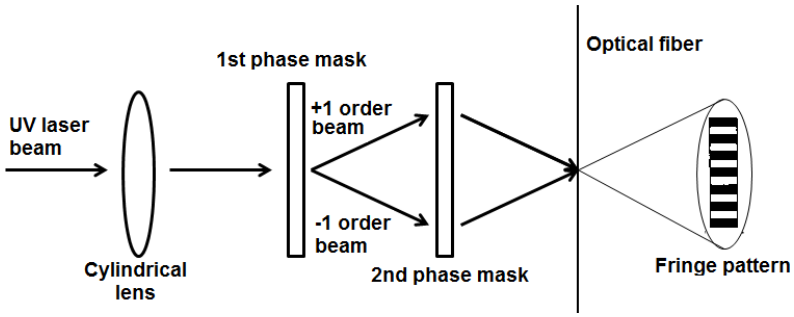

Figure 2.4: Set-up for a double phase mask interferometer.

densities on the last optical element, preventing the optics damage. With this technique the inscription of FBGs in a fluorine depressed cladding silicate glass optical fiber and in a SMF, using a 500 fs, 248 nm laser radiation, was possible [80]. This was shown to be an efficient way to write FBGs in low defect silicate glass optical fibers.

Point by point technique

The fabrication of FBGs by the point by point technique is accomplished by inducing a refractive index change exposing the fiber core step by step to UV laser radiation [81]. The modulation of the refractive index is then obtained by separately focusing the laser pulse along the fiber core, by moving every time the fiber of a distance Λ_G, the grating period. For such kind of system it is of course essential to have a very stable and precise submicron translational unit.
The main advantage of this technique is that there is complete freedom in deciding the grating pitch or length, choosing different Bragg wavelengths, or modulating the pitch in the same grating producing for example chirped gratings. One disadvantge is that since it is a step by step procedure it is quite a relatively long process. In second instance errors in the grating pitch due to thermal effects and/or small variations in the fiber strain can occur. This limits the grating to a very short length.

Mask image projection

For the fabrication of FBGs is also possible to use a high resolution mask projection [82]. The system consits of a UV beam, coming from an excimer laser source, incident on a transmission mask. The transmitted beam is imaged onto the fiber by a multicomponent fused silica high resolution demagnifing system.

2.3.2 LPGs fabrication techniques

The most widely utilized method for the fabrication of LPGs is the exposure to UV radiation [83], but in addition to this method others are employed that can induce the refractive index change in the fiber core, as well as small deformations of the fiber structure.

UV exposure

The refractive index modulation by means of exposing the fiber to UV laser radiation can be achived by a point by point technique [84], that is very flexible for the reasons already said in the part dedicated to FBGs. An other method that can be employed with the UV exposure is the use of an amplitude mask [85], similar to the phase mask technique used for FBGs. In this case a UV laser beam illuminates the fiber throught the amplitude mask, inducing in the fiber core a modulation of the refractive index whose period is the same as the one of the mask. A typical amplitude mask configuration is represented in Fig. 2.5. These kind of masks can be made of a metal foil in which a periodic structure has been fabricated. This technique allows the fabrication of LPGs in a fast and reproducible way. Differently from FBGs where a stabilized system against mechanical vibrations is needed, the LPGs inscriptions is poorly affected by mechanical vibrations, and an anti vibrational system is not strictly necessary.

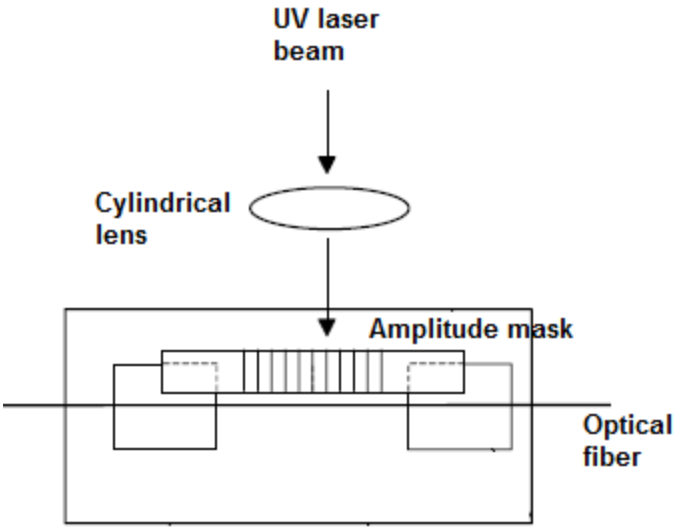

Figure 2.5: Schematic of the set-up for LPGs writing with an amplitude mask.

Near infrared irradiation

The fabrication of LPGs is possible by exposing the fiber to a laser radiation in the near infrared region, at the wavelength of 800 nm. The irradiation at this wavelength it is believed to cause a densification of the glass, that means a change in the refractive index.

CO_2 exposure

The irradiation with a CO_2 laser, at the wavelength of 10.6 μm, can induce a refractive index change in the core of an optical fiber [86]. With this method the modulation of the refractive index along the fiber core is obtained by a point by point configuration. The exposure to CO_2 radiation was thought to induce densification in the glass, as for the near infrared irradiation. There is anyway evidence that suggests that the refractive index change is due to the breakage os Si-O-Ge chains. LPGs written with this technique showed unchanged characteristics after annealed at 1200 $^{\circ}C$.

Electric arc discharge

The LPGs fabrication can be performed applying electric discharges with the electrodes of a splice machine. The fiber properties modulation is possible due to the combination of four different effects, this includes the formation of microbendings in the fiber structure. Typically applying an electric discharge will expose the fiber to a length of 100 μm, this will limit the minimum period of the grating. It seems that LPGs fabricated with this technique show a better thermal stability compared to the ones fabricated with UV exposure [87].

Mechanical induced

By mechanically pressing a periodic structure on the fiber it is possible to induce a periodic variation in the fiber cladding. This results in a periodic refractive index change via the photoelastic effect [88]. The coupling strength increases with the applied load with a short change in the resonance wavelength.

2.3.3 Types of fiber Gratings

Different kind of fiber gratings can be written with the techniques described above. FBGs can be of different types, a short list will introduce some of them:

- **Common Bragg reflectors.** These are the simplest and most used FBGs, they are characterized by a constant refractive index change and period, Fig. 2.6(a).
- **Chirped gratings.** A chirped grating is obtained by monotonically varying either the grating period, or the grating refractive index modulation, or both, Fig. 2.6(b).
- **Blazed gratings.** If the grating planes are tilted, of a certain angle respect to the fiber core axis, blazed gratings are obtained, Fig. 2.6(c). The tilting of the grating planes has the effect of coupling part of the light propagating in the core, into the cladding. With the formation in the transmission spectrum of cladding modes.

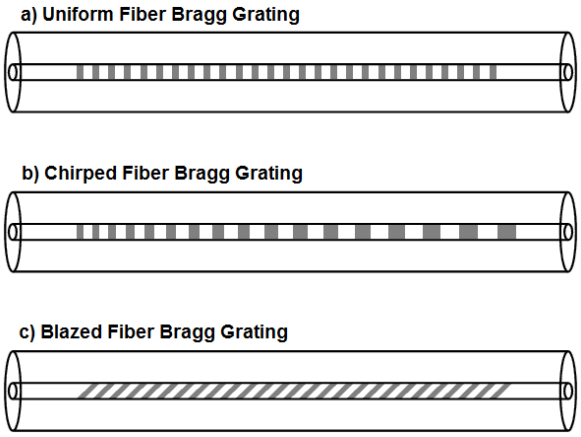

Figure 2.6: Represantation of the refractive index modulation of different kinds of FBGs. a) Common Bragg reflector. b) Chirped Bragg reflector. c) Blazed Bragg reflector.

- **Type II gratings.** FBGs that have a high refractive index modulation are labelled as *type II*, while the one with low refractive index modulation are labelled as *type I*. Type II gratings are fabricated exposing the fiber to very high laser intensities, above the glass damage threshold. In these kind of gratings damages at the core cladding interfaces have been observed. This happens only for type II gratings, suggesting that it may be responsible for the large index modulation.

  A characteristic of type II gratings is their high stability to high temperatures. It has been found that still at the temperature of 800 $^{\circ}C$ there is almost no degradation in the grating reflectivity. It is worth to notice that at the same temperature a type I grating is completely erased.

  An other type of gratings are labelled as *type IIA*, even if they are not fabricated using laser intensities above the damage threshold, they perform the same performances as type II gratings when heated at very high temperatures [89] [90]. Type IIA gratings are characterized by a blue shift and negative refractive index

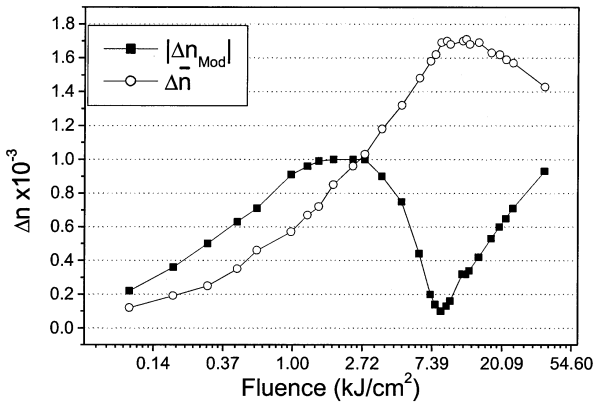

Figure 2.7: The typical evolution of the refractive index change (black squares), and of the average refractive index change (white dots), of a type IIA Bragg grating.

variations. At the beginning of the inscription the grating performs a positive refractive index variation and a red shift of the Bragg wavelength, like for the type I gratings. Continuing with the exposure the refractive index variation decreases and a blue shift starts, and at the same time the grating strength decreases. The Bragg wavelength keeps on having blue shift but at a certain point the grating strength starts to increase again resulting in an increase of the refractive index modulation. In Fig. 2.7 is well represented the evolution of the refractive index change.

LPGs can be as well written in a uniform way with a constant period and constant refractive index change. There are anyway records of tilted LPGs fabricated by mechanically induced refractive index modulation [91] or similarly to FBGs, via UV exposure by tilting the fiber respect to the amplitude mask [92]. Chirped LPGs are also possible by simply changing the step in a point by point fabrication through CO_2 laser exposure [93]. While it does not seems that there are records of type II LPGs.

2.4 Applications

Fiber gratings can be employed in different kind of applications from the telecommunications to the sensor field.

2.4.1 FBGs applications

The different applications on which FBGs are employed are enlisted below:

Lasers

A FBG may be coupled to a semiconductor laser in order to obtain a fiber Bragg laser. If the FBG reflects at a wavelength in the gain bandwidth of the semiconductor diode it is possible to obtain a laser diode emitting at the Bragg wavelength of the grating. An advantage of this system is that the FBG has a temperature sensitivity round 10 % of that of semiconductor lasers [68] resulting in a device less affected from wavelength drift due to temperature.
An other way to obtain lasers from Bragg gratings is to use an erbium doped fiber as the lasing medium inserted in an optical cavity, along with some tuning element. This can result in a continuous tunable laser source due to the broad bandwidth of the erbium emission spectrum. A possible configuration can be the presence of an external grating [94], or the presence of a broadband Bragg mirror and a narrow band Bragg grating that serve as the high reflector and the output coupler respectively [95].

Filters and couplers

If two identical Bragg gratings are placed in two arms of a coupler, as in a Michelson arrangement, it is possible to obtain a band-pass filter. This filter lets to pass only the wavelengths that are around the Bragg resonance and discards all the others. The only drawback of this implementation is that the non reflected wavelengths suffers from a 3 dB loss in output, this can be overcome just recombining the two output arms like in a Mach-Zender arrangement.

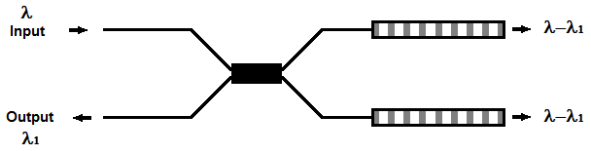

Figure 2.8: A band-pass filter schematic. The wavelength that corresponds at the grating Bragg wavelength are rejected.

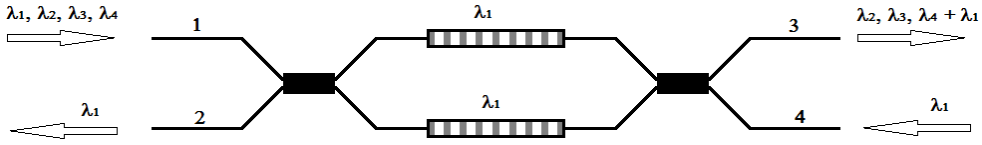

Figure 2.9: Schematic of a add and drop filter. The channel corresponding to the Bragg wavelength entering from port 1 will be dropped to port 2. While the channel entering from port 3 will be added to port 4.

Optical fiber communication systems employing wavelength division multiplexing/demultiplexing (WDM/D) techniques require componests able to select or deselect one or more particular wavelength. If a second coupler is added to the configuration described to realize a band-pass filter, forming a Mach-Zender configuration. With such a component it's possible to add and drop particualar channels, i.e. wavelengths, from the transmission line.

Dispersion compensation

Chromatic dispersion is one of the most limiting factors in high data rate transmission systems. Without compensation modules dispersion would limit the transmission of data to few kilometers. Chirped grating can act as dispersion compensation modules via pulse compression [78]. A chirped grating is formed by a monotonous change of the grating period, or the refractive index modulation, this means that different parts of the grating will reflect different wavelengths. Then the wavelengths that compose

a pulse will be reflected in different position of the grating resulting in a compression of the reflected pulse.

Temperature sensor

FBGs are sensitive to temperature, and by observing a shift in the Bragg wavelength it's possible to detect a temperature change. The wavelength shift due to temperature occurs by affecting both the refractive index and the thermal expansion coefficient of silica glass. The following equation relates the wavelength shift to the temperature change:

$$\Delta\lambda_B = \lambda_B(\alpha + \xi)\Delta T, \tag{2.17}$$

where $\alpha = \frac{1}{\Lambda_G} \cdot \frac{\delta\Lambda_G}{\delta T}$ is the thermal expansion coefficient of the fiber, and $\xi = \frac{1}{n} \cdot \frac{\delta n}{\delta T}$ is the thermo optic coefficient. For silica glass α has approximately a value of 0.55×10^{-6} while ξ for germania doped silica core fiber has a value approximately of 8.6×10^{-6}. The thermo optic effect is then dominant in the wavelength shift due to temperature change.

Strain sensor

If a strain is applied to the optical fiber a change in the Bragg wavelength will result. The shift is induced through the expansion or contraction of the grating elements and through the strain optic effect. The wavelength shift due to strain is expressed by the following equation:

$$\Delta\lambda_B = \lambda_B(1 - p_e)\varepsilon_z, \tag{2.18}$$

where $p_e = \frac{n^2}{2}[p_{12} - \nu(p_{11} + p_{12})]$ is the effective strain optic constant, and ε_z is the strain applied to the fiber. In the p_e relationship p_{11} and p_{12} are the components of the strain optic tensor, n is the core index, and ν is the Poisson's ratio. For a standard optical fiber: $p_{11} = 0.113$, $p_{12} = 0.252$, $\nu = 0.16$ and $n = 1.482$. With the values of these parameters at the wavelength of 1550 *nm* it is possible to expect a sensitivity of 1.2 *pm* for every applied $\mu\varepsilon$.

Refractive index sensor

Considering the relationship of the Bragg wavelength, eqn. 2.10, if a change in the refractive index occurs this induce a change in λ_B. Then it is possible to make a sensor for chemicals [96], and biological molecules [97], considering the fact that sensors for these analytes are usually based on refractive index measurements. In order to devise such a sensor two things are needed: first the evanescent field of the grating must be in contact with the sample, and it must be sure that the grating is not affected by strain and temperature changes that can affect the measurements.

2.4.2 LPGs applications

LPGs have found many applications as well, and they are enlisted below:

Telecommunications

In the telecommunications field LPGs have found application as band rejection filters [98], dispersion compensation [99], and WDM isolation filters [100]. As a band rejection filter a LPG can be employed as ASE suppressor in erbium doped amplifier, or for removing unnecessary Stokes' orders in cascades Raman amplifier. Chirped LPGs can be employed, as well as chirped FBGs, to compensate dispersion along a data transmission line. If two chirped LPG are concatenated one after the other the realization of a WDM isolation filter is feseable.

Temperature sensor

As well as FBGs, LPGs are sensitive to temperature, and the shift of the wavelength due to temperature can de expressed by the following differential equation:

$$\frac{d\lambda}{dT} = \frac{d\lambda}{d(\delta n_{eff})}\left(\frac{dn_{co}}{dT} - \frac{dn_{cl}}{dT}\right) + \Lambda_G \frac{d\lambda}{d\Lambda_G}\frac{1}{L}\frac{dL}{dT}, \tag{2.19}$$

where λ is the central wavelength of the attenuation band, T is the temperature, n_{co} and n_{cl} are the effective refractive index of the core and the cladding respectively, while $\delta n_{eff} = n_{co} - n_{cl}$ is the difference of the two, L is the length of the LPG,

and Λ_G is the period. In the same way for FBGs the wavelength shift is due to two different contributions. The first term of eqn. 2.19 is the effect of the material, while the second one is the effect of the waveguide. The difference with FBGs is that an other parameter is involved here, the coupling with cladding modes. The contribution due to the material takes in account the composition of the glass of which the fiber is made and the order of the cladding mode to which the core mode is coupled. If the coupling to low order cladding modes occurs the temperature sensitivity is dominated by the material effect. While the coupling to high order cladding modes can make negligible the material effect. The second contribution is due to the change in the LPG period. The magnitude and the sign of this term of the equation depends on the order of the cladding mode. If the coupling to low order cladding modes occurs the parameter $d\lambda/d\Lambda_G$ has a negative sign, while the coupling to high order modes induces a positive sign.
LPGs fabricated in standard telecommunication optical fiber have sensitivities that are in the range between 3 $nm/100°C$ and 10 $nm/100°C$ [68].

Strain sensor

LPGs are also sensitive to strain, and the strain sensitivity can be expressed by the following equation:

$$\frac{d\lambda}{d\varepsilon} = \frac{d\lambda}{d(\delta n_{eff})}\left(\frac{dn_{co}}{d\varepsilon} - \frac{dn_{cl}}{d\varepsilon}\right) + \Lambda_G \frac{d\lambda}{d\Lambda_G}, \tag{2.20}$$

where λ is the central wavelength of the attenuation band, ε is the applied strain, n_{co} and n_{cl} are the effective refractive index of the core and the cladding respectively, while $\delta n_{eff} = n_{co} - n_{cl}$ is the difference of the two, L is the length of the LPG, and Λ_G is the period. As well as for temperature the strain sensitivity is due to two contributions, one given by the material and one given by the waveguide. Similar considerations to the temperature sensitivity can be done, in particular the second term has negative sign if the coupling to low order modes occurs, or positive sing in case of coupling to high order modes.

Refractive index sensor

The sensitivity to the refractive index changes comes from the phase matching conditions, eqn. 2.14. The effective refractive index of the cladding modes is the difference between the index of the cladding and the index of the medium surrounding the fiber. Thus from eqn. 2.14 the resonance wavelength of the attenuation bands depends on the refractive index of the medium surrounding the fiber. Then a change in the surrounding refractive index can be detected by observing a shift in the resonant wavelength.
The sensitivity to the refractive index can be exploited to detect different chemical elements [39], concentrations of chemical solutions [38], and the feasibility of biological molecules sensors [101] considering the fact that the bonding of molecules to the fiber surface can be seen as a change in the refractive index of the external surface of the fiber. Differently from FBGs due to the coupling to cladding modes an evanescent field is present outside the fiber, and treatments of the fiber, like HF etching, are not needed in order to put in contact the evanescent field with the analyte. Treatments of the fiber can be done to increase the sensor sensitivity [37] [38]. A drawback of LPGs is the high sensitivity to temperature, and in order to have reliable refractive index measurements these should be performed in a temperature controlled enviroment.

Chapter 3

Fiber surface functionalization

The optical fiber surface functionalization is a fundamental step in the realization of a optical fiber biosensor. The functionalization is basically the chemical modification of the surface that makes possible the binding of biological molecules by means of a stable intermediate layer between the probe and the fiber surface. Without this procedure it would be impossible to bind the probes to the surface. Depending on which is the analyte different kind of probes must be used, and different kind of functionalization procedures must be performed in order to bind the probes to the surface.
In [36] three different methods are reported to bind the probe protein Bovine Serum Albumin (BSA) to the fiber surface. These three methods consists on ionic bondings only, ionic bonding combined with an avidin-biotin linkage, and covalent bondings combined with avidin-biotin linkage.
The ionic bonding method is based on the Electrostatic Self-Assembled (ESA) film deposition. Here the electrostatic attraction between oppositely charged molecules in each monolayer deposited is involved. At first the fiber surface is treated with cloridic acid (HCl) and sodium hydroxide (NaOH) in order to form a negatively charged surface. Subsequently the fiber is dipped into cationic and anionic polymer solutions in order to form polyelectrolyte multilayers. The sensitivity of the sensors depends on how many layers are grown on the fiber surface. The authors declare a good sensitivity by only growing four layers, with the external layer positively charged to ensure

the immobilization of the negatively charged BSA probes.
The ionic bonding method can be combined with an avidin-biotin immobilization technique. This technique is an extremely specific non-covalent binding method. Moreover the avidin binding to the ESA film has the effect of passivate the surface preventing non-specific binding of biomolecules on the surface. The avidin coated substrate can be homogeneously linked to biotinylated proteins, like BSA in this case. The easiest method to attach the avidin to the transducer platform is then the electrostatic adsorption on self-assembled multilayers. The main disadvantage of a ionic method is that electrostatic adsorption methods suffer from low long term stability.
In order to improve the long term stability a covalent bonding is needed. The covalent bonding is performed via a silanization procedure. Before the silanization the fiber is treated with a strong acidic solution in order to activate the surface. The activated silica surface is then silanized with 10 % 3-aminopropyl-trimethoxysilane (APTS). The silanization is then followed by subsequent steps that lead to the formation of a polyacrylic-acid (PAA). The PAA layer is then coated with extravidin via covalent bonding with the terminal carboxyl groups on the PAA. The immobilization of the BSA biotinylated probes occurred via avidin-biotin interactions.
The above described methods refer to a particular experiment, but it shows that it is possible to bind the same probe to the same sensing platform in different ways. In an other work [102] the covalent bonding, similar to the described above, has been used. Antibodies of goat anti-human IgG were immobilized on the surface of an optical fiber using the covalent bonding through silanization. But in this case the antibodies were immobilized not through an avidin-biotin interaction but directly after having treated the fiber surface with glutaraldehyde in water solution.
The DNA detection was the aim for the biological sensors presented here. Then a specific and selective probe for the DNA was nedeed.

Figure 3.1: The double helix DNA structure.

3.1 DNA

Deoxyribose Nucleic Acid is a biological molecule that has a double helix structure, first discovered by Watson and Crick in 1953 [103] thanks to the X ray diffraction technique, represented in Fig. 3.1.

The double helix is composed by two strands of nucleotides. Every nucleotide is composed by three distinct parts: a pentose sugar (5 carbon atoms), a nitrogen base, and a phosphate group. The nitrogen bases are divided into two classes: the purines with a double ring structure, and the pyrimidines with a single ring structure. In the DNA molecule there are two kind of purines: adenine (A) and guanine (G), and two kind of pyrimidines: thymine (T), and cytosine (C), the chemical structure of the four bases are visible in Fig. 3.2. In order to form a strand with more than one nucleotides the phosphate group that is bound to the carbon atom in position five (5') of the pentose sugar is linked to the 3' carbon atom of the other nucleotide. These kind of

5'-3' bonds are relatively strong, and the skeleton of the strand composed by repeated sugar-phosphate-sugar-phosphate bondings gives stability to the structure [104]. The terminations of a DNA single strand are not the same, on one side a 5' carbon atom is present, while on the opposite side a carbon 3' is present, see Fig. 3.2.
The bonding between the two single DNA strands is due to the binding between the bases that form each strand. In particular A links to T, and G links to C, and no other pairs are possible. The links A-T and G-C are possible through hydrogen bondings between the bases, two for the A-T pair and three for the G-C pair. Hydrogen bondings between the bases are a relatively weak, and because of this the two strands of DNA can be easily separated for example by heating the molecule.
The formation of the pairs A-T and G-C determines a complementary relationship between the two strands that form a molecule, giving to the DNA a self-coding character [105]. For example if a single DNA strand has the following sequence: 5'-ACTTGTAC-3' the complementary strand that binds to this will be: 3'-TGAACATG-5'. It is important to notice that the "head" and the "tail" of the two strands are different, if the head of one strand is 5' the end will be 3', it has 5'-3' direction, the opposite will be for the complementary strand that will have 3'-5' direction.
The specificity of A-T and G-C pairs makes DNA suitable for being a probe for detecting DNA itself. If a single strand of DNA is linked to the sensor surface it will be able to capture the complementary strand, and in this way the specificity of the detection is also guaranteed.

3.2 Peptide Nucleic Acid Functionalization

In the work presented here the fiber surface has been functionalized with Peptide Nucleic Acid (PNA). PNA is a synthetic analogue of DNA strand, whose sequence is designed to be complementary to the one of the traget DNA, its molecular structure is represented in Fig. 3.3. PNA molecules are well known to bind in a very effective way and have a high specificity to complementary DNA strands [106], and they are considered to be one of the best types of probes for DNA recognition, being able to discriminate very efficiently between DNA sequences differing for a single base

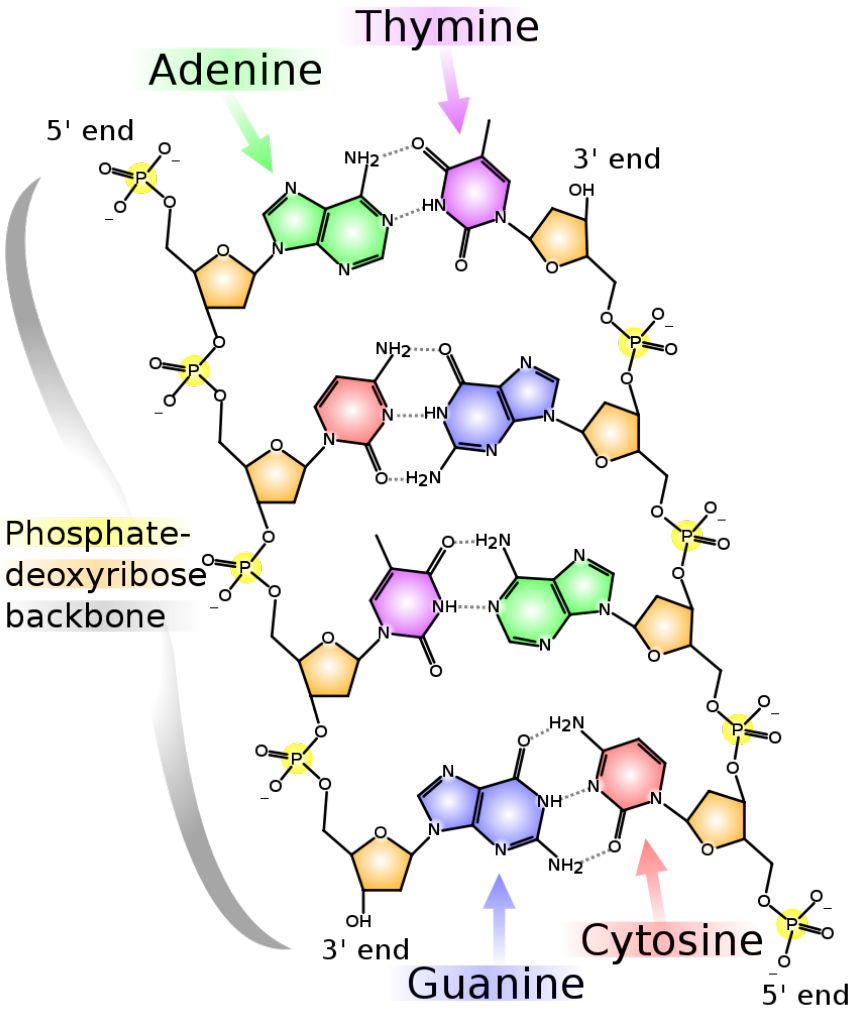

Figure 3.2: Example of the chemical structure of a double stranded DNA molecule.

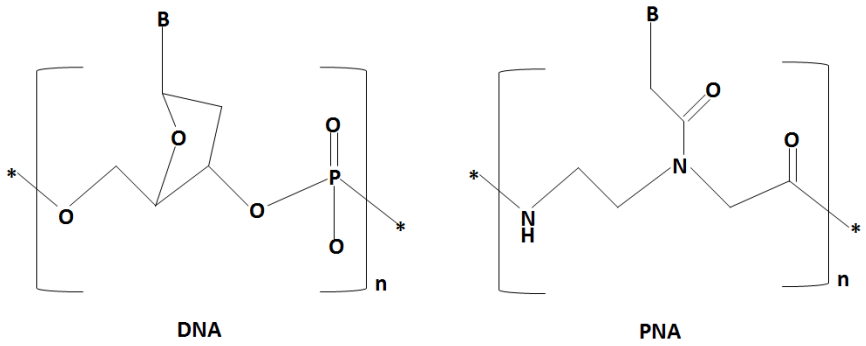

Figure 3.3: Structure comparison of a DNA and a PNA molecule. B denotes DNA nucleobases.

mismatch [107], known as Single Nucleotide Polymorphism (SNP).
PNA is not able to be strongly adsorbed to the fiber surface, then a functionalization is needed. The PNA functionalization on a glass surface has been already carried out with success [11] [12] on microarray glass slides. The same procedure has been applied to the optical fiber surface, since the material of which microarray slides and the optical fiber are made is the same, silica glass.
The chemical modification of the fiber surface was carried on following the steps described below:

1. cleaning and activation of the fiber surface with a solution of HCl:MeOH (1:1);

2. silanization with (3-aminopropyl)triethoxysilane (5% in ethanol), according to the literature the silanization procedure [44] [108], is considered as the most stable for silica glass;

3. reaction of the amino groups with succinic anhydride (0.25 *M* in *N,N* - dimethyl-formamide (DMF)) overnight, in order to have carboxylic acid functional groups bound to the fiber;

4. activation of the carboxylic function with *N,N*-diisopropylcarbodiimide (DIC)

and N-hydroxysuccinimide (NHS) in DMF dry as a solvent (0.25 *M* both);

5. PNA binding to the carboxylic functional groups by reaction of the activated ester to the PNA probes terminal amino group;

6. quenching of the excessive activated esters with an excess of ethanolamine, the quenching of the activated esters that are not bound to PNA probes is done in order to prevent the binding of DNA during the hybridization.

All the steps described above are represented in Fig. 3.4.
A more detailed description of this procedure will be given later.
It has been recently demonstrated the possibility of binding DNA probes by growing a hydrogel matrix on the fiber surface [109]. This is an alternative way to covalently bind DNA probes to the fiber surface.
Once the fiber surface has been functionalized with PNA probes, it is ready for the target DNA detection, the hybridization phase. During this phase an optical signal is measured and the observation of a signal change is to attribute to the DNA binding. Of course hybridizations with mis-matched DNA must be carried on in order to prove that the successful hybridization is not due to non-specific absorption, or to the poor selectivity of the probes.

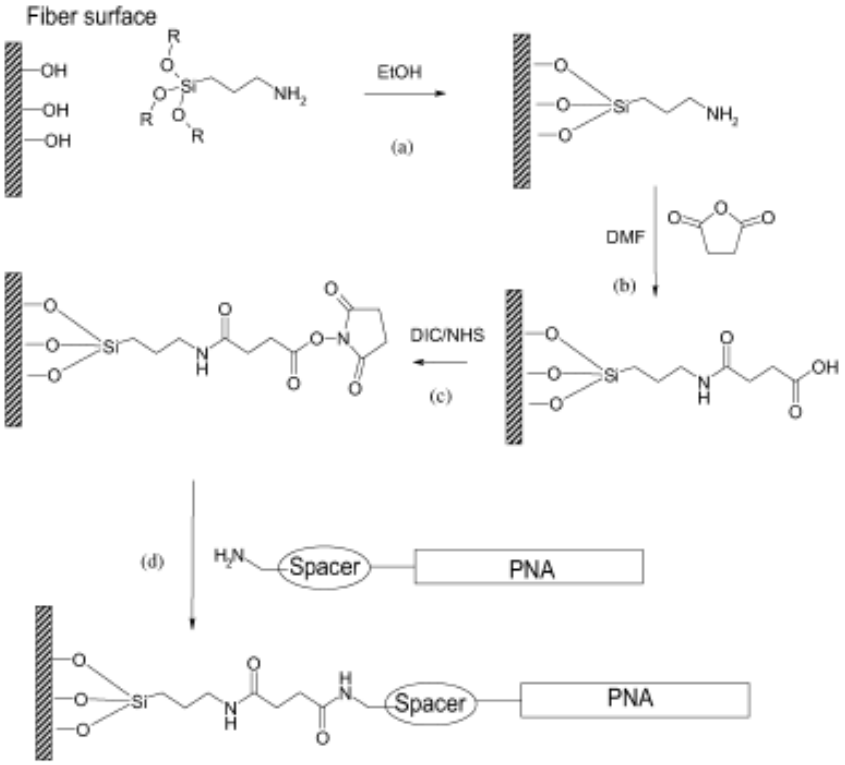

Figure 3.4: The PNA functionalization procedure used in the experiments. (a) Silanization. (b) Reaction with succinic anhydride. (c) Activation of the carboxylic moiety. (d) Covalent link to the PNA through terminal amino group. Experimental details are described in the text.

Chapter 4

Fiber Bragg grating fabrication

In this chapter the fabrication of FBGs is presented. In the first section the refractive index engineering of phosphate glass optical fibers is investigated, the gratings have been made by exposing the fiber samples to UV laser radiation in order to induce the refractive index change.
In the second section the fabrication of Surface Relief Fiber Bragg Gratings (SR-FBGs), a kind of gratings obtained by physically removing the material in order to induce the refractive index change, is invesitgated. SR-FBGs have been fabricated inside the holes of PCFs.

4.1 Non-monotonous refractive index changes recorded in a phosphate glass optical fiber

Several studies have been presented on the photosensitivity and index engineering of phosphate glasses using high intensity ultraviolet [110], [111], [112] and infrared [113] laser sources. These studies are of particular interest due to the increased number of applications of rare-earth codoped phosphate glasses in the development of high efficiency planar and fiber active components [114]; but also due to the specific micro-structure and physical properties of the phosphate glass. The pentavalent phosphorus defines the micro-structure of phosphate glass, leading to a linear-like

polymerisation chain built in combination with oxygen and other ion modifiers; a micro-coordination structure which is substantially different from that of common silicate glasses [115]. The specific microscopic properties define the photosensitivity characteristics of phosphate glasses: the refractive index changes induced in those glasses are rather low ($10^{-5} - 10^{-4}$) by utilizing standard ultraviolet lasers [110] [111]. The photosensitivity origin of phosphate glasses has been investigated employing a number of diagnostics [110], [111], [113], [116]; however, there is still an open question related to the sign of the refractive index changes induced in phosphate glasses using different laser wavelengths and exposure conditions. In the past, transient and low strength gratings have been recorded in phosphosilicate glass fibers using nanosecond 193 *nm* and 240 *nm* laser radiation [117]. However recently, strong Bragg gratings were inscribed in a rare-earth doped all-phosphate glass optical fiber, using standard phase mask approach and 193 *nm* excimer laser radiation, by Albert, et al [118]. The Type I refractive index changes presented in [118] are of the order of $4\text{x}10^{-4}$, while the inscribed gratings exhibited interesting thermal regeneration characteristics at relatively low annealing temperatures. Grobnic, et al, have inscribed refractive index changes greater than $1.5\text{x}10^{-3}$ in a similar phosphate glass fiber [119]; while Bernier, et al, have recorded negative refractive index changes in ZBLAN glass fibers [120], both of them using 800 *nm* femtosecond radiation. Herein, results on the photosensitivity and Bragg grating recording behavior of an all-phosphate glass rare earth doped optical fiber, utilizing 248 *nm*, 500 fs laser radiation are presented. In the grating inscription results presented, non-monotonic refractive index changes are observed versus accumulated energy density dose. This specific behavior resembles that of the Type IIA (belonging to the greater family of Type In grating types [121]) photosensitivity mechanism that usually occurs during grating recording in high-Ge doped silicate glass optical fibers using deep ultraviolet laser sources; however, it has never been observed before in grating recording in soft glasses [120], including phosphate glass fibers. The results presented refer to average and modulated refractive index changes, accompanied by a specific thermal study of the inscribed gratings. Moreover, the origin of the non-monotonic refractive index changes inscribed is further investigated utilizing Knoop hardness (HK) micro-indentation measurements,

performed in irradiated fiber samples.

4.1.1 Experimental

The Bragg grating inscription was performed using a 248 *nm* KrF excimer-dye laser system, Lambda Physik EMG 150MSC, with 500 fs pulses at a repetition rate of 10 Hz. The experimental set-up used for grating recording was a double phase mask interferometer, described in detail elsewhere [80]. The first phase mask used had a period of 1084 *nm*, while the second had a period of 535 *nm*, and they are both made from fused silica and being optimized for 248 *nm* wavelength operation. The resulting grating period recorded in the fibers exposed was 528.1 *nm*. Before the two phase gratings interferometer, a 0.4 *cm* long $\times$ 1 *cm* wide rectangular, metallic aperture was used for selecting the most uniform part of the beam, while a 6 *cm* focal length CaF_2 cylindrical lens that was placed after, was used for focusing this beam along the longitudinal axis of the fiber. The distance between the second phase mask and the fiber was 2.5 *cm* [80]. The grating transmission was monitored online using a broadband superluminescent source and an optical spectrum analyzer.

A phosphate glass single clad, Er/Yb codoped phosphate glass optical fiber, manufactured by INO, was used for the grating inscription. The concentration of the rare earth dopants in the fiber are 0.90 $wt\%$ for Er, and 7.0 $wt\%$ for Yb. Energy dispersive X-ray spectroscopy (EDX) measurements of the fiber glass showed that both core and cladding areas exhibit a similar stoichiometric composition, as well as, revealed the existence of Al and Ba ion modifiers. These two ion modifiers were traced at higher concentrations in the fiber core area. A short length of $\approx$10 *cm* of the Er/Yb codoped phosphate fiber was spliced at both ends to SMF28 telecom fiber, using a standard arc fusion splicer. The splicing process resulted in an additional transmission loss of 15 *dB* per splice, as that was measured at the wavelength of 1580 *nm*, and the generation of a smooth and long range Fabry-Perot spectral ripple of 4 *dB* extinction ratio.

For performing Knoop hardness measurements, the phosphate glass optical fibers were exposed using an un-modulated beam, embedded in a hard resin, and then they were side polished to optical quality until the centre of the fiber core was revealed. Knoop hardness measurements were performed using a Matsuzawa, MXT70, digital

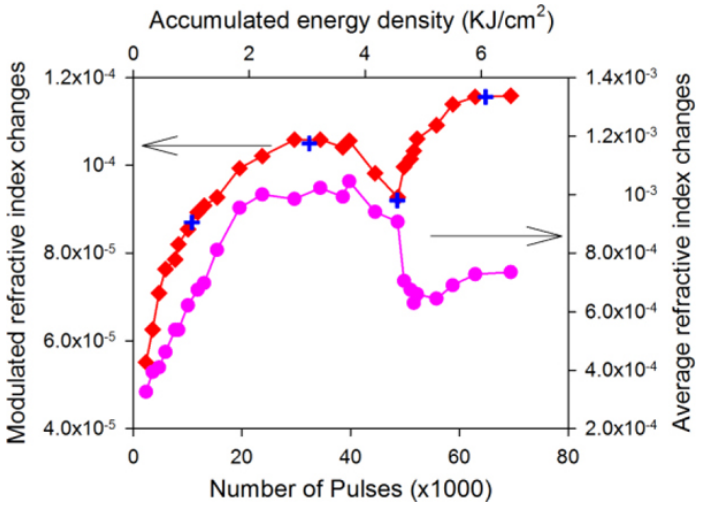

Figure 4.1: Index modulation Δn_{mod} (red points) and average refractive index Δn_{ave} changes (purple points) versus accumulated energy density, for grating exposure of the phosphate glass fiber using 248 nm 500 fs excimer laser radiation. The blue cross-points denote the exposure instances (number of pulses for fixed energy density) where Knoop micro-indentation measurements were performed.

indentation microscope, and by applying a 100 gf load for 20 s indentation time. Under these micro-indentation conditions the HK of the pristine glass was measured to be ≈292, for ten imprinting samples.

4.1.2 Results and discussion

The average and modulated refractive index change results obtained for a grating exposure using 93 mJ/cm^2 average energy density (0.37 TW/cm^2 intensity at the bright fringe) are shown in Fig. 4.1. Lower energy densities (by a ratio of 25%) led to observation of monotonous, photo-induced refractive index engineering process, for similar accumulated energy density doses. No evident cladding or core damage was revealed after inspecting the exposed fiber using optical microscopy, thus, no Type

II heat-induced damage changes were inscribed. After the inscription was initiated a spectral peak corresponding to the Bragg reflection was observed at the spectral vicinity of 1625 *nm*, scattering far away from the Er-doped absorption peak. The maximum refractive index changes measured are of the order of $1.2\text{x}10^{-3}$, manifold greater than those induced using 248 *nm* nanosecond [110] and 213 *nm*, 150 *ps* exposures [112] in a similar phosphate glass matrix. For an accumulated energy density of 4.5 KJ/cm^2 a characteristic turning point similar to that of the Type IIA photosensitivity behavior is observed in the modulated refractive index change data; while in the corresponding average refractive index changes, a significant blue shift singularity appears. At this characteristic turning point, the grating does not reach zero strength (namely becomes 3.1 *dB*). There are two possible factors that can be related with this non-zero turning point. The first is associated with irregularities in the intensity profile of the beam (herein measured to be between $\approx 30\%$), which in turn affect the progression of index engineering and the photosensitivity type along the grating length [90]. Namely, spatial irregularities in the beam intensity profile affect the accumulated energy dose at different points of the grating length; triggering positive or negative refractive index changes photosensitivity mechanisms asynchronously during exposure. The second factor is related with the underlying photosensitivity mechanisms occurring in the phosphate glass under 248 *nm*, 500 fs irradiation, and specifically the actual generation and progression of positive and negative refractive index changes. The non-zero turning point of Fig. 4.1 can be associated with a positive refractive index changes residue which is formed during the whole duration of the grating exposure. This specific point will be discussed in the following paragraphs.The aforementioned considerations related with the laser beam quality may be also supported by the broad shape transmission spectrum of the grating inscribed (see Fig. 4.2). The shape of the grating spectra presented in Fig. 4.2 indicates the recording of a rather chirped grating with possible phase imperfections due to the spatial distribution of the beam intensity and slight misalignment with the interference pattern. The final grating strength is 6.3 *dB* approximately, over a length of 4 *mm*, while the red-band transmission notch is believed to be related with strong phase imperfection and not with radiation induced birefringence. An annealing study was performed six months after the inscription,

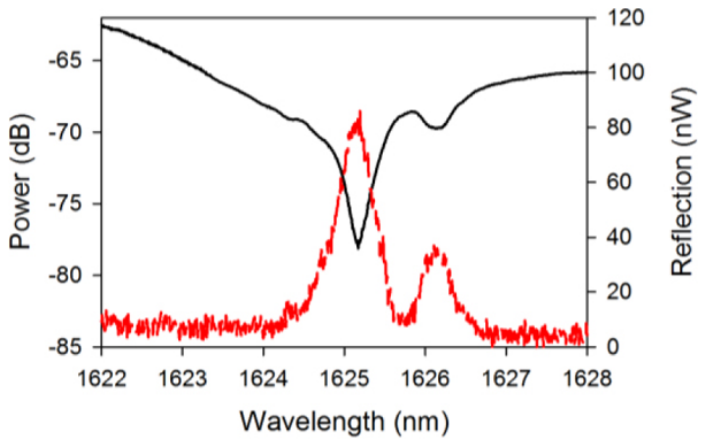

Figure 4.2: Transmission (black line) and reflection (red line) spectra of a 4 *mm* long Bragg grating fabricated in a phosphate glass fiber using 248 *nm*, 500 fs excimer laser radiation, for an accumulated energy density of 6.5 KJ/cm^2.

while the 93 mJ/cm^2 grating was kept at room temperature and low humidity conditions. Comparative spectral measurements show that the grating remained spectrally stable after this prolonged storage period. Then, the grating inscribed was placed into a copper capsule resting onto a hot plate and was isothermally annealed up to 377 $^{\circ}C$, at increasing steps of 30 *min* duration. Grating decay results are presented in Fig. 4.3 . The annealing process was interrupted at 310 $^{\circ}C$, letting the grating cool down to room temperature and measuring its relaxed spectral characteristics. Accordingly, the grating was then re-annealed to 377 $^{\circ}C$ for a 30 *min* slot and then left to cool down at room temperature. The data of Fig. 4.3 show that the grating retains the 75 % of its strength at the end of the annealing cycle at 377 $^{\circ}C$, thus, a significant part of the refractive index changes inscribed (see Table 4.1). The annealing data presented for the 93 mJ/cm^2 exposure, are rather similar to those obtained for Type IIA grating recordings, exhibiting a slow demarcation trend versus increased temperature, with a minor regeneration point at 100 $^{\circ}C$. For comparison, gratings recorded using $\approx$ 25% lower energy densities, were erased faster at lower temperatures; however, they exhibited

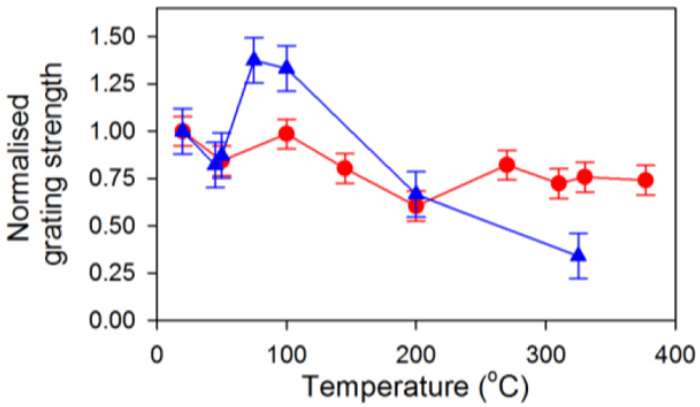

Figure 4.3: Isochronal annealing results for Bragg gratings recorded in the phosphate glass fiber, using 248 nm, 500 fs laser radiation. Red circles: 93 mJ/cm^2 energy density, 6.5 kJ/cm^2 accumulated energy dose. Blue triangles: 78 mJ/cm^2 energy density, 3.6 kJ/cm^2 accumulated energy dose.

prominent regeneration effects at the aforementioned annealing vicinity of 100 $^{\circ}C$ (see Fig. 4.3), similarly to the results presented by Albert, et al [122]. This specific behavior may be associated with slow structural relaxation process of defects that are not transformed/exhausted during the Type I photosensitivity regime. Since in a saturated Type IIA grating these defect states are rather transformed/exhausted, such regeneration effects are expected to be of lower magnitude [122]. The non-monotonous index engineering data presented here come to augment studies previously presented on the photosensitivity of phosphate glasses [111], [112]. It has been shown that an alumino-phosphate glass matrix undergoes substantial, non-monotonic Knoop hardness changes upon irradiation using 248nm [123] and 193 nm excimer lasers [116]. Similarly in this work, a pristine fiber sample was exposed to 186 mJ/cm^2 energy density 248 nm, 500 fs radiation, resembling the energy flux conditions occurring in the bright fringe of interference. Such Knoop micro-hardness measurements have been repeated here, however performed onto the exposed and side-polished, optical fiber core (see Fig. 4.4). The accumulated energy density figures employed in those

Table 4.1: Summary of the Bragg Wavelength Shift and Erased Average Refractive Index for Different Annealing and Cooling Cycles of the Phosphate Glass Fiber Bragg Reflector for 93 mJ/cm^2 Energy Density Exposure

Temperature ($^{\circ}C$)	**Bragg Wavelength** (*nm*)	**Average refractive index changes erased**
22	1625.09	-
310	1624.74	-3.1x10^{-4}
377	1624.46	-5.4x10^{-4}

fiber exposures for performing Knoop hardness indentations were determined after considering the modulated refractive index change data of Fig. 4.1. The targeted accumulated energy densities/number of pulses points refer to the initial stage of the exposure (where refractive index changes progress rapidly), the saturation plateau of the Type II regime, the turning point in grating strength, and finally, the saturation point of the Type IIA regime (see cross-points in Fig. 4.1).

As the data of 4.4 show, the Knoop hardness of the glass increases during the early stages of exposure, while after follows a clear declining trend towards lower values. The actual decrease of the Knoop hardness due to the irradiation processing is greater than 10 %. That significant change of the Knoop hardness is associated with volume densification/or dilation effects [111], [116], [123] and corresponding changes to Young's modulus of the material that are dependent upon irradiation conditions [116], [124]. The initial increase of the hardness (which is associated with positive refractive index changes) may be attributed to the dissociation of the O-P-O bond and its transformation to either a double P = O bond or an Al-O-P of higher energy and size. Also, P-O hole centers are expected to contribute to the positive refractive index changes saturated at the early stages of the irradiation [125]. Accordingly prolonged exposures using high intensity ultraviolet radiation, induce extended de-polymerisation of the phosphate glass matrix irrespectively of defect type while increasing glass randomness; facts which have been also verified using micro-Raman

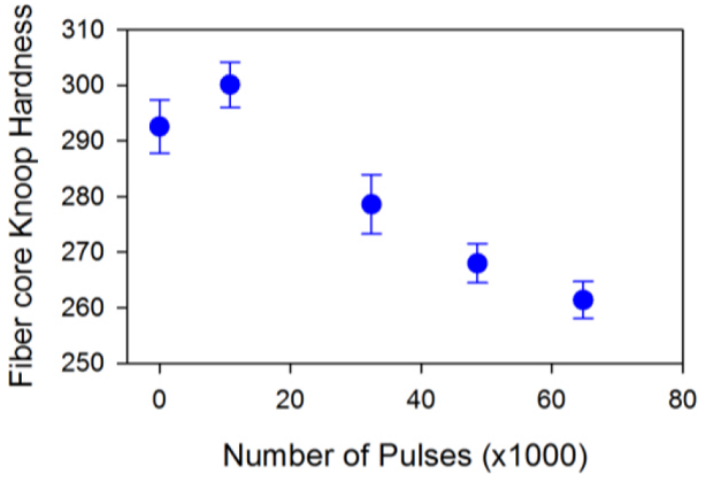

Figure 4.4: Knoop micro-hardness indentation measurements performed in the core of the exposed phosphate glass fibers, for different number of irradiation pulses, and 186 mJ/cm^2 energy density per pulse.

spectroscopy [111], [116]. Volume dilation will progress faster at the later phase of the exposure after the P-O defect transformations have been saturated. This assertion appears taking place during grating inscription (see Fig. 4.1), where the modulated refractive index changes turning point occurs at an energy density close to that of the saturation of the grating.

After considering the refractive index change and Knoop hardness data presented above, a hypothesis can be made for the anomalous photosensitivity behavior of the phosphate glass fiber, under 248 nm, 500 fs irradiation. The density decrease of the exposed phosphate glass that was revealed using Knoop hardness measurements, takes place at the bright fringes of interference, while contributing a negative refractive index change component in the grating recording process. That glass softening effect occurs in an analogous extend along the whole transversal section of the phosphate glass fiber, since both the core and cladding are of quite similar stoichiometric composition, while being subjected to energy density doses of almost the

same magnitude. Subsequently, the localized density decrease and volume dilation, can lead to compressive axial stress generation in the dark fringes of the exposure [126], [127]. That compressive stress generation leads to positive refractive index changes. Together with the other positive refractive index change mechanism that of the glass hardening (see Fig. 4.4) and P-O hole centers, saturated at the initial phases of the ultraviolet radiation exposure, they can form an overall positive refractive index changes background. This non-saturated positive refractive index background can be associated with the non-zero turning point of the Δn_{mod} refractive index change data [90], as well as, with the overall positive, average refractive index changes, presented in Fig. 4.1. The positive refractive index change mechanisms are initiated and progress at different instances of the exposure; and in parallel with the underlying volume dilation, which dominates the later phase of the exposure and drives the non-monotonous refractive index engineering. The above photosensitivity hypothesis may be interpreted as the mirror counterpart of the Type IIA of the highly doped germanosilicate fibers, where the exposed regions undergo compaction and the induced stress effects are tensile [126].

4.1.3 Summary

The observation of non-monotonic photosensitivity and refractive index engineering of a phosphate glass fiber during Bragg grating recording using a double phase mask interferometer and 248 *nm*, 500 fs laser radiation, has been reported. The results obtained show a photosensitivity behavior with similar growth characteristics to the Type IIA observed for exposures in high-Ge doped silicate glass fibers. The results presented are discussed according to the volume dilation model that has been proposed before for phosphate glasses.

4.2 Surface relief fiber Bragg gratings

SR-FBGs have the same basic operational characteristics as standard FBGs. The main difference between these devices is in the method used to fabricate the gratings into

the fiber. The gratings of standard FBGs come from a periodic modulation of the refractive index in the core. However, in SR-FBGs the gratings are physically etched into the fiber. This allows SR-FBGs to operate at elevated temperatures where the gratings in standard FBGs are erased. As a result, SR-FBGs are ideal for sensing applications where high temperatures would limit the operation of standard fiber Bragg gratings. Ideally, an SR-FBG will maintain functionality as a sensor in temperatures up to the melting point of glass.
SR-FBGs have been fabricated in D-shaped optical fibers [128], [129]. On the flat region of the fiber a SR-FBG is fabricated by first etching the cladding, then applying a photoresist layer, and then performing a second ecthing of the photoresist and the glass as well. Measurments performed with this kind of gratings are possible till a temperature of $1100°C$ [129], a temperature at which standard FBGs don't survive.
Micromachining lasers techniques can be applied to perform etching on dielectrics materials. These techniques are based on the laser induced backside ecthing, a finely polished sample is irradiated with a laser beam at a wavelength at which it is transparent. On the opposite side, of the irradiation, the dielectric is in contact with a material which absorbs the laser beam. There an etching is performed.
The possibility of infiltrating liquid or vapours phase materials in the holes of a PCF can lead to the possibility of fabricating SR-FBGs inside them. In particular in the holes surrounding the core so that the etched structure can be felt by the evanescent field of the core propagating modes. Exploiting laser induced etching to fabricate SR-FBGs inside PCFs can avoid all the fiber preparation steps needed for the D-shaped fibers.

4.2.1 Laser induced backside etching

Nowadays a number of indirect laser processing methods is in development, the aim is to induce a near surface absorption of the laser energy at the backside of transparent samples. However, the enhanced surface/interface absorption is achived at these methods by additional materials. Depending on the additive material used to enhance the energy deposition near the sample surface different techniques can be distinguished.

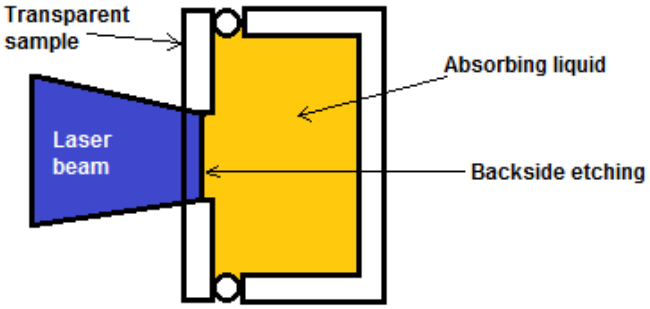

Figure 4.5: Basic set-up configuration for LIBWE.

Laser Induced Backside Wet Etching (LIBWE) makes use of high absorption of organic liquids (hydrocarbons or solutions of hydrocarbons) or liquid metals for excimer lasers wavelengths [130].
The Laser Etching by Surface Adsorbed Layer (LESAL) similarly to LIBWE makes use of hydrocarbons vapours adsorbed at the backside of the sample to enhance the laser beam absorption [131], [132].
Laser Induced Backside Dry Etching (LIBDE) has been also demonstrated, this technique makes use of a thin metal film for laser energy deposition [133].
For our purposes the LIBWE and LESAL techniques are the ones of our interest.
In the LIBWE technique the use of hydrocarbons as absobers imply the employment of UV excimer laser sources in order to have enough absorption of the organic liquids.
The basic configuration of the experimental set-up used for LIBWE is represented in Fig. 4.5 [130]. The etching chamber holds the substrates and at the same time contains the absorbing liquid.
Different kind of etching are possible, in Fig. 4.6(a) [130] a $100\mu m \times 100\mu m$ square pattern has been etched on a sample of fused silica using a 248 *nm* laser radiation and a 0.5 *M* solution of pyrene:toluene. This technique gives also the possibility of etching periodical pattern, as shown in Fig. 4.6(b) [130] where a 530 *nm* periodicity structure has been etched on a fused silica sample, the image also show the high

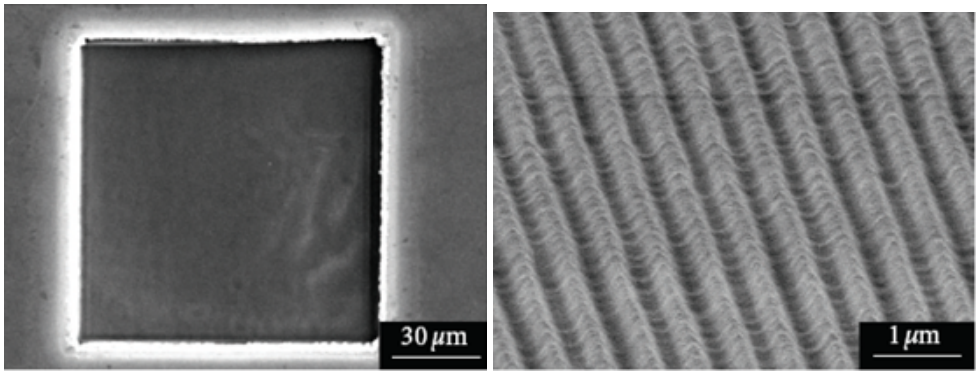

(a) (b)

Figure 4.6: (a) A 100 μm × 100 μm square pattern etched on a fused silica sample using a 248 *nm* laser radiation and a pyrene:toluene solution. (b) 530 *nm* periodic pattern etched on a fused silica sample with a 266 *nm* laser radiation.

quality of the obtained etching.

The mechanism that governs the laser backside etching is quite complex. The irradiation of the solid/liquid interface by pulsed lasers results in a number of processes in both materials, that involve fast heating, transient pressure, shock waves, melting and boiling, bubble formation and collapse, and modification or decomposition of the materials. These processes are linked together and they finally cause material erosion. However, it is generally accepted that laser absorption and heating of the near interface regions of both materials is the main process for backside etching [130]. In consequence of the laser heating during LIBWE, the softened, destabilized, weakened, or even melted material region near the surface might be expelled by mechanical forces resulting from the fast heating, shockwaves, or bubble formation.

More precisely the laser radiation is absorbed by the organic liquid and heats up to temperatures below the solid melting point. However, the organic solution vaporizes and decomposes due to photothermal and photochemical processes so that the formation of bubbles is forced. Due to heating decomposition and bubble formation, the surface is modified increasingly with the pulse number by liquid decomposition

products, for exmple, carbon, resulting in a thin highly absorbing film on top of the solid. The solid surface temperature increases with the pulse number and exceeds a critical temperature, at this point the transparent solid material is etched. Very high temperatures can be achived at the etching point so that processes similar to ablation occur at the solild surface that is confined by the liquid. This confinement may enhance the interaction of secondary processes with the solid and results in a modified near-surface solid region, that highly absorbs UV laser radiation with a result in an efficient interface heating. At this point the process of surface modification is self-mantaining but needs the absorbing liquid.
The kind of liquid solution or the solid material used can affect the rate and the quality of the etching. For example the etching rate of fused silica by using pure toluene or a 0.5 M pyrene:toluene solution is different, in particular a higher etch rate is perfomed using pure toluene, considering the same laser fluence [130]. The etching results can be affected also by the etched solid material, as shown in [130] comparing the etching of sapphire, calcium fluoride, and fused sillica. The etched fused silica shows a better quality etching compared to the other two that appears more grainy and irregular.
The LESAL technique similarly to the LIBWE technique causes the etching at the backside of a transparent material by means of a thin layer adsorbed onto the backside surface capable of absorbing the laser radiation. The laser beam only interacts with the adsorbed film at the back side with a result in smooth etching with low etch rates [132]. The adsorbed layer is formed by the vapour phase of organic solvents, such as toluene. In Fig. 4.7 is represented the basic experimental set-up for this technique.
This method was applied to fused silica showing remarkable attributes of the laser etch process and the etched surface [131] [132].
In the case of this technique the laser beam penetrates the trasparent sample and it is absorbed by the thin layer of hydrocarbons, which is continuously formed by adsorption from the vapour at the back side of the transparent sample.
The processes involved in the etching of the material are complex. As for the LIBWE the main cause of the etching is the fast heating at the solid/adsorbed layer interface. This fast heating involves other secondary processes like desorption of the adsorbed layer, formation of shock waves, and the decomposition of the adsorbed hydrocar-

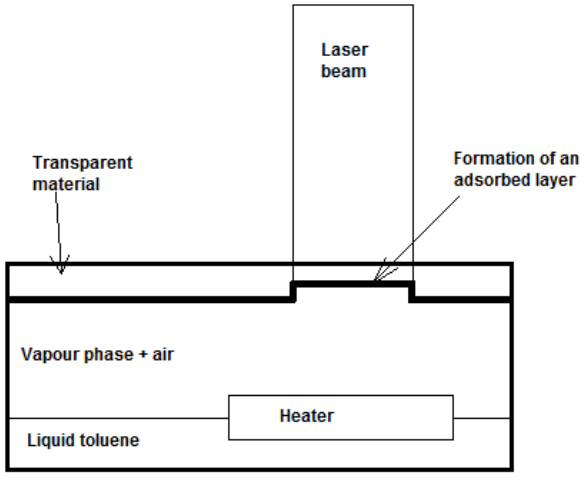

Figure 4.7: Basic set-up configuration for the LESAL technique.

bons [132].
The use of different solid material can affect the quality of the etching. Comparing etching performed on fused silica, quartz and magnesium fluoride, using toluene vapours to form the adsorbed layer and a *ns*, 248 *nm* excimer laser. The fused silica sample shows a lower roughness than the other two [131].
The main differences of the LESAL technique compared to the other backside etching techniques are the use of an adsorbed hydrocarbon layer, the low etch rates, the low roughness of the etched surfaces and the absence of secondary effects like the bubbles formation.

4.2.2 Results and discussion

Experimental set-up

Laser exposures have been made with three different PCFs: a Penda fiber Fig. 4.8(a), a LMA10 Fig. 4.8(b), and a ESM12 Fig. 4.8(c). Two different lasers have been used for the exposures, a KrF 248 *nm* excimer laser, and a ArF 193 *nm* excimer laser. A

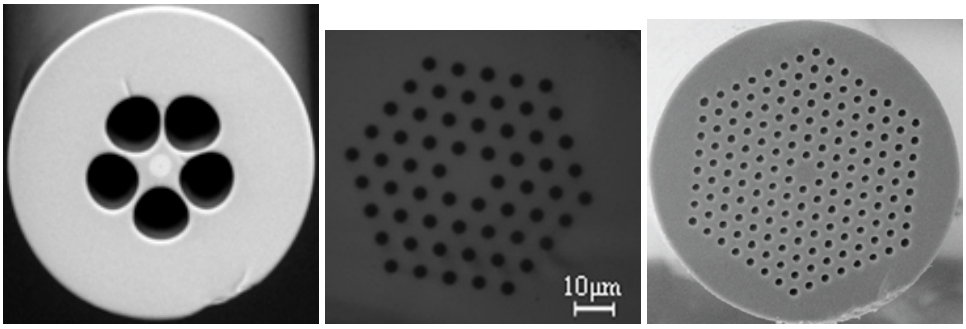

(a) (b) (c)

Figure 4.8: (a) Penda fiber provided by Acreo. (b) LMA10 produced by NKT Photonics. (c) ESM12 produced by NKT Photonics.

single phase mask set-up has been used, the phase mask had a 1070 *nm* period. A small part of the PCFs, about 3-4 *cm*, has been infiltrated with organic solvents, in order to have vapours inside the fiber capillaries in particular in the part exposed to the laser beam.

Experimental results

At first LIBWE technique has been employed, a sample of LMA10 has been infiltrated with liquid toluene and spliced both sides with SMF. The fiber has been exposed to a ArF 193 *nm* laser radiation with a fluence of 133 mJ/cm^2. Optical microscpoe images, Fig. 4.9, show that exposing the fiber with liquid toluene inside the capillaries leads to the destruction of the capillaries themselves. From the results obtained it has been decided to apply the LESAL technique, in order to avoid the capillaries destruction, and vapours from different organic compounds have been used.
Exposures of the Penda PCF samples have been carried on with three different organic solvents, toluene, carbon tetrachloride (CCl_4), and dibromodifluoromethane (CBr_2F_2), and two different laser wavelengths. The experimental conditions used with the Penda fiber are reported in detail in Table 4.2. Observing the exposed samples at the optical microscope, Fig. 4.10, etching has been observed for the 193 *nm*

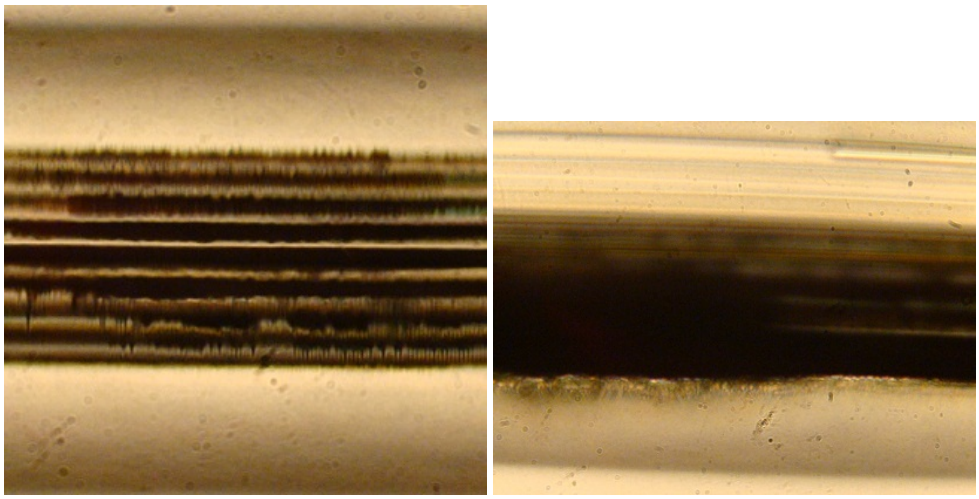

(a) (b)

Figure 4.9: (a) It is possible to recognize the periodical etching inside the capillaries. (b) From a different focus the disruptive etching of the capillaries is clear. The black color is due to the formation of carbon during the etching process.

Table 4.2: Experimental conditions for the Penda fiber exposures

Organic solvent	**Laser Wave-length** (*nm*)	**Pulse width**	**Energy density** (mJ/cm^2)	**Repetition rate** (Hz)	**Number of pulses**	**Grating length** (*mm*)
Toluene	193	10 *ns*	133	2	7200	14
Toluene	248	5 *ps*	71	2	7200	4
CCl_4	193	10 *ns*	133	2	7200	12
CCl_4	248	5 *ps*	71	2	7200	4
CBr_2F_2	193	10 *ns*	133	2	7200	12
CBr_2F_2	248	5 *ps*	71	2	7200	4

exposure with toluene, and for the 248 *nm* exposure with CCl_4 and CBr_2F_2. But SEM scans showed that etching was performed only for toluene with 193 *nm* laser radiation, and CBr_2F_2 with 248 *nm* laser radiation, most probably the features of Fig. 4.10(b) were just due to carbon deposition. In Fig. 4.11(a) is represented the SEM scan of the etching performed with toluene, while in Fig. 4.11(b) the etching performed with CBr_2F_2. From the SEM images it is possible to notice that the toluene etching quality is better than the one obtained with CBr_2F_2. The periodic structure has a better definition, and there is almost no presence of debris produced by the etching process. In both cases it was not possible to detect any spectra of the grating, both reflection and transmission. This may be due to the fact that the etching is performed in the part of the hole surface opposite to the core region. In this case it is impossible for the evanescent field of the propagating mode to feel the etched periodic structure. The reason why the etching didn't occurred in the core region may be due to the large holes of the fiber, 20 μm diameter, and because of this most of the laser intensity has been absorbed by the vapours, and the one which reached the core region was not enough in order to perform an etching. For this reason fibers with smaller holes as LMA10 and ESM12 have been chosen for the following exposures.

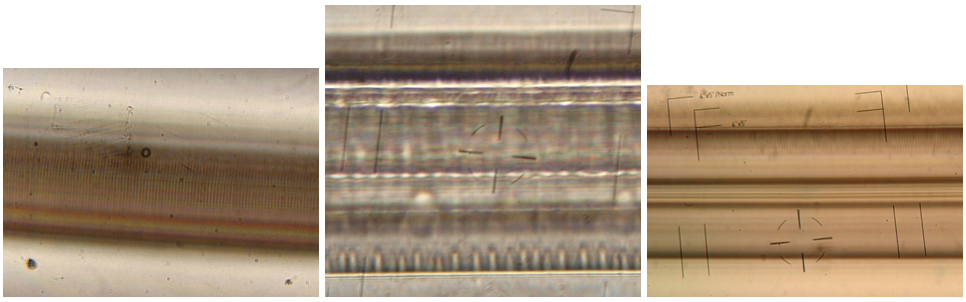

(a) (b) (c)

Figure 4.10: (a) Penda fiber infiltrated with toluene vapours exposed to 193 *nm* 10 *ns* laser radiation. (b) Penda fiber infiltrated with CCl_4 vapours exposed to 248 *nm* 5 *ps* laser radiation. (c) Penda fiber infiltrated with CBr_2F_2 vapours exposed to 248 *nm* 5 *ps* laser radiation.

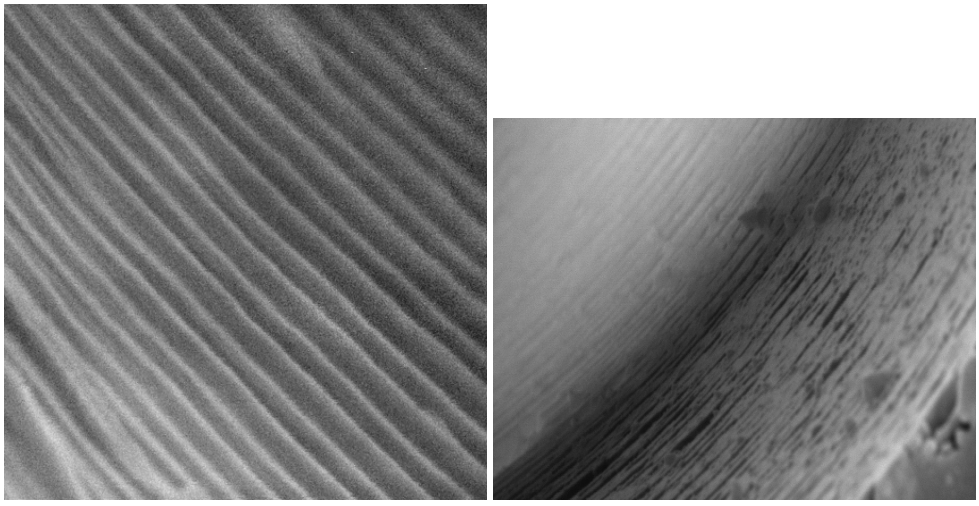

(a) (b)

Figure 4.11: (a) SEM image obtained from the sample etched with toluene. (b) SEM image obtained from the sample etched with CBr_2F_2.

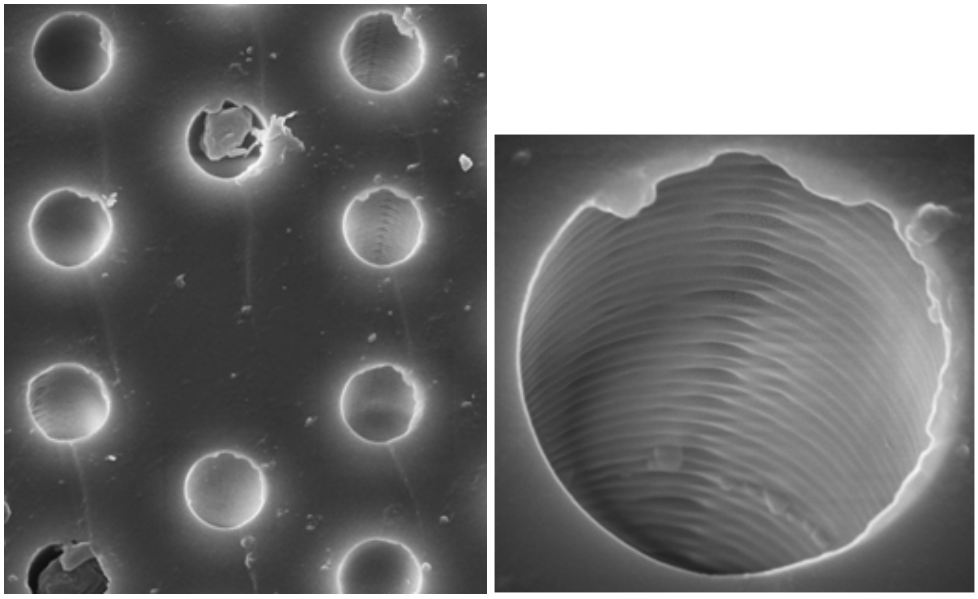

(a) (b)

Figure 4.12: (a) SEM scan of the LMA10 cross section, in the holes the presence of a periodic structure is visible. (b) Magnification of one of the holes near the core region, the periodic structure is clearly visible.

The results obtained with the Penda fiber showed anyway that the etching is feasible with the technique used, and that toluene is the most suitable solvent to use.
Samples of LMA10 and ESM12 have been exposed to a 248 *nm*, 10 *ns*, laser radiation. This laser radiation gives the possibility of having higher energy densities up to 400 mJ/cm^2, after that the fiber is damaged.
LMA10 samples have been exposed to a 390 mJ/cm^2 laser fluence, at the repetition rate of 5 *Hz*, and to a 27000 total number of pulses. In Fig. 4.12 are representetd the SEM scans of one of the exposed samples. In Fig. 4.12(a) it is possible to recognize the presence of the etching in the holes, and in particular in the holes in the core region. In Fig. 4.12(b) a magnification of the inside of one of the holes near the core is reported. A periodic structure of the same quality of the one in Fig. 4.11(a)

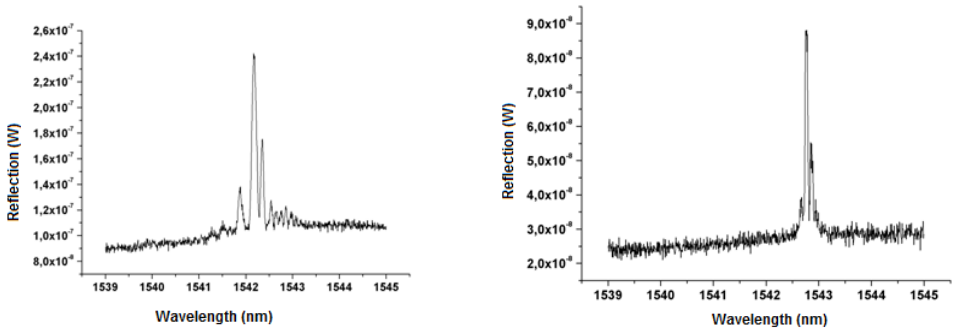

(a) (b)

Figure 4.13: (a) Reflection spectrum of the grating inscribed in the LMA10 fiber. (b) Reflection spectrum of the grating inscribed in the ESM12 fiber.

is clearly visible. But in this case the etching is all around the hole and then in the core region as well. During the exposure the growth of a weak reflection spectrum of the grating has been recorded. In Fig. 4.13(a) is represented the reflection spectrum of the grating just after the exposure. The presence of a reflection spectrum suggests the fact that the evanescent field of the propagating core mode feels the etching in the holes. A transmission spectrum was not recorded, most probably because the depth of the etching was not enough in order to detect the transmission as well.
ESM12 samples have been exposed to a 355 mJ/cm^2 laser fluence, at the repetition rate of 5 Hz, and to a 27000 total number of pulses. The growth of a weak reflection spectrum of the grating has been recorded as well, in Fig. 4.13(b) is represented the spectrum after the exposure.
The results obtained for the two fibers are similar, the grating in both fibers shows approximatively the same Bragg wavelength, 1542.17 *nm* for the SR-FBG etched in the LMA10, and 1542.77 *nm* for the SR-FBG etched in the ESM12. This is consistent with the fact that the two fibers have similar geometry, and that the experimental conditions applied are almost the same. Moreover the effective refractive index cal-

culated from the obtained Bragg wavelengths, and considering the grating period as half of the phase mask one 535 *nm*, is 1.44 that is consistent with the pure fused silica refractive index in the 1.55 μm region.

4.2.3 Summary

In summary the possibility to realize SR-FBGs in photonics crystal fibers have been demonstrated. Despite the obtained results are still preliminary the application of the LESAL technique to different kinds of PCFs has been found successful. The FBGs etched in a LMA10 PCF showed a good quality of the etching and a reflection spectrum was also detected, as for the ESM12 fiber.
The fabrication of such kind of gratings can lead to Bragg gratings that can survive to very high temperatures, moreover the employment of the LESAL technique can ease their fabrication compared to the procedure so far used for the D-shaped fibers.

Chapter 5

Fiber optics biosensors

In the literature, several optical designs have been widely reported that utilize optical fibers to implement biosensors. By using PCFs with the aim of exploiting their unique characteristics to produce highly sensitive chemical and biological sensors [134], [135]. In fact, air-holes can be easily inflated or filled with gases or liquids without compromising the fiber robustness, obtaining a very long interaction length, even in the presence of very limited quantity of sample. Moreover, a hollow-core PCFs capability to obtain light confinement in a low-index core yields the possibility to realize sample-filled core sensors [136], [137]. Sensing can also be performed through solid-core fibers, exploiting the evanescent tails of the guided mode field. Even if these fibers provide a lower field sample interaction with respect to the hollow-core fibers, due to the fact that only a small fraction of the optical power travels in the sample-filled region, their confinement losses are lower on a broader wavelength range. Moreover, it is possible to speed up the diffusion of the sample into the holes of solid-core fibers with the realization of side accesses [138], given the fact that the presence of a periodic cladding lattice is not required by their guiding mechanism.

It is also possible to realize a biosensor using a standard single mode fiber, and having anyway an interaction between the light and the analyte, by inscribing a Tilted Fiber Bragg Grating (TFBG) [36], or a Long Period Grating (LPG) [101], [102], in

the core of the fiber. With these devices it is possible to couple part of the light of the fundamental mode to the cladding modes, thus providing light interaction at the air-cladding surface. If the external surface of the optical fiber is functionalized with biological molecules, the light will interact with them. This interaction can yield to a change of the optical signal, in particular of the resonant wavelength of a LPG, or the predominant frequency of the Fourier transform of the TFBG spectral response [36]. Another advantage of this is also the possibility of performing a label-free detection. Different types of biosensors have been investigated, in this chapter all the platforms realized during the activity are reported.

5.1 Suspended core fiber DNA sensor

Among solid-core fibers, suspended-core PCFs (SC-PCFs) appear to be most promising for developing efficient biological sensors, due to their high evanescent-field power fraction, which can almost reach 30 % at 1550 *nm* for a submicrometer core diameter [54], and the capability to be designed with large air holes, which facilitate the filling with samples. Applications of SC-PCFs spanning from chemical sensing of gases and liquids to biological species detection have already been reported [54], [47], [13]. A detailed description of SC-PCFs will be given in Section 5.1.2.
One of the most intriguing possible applications of SC-PCFs is the selective detection of DNA. Well-established DNA analysis techniques are usually performed by immobilizing a single strand of DNA on a glass chip and checking the hybridization of this strand to its complementary. A so-called functionalization treatment is required in order to allow the binding of biological species to the glass surface [139]. Hybridization is then proved through the measurement of the fluorescence signal produced by the labeled sample. The ability to perform this kind of analysis, by exploiting the SC-PCFs hole surfaces instead of glass chips and by recollecting the fluorescence signal into the fiber core, can lead to a significant improvement of the sensitivity, with respect to the present technology.
The functionalization of internal surfaces of the holes of a silica SC-PCF and preliminary experimental studies on selective DNA detection are reported. Selective detec-

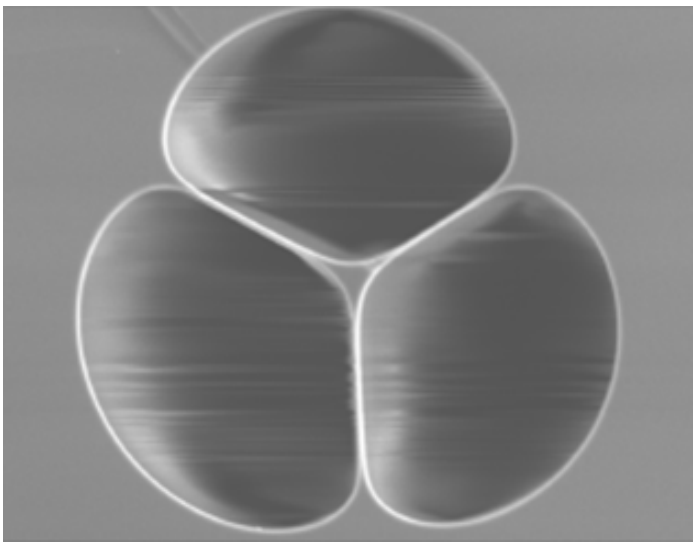

Figure 5.1: SEM of the SC-PCF.

tion of DNA strands has already been demonstrated with polymer optical fibers [140], which have the advantage, through proper modifications of their surface, of allowing biomolecules to be attached directly. With respect to polymer fibers, silica fibers have the main advantages of lower material losses and higher thermal resistance.

5.1.1 Suspended core fiber

An SEM of the silica SC-PCF used in the experimental part was provided in the frame of the European Cooperation in Science and Technology COST 299 action "Optical Fibres for New Challenges Facing the Information Society", is shown in Fig. 5.1. The fiber has a core diameter of 1.17 μm, a cladding diameter, which is the diameter of the smallest circumference inscribing the holes, of 24.5 μm, and a strut width of 0.19 μm. The evanescent-field power fraction for this fiber was calculated for different wavelengths by means of a full-vector modal solver based on the finite-element method, as reported in detail in [58].

5.1.2 Surface functionalization with PNA probes

In several works, the modification of optical fiber and waveguide silica surfaces has been described. The most stable modification can be obtained by tethering of sensors or biomolecules to the silica surface through a silanization procedure [44], [101], [108]. In order to test the applicability of sequence-selective detection of DNA by SC-PCF, a series of tests aimed at the introduction of very selective DNA-binding molecules at the fiber surface has been carried out. Peptide nucleic acids (PNAs), which are nucleic acid analogs known to bind very effectively and with high sequence specificity to complementary DNA [106], were chosen as probes. Due to their exceptional performances in DNA recognition, PNAs are considered to be among the best probes for the detection of even single-base mismatches in the target DNA sequences [107], showing a very high sensitivity [141].
In order to obtain a PNA-modified surface, first, the functionalization at the external surface was carried out according to the scheme reported in Fig. 3.4, Chapter 3, in order to rapidly test the feasibility of the derivatization reactions on the fiber material; then it was performed on the internal channels, with the same reaction steps. In both cases, the protocol used is described by the following steps:

1. cleaning and activation of the silica surface with acidic treatment (HCl:methanol = 1:1), which, according to the literature, is the best performing technique for subsequent functionalization [139];

2. silanization with (3-aminopropyl)triethoxysilane (5 % in ethanol) overnight [139];

3. reaction of the amino group with succinic anhydride (0.25 *M* in *N,N* - dimethylformamide (DMF), overnight) in order to obtain a carboxylic acid functional group attached to the fiber;

4. activation of the carboxylic function with *N,N* - diisopropylcarbodiimide (DIC) and *N*-hydroxysuccinimide (NHS) in DMF as a solvent (0.25 *M* both) overnight;

5. reaction of the activated ester with the end terminal amino group of the PNA

probe overnight (30 μM of probe in 100 mM carbonate buffer in water: acetonitrile = 90:10 containing 0.001 % sodium dodecylsulfate, pH = 9), according to previous procedures used for microarray spotting [11], [12];

6. quenching of the excessive activated esters with an excess of ethanolamine (50 mM in aqueous Tris buffer pH = 9.0, room temperature for 3 h).

For the derivatization of the external fiber surface, the coating was removed from a 2.5 cm long sample of the fiber and the exposed part was immersed in the corresponding solutions.
Internal derivatization was obtained by applying a nitrogen pressure of 2 atm to a poly(tetrafluoroethylene) (PTFE) tubing reservoir (100 μL), connected to the terminal part of the fiber through a polyetheretherketone (PEEK) ferrule junction and a PTFE adapter. In the latter case, the flow through the fiber was checked by the appearance of a liquid flow at the opposite end. After each treatment, the liquid was removed from the fiber by means of at least 30 min nitrogen flux, as checked by optical microscope inspection.

5.1.3 Experimental results

In order to test whether the PNA probes were effectively attached on the surface, hybridization experiments were performed with fluorescently labeled full complementary and single mismatched DNA oligonucleotides, reported in Table 5.1. The hybridization was evaluated by means of a microarray fluorescence reader, the ScanArray Express by Perkin Elmer, which performs fluorescence scanning of the samples deposited on a glass slide, using two different laser sources for excitation of the fluorophores (543 nm for Cy3 channel and 633 nm for Cy5 channel) and different emission filters for selecting the fluorescence emitted.
For the externally modified fiber, a Cy3-labeled full-match DNA 1 and a Cy5 single-mismatched DNA 2 in a 1:1 mixture (100 nM each in phosphate buffer saline (PBS), pH = 7) were used.
Unmodified fibers and a functionalized fiber were considered. The uncoated parts of these fibers were immersed overnight in the same mixture for hybridization, at room

Table 5.1: Sequences of the PNA probes and the DNA targets

Oligo	**Sequence**	**Role**
PNA	H-O-O-TTACTCATTCACC-NH2	Probe
DNA 1	Cy3-GGTGAA**T**GAGTAA	Cy3 full-match
DNA 2	Cy5-GGTGAA**A**GAGTAA	Cy5 mis-match
DNA 3	Cy3-GGTGAA**A**GAGTAA	Cy3 mis-match

temperature in the dark, and then washed three times with PBS (10 *mM* phosphate, 0.1 *M* NaCl, 0.1 *mM* ethylenediaminetetraacetic acid (EDTA), pH = 7.0), dried in air, and put on a glass slide for microarray analysis, together with a third unfunctionalized fiber, to be used as reference, on which a drop of the DNA mixture was deposited.
Under these conditions, if the PNA is present on the surface of the modified fiber, a sequence-specific DNA binding should be revealed by the following evidences: 1) the higher uptake of fluorescently labeled DNA by the functionalized fiber and 2) the higher uptake of the full-match target DNA 1 (Cy3 labeled) than that of the mis-matched DNA 2 (Cy5 labeled) of the derivatized fiber, as compared to the starting solution and the underivatized fiber. The results are shown in Fig. 5.2. In particular Fig. 5.2 compares the mean fluorescence intensities and standard deviation observed after hybridization for the PNA-modified SC-PCF and the unmodified SC-PCF, normalized to that of the hybridization solution simply deposited on an unmodified fiber. The image show that the PNA-derivatized fiber maintains higher fluorescence in the analysis performed using the Cy3 channel, with an increased ratio between the Cy3 (full-match) and Cy5 (mismatch) signals, whereas in the unmodified fiber, only small retention of both oligonucleotides was observed, due to unspecific adsorption. There-

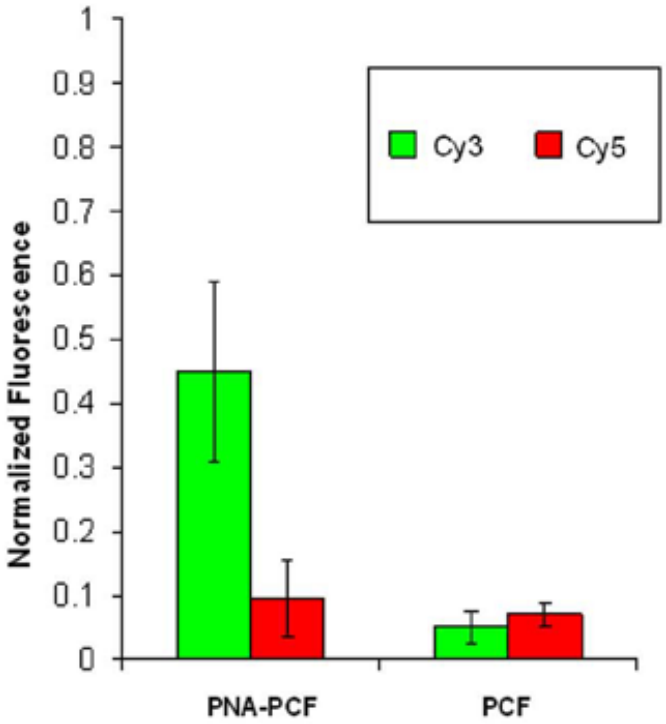

Figure 5.2: Fluorescence intensities observed after hybridization for PNA-modified SC-PCF and unmodified SC-PCF, compared to those obtained for the initial solution deposited on an unmodified fiber. Data are normalized for each channel to the intensity of the initial solution, in order to take into account the different sensitivity of each channel. Vertical bars indicate standard deviations.

fore, the PNA-modified fiber was shown to be able to retain full-match DNA more effectively only if it contains the full-matched sequence, suggesting a PNA-mediated retention.

Successively, the possibility to obtain internal functionalization was tested using a similar strategy, as described in Section 5.1.2. Several 5 *cm* long samples of the same fiber, internally modified with PNA, were treated separately, one series with the Cy3-modified full-match (DNA 1) and the other with the mismatched (DNA 3) oligonucleotides, as described in Fig. 5.3(a). The solutions were diluted to 100 nM concentration and their fluorescence emission intensities were checked to be exactly the same, before hybridization. The hybridization was performed by flowing each solution through the fiber by means of a high-performance liquid chromatography 100 μL syringe with a moderate pressure of 2 atm. Thirty-four microliters of each solution were passed through either of the two fibers, in large excess if compared to the ultrasmall internal volume (around 23 nL). The fibers were then dried with a flux of air and washed with excess PBS (15-20 μL), and then dried again. The two fibers were then analyzed using the ScanArray Express reader and the fluorescence was quantified using the instrument software. An example of the results is reported in Fig. 5.3(b). The same measurement was repeated in triplicate, with reproducible results. Unmodified fibers treated with the 100 nM solution of the DNA 1 using the same procedure showed very low fluorescence, while the intensity of the PNA-modified fibers treated with the same solution was significantly higher (fluorescence ratio PNA modified/unmodified fibers = 53 and standard deviation = 14), thus showing that the PNA induces efficient capturing of the target DNA within the fiber.

Furthermore, the full-match DNA 1 was captured by the PNA modified fibers more efficiently than the single-mismatched DNA 3 (fluorescence ratio DNA 1/DNA 3 = 3.0 and standard deviation = 0.9).

This again indicates a role of the PNA probe in binding to the target DNA and discriminating the DNA with only a single-base difference. In this case, the fluorescence signal was localized in the internal part of the fiber.

The successful modification of the fiber with PNA and the capability of these probes to make the SC-PCF sequence-selective sensors for DNA targets have thus been

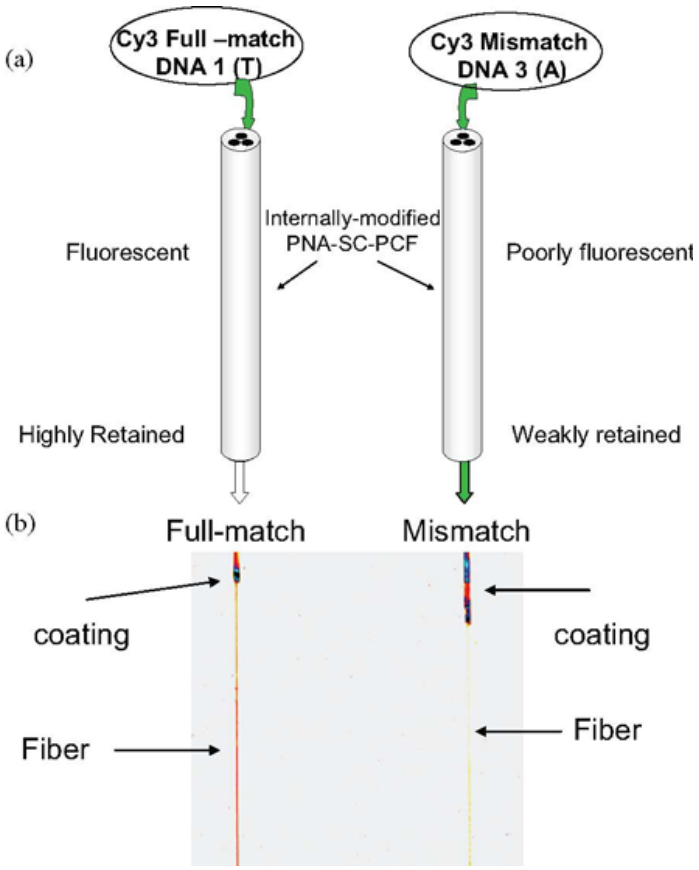

Figure 5.3: (a) Schematic representation of the hybridization experiment using PNA internally modified SC-PCF. (b) ScanArray images (Cy3 channel; $\lambda_{ex} = 543\ nm$ and $\lambda_{em} = 570\ nm$) of the fibers after hybridization; PNA SC-PCF hybridized with (left) full-match DNA 1 and (right) mismatched DNA 3. Negative image, intensity is color-encoded from (low) yellow to (high) blue; full scale: black.

demonstrated.
This approach can therefore lead to nanoliter readout systems with high biological specificity for the detection of ultrasmall samples. The confinement of the target solution within the fiber allows to have a microfluidic channel with large surface to solution ratio, thus with faster hybridization rates, and highly localized fluorescence signals.

5.1.4 Summary

The feasibility of a biosensor for DNA detection based on SC-PCFs has been demonstrated. After a proper functionalization of the silica hole surfaces, which allows the immobilization of PNA, the fluorescence signal has been detected, showing the selective binding with full-complementary DNA strand. Experimental results confirm the unique selectivity of the probe that is able to discriminate the DNA with only a single-base difference.
Tests were made with 100 *nM* DNA solution concentration, infiltrating the fibers with 34 μL of the solution, considering the fact that this is a large excess of the reagent used if compared to the internal volume of the fibers, around 23 *nL*. The fluorescence measurements have been obtained by means of a microarray fluorescence reader after the fiber samples have been hybridized overnight, while the functionalization had a duration of five days.
These achievements open up a new path toward the development of biosensors with high accuracy and selectivity, despite the ultrasmall sample volume required to fill the fiber holes. Further activities will consider the design of label-free probes, which could provide a faster analysis, keeping the proved advantages of the optical fiber technology.

5.2 Label-free DNA detection based on LPG

The fundamental characteristic of a LPG is that the resonant wavelength of the grating is sensitive to the external refractive index, thus the change of the refractive index

of the medium surrounding the fiber induces a subsequent change in the grating resonant wavelength. So it is straightforward to understand that modifying the external surface of the optical fiber with biological molecules it is possible to induce a change in the resonant wavelength of the grating. This change therefore allows to detect the interaction between the probe and the analyte.
The feasibility of a DNA biosensor has been demonstrated, using a LPG as the sensing platform. The grating has been inscribed in a single mode standard fiber, with a boron germania co-doped core, exposing the fiber to an Ultra Violet (UV) laser radiation. In particular, in this work the external surface of the fiber has been functionalized with PNA. The functionalization has been carried on following the same procedure used for the suspended core fiber. With the help of a teflon tubing system, a real-time measurment of the resonant LPG wavelength shift has been performed. The wavelength shift has been measured in real time while the DNA solution was flowning in a sealed cell containing the functionalized fiber.

5.2.1 LPG

The LPG used has been inscribed in a boron germania co-doped standard single mode fiber. The grating period is 407 μm, and it has a length of 20 *mm*. The fiber has been exposed to a UV laser radiation, at the wavelength of 248 *nm*, with pulses of duration of 10 *ns*. The experimental set-up used for the fiber exposure is composed by a cilindrical lens, with a 20 *cm* focal length, in order to focus the laser beam along the fiber axis, and a titanium amplitude mask. Between the mask and the cilindrical lens an iris has been inserted, with the aim to control the grating length. In Fig. 5.4 a transmission spectrum of the grating is reported. It is possible to observe that the grating is characterized by five attenuation bands.
The grating has been subsequently immersed in isopropanol ($n_{iso} = 1.375$). As expected, a shift of the resonant wavelengths has been observed. A graph comparing the transmission spectra of the grating surrounded by air and isopropanol is reported in Fig. 5.4. It is possible to observe that not all the wavelengths experience the same shift amount. In Table 5.2.1 the wavelengths shift of the five attenuation bands is reported. The highest shift, that is 5.6 *nm*, has been obtained for the first attenuation

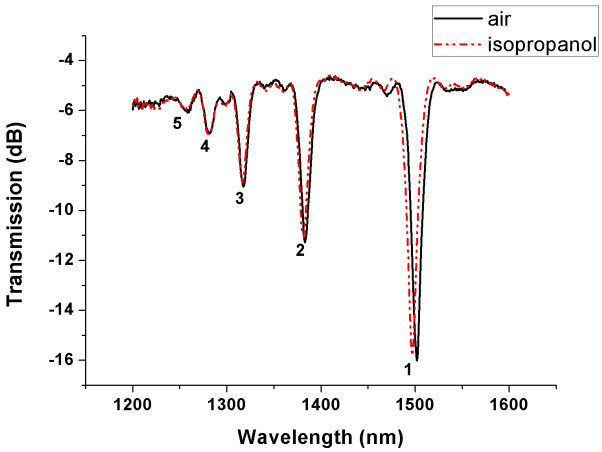

Figure 5.4: Transmission spectra of the grating surrounded by air, full line, and by isopropanol, dotted line. It is possible to recognize the presence of five attenuation bands.

band. Since this is the attenuation band with the highest sensitivity, its resonant wavelength has been chosen as the one to be monitored during the experiment.

5.2.2 Fiber functionalization

In order to bind PNA molecules to the fiber external surface, a functionalization of the surface is needed. The functionalization has been performed in the part of the fiber where the grating was inscribed. The procedure followed for the functionalization is the same used for modifying the holes of the suspended core fiber, but with a different set-up. All the steps of the procedure are described below:

1. Cleaning and activation of the external surface of the optical fiber by immersion of the gratings in a bath of the solution for 30 minutes, then rinsed with distilled water three times, and dried with nitrogen;

Attenuation band	λ_{res} air (nm)	λ_{res} isopropanol (nm)	$\Delta\lambda_{res}$ (nm)
1	1502.4	1496.8	5.6
2	1383.2	1381.6	1.6
3	1317.6	1316.8	0.8
4	1281.6	1281.6	0
5	1256	1255.6	0.4

Table 5.2: Resonant wavelengths of the attenuation bands, with air and isopropanol, and wavelengths shift.

2. Silanization: immersion of the gratings in a bath of the reagent and subsequently washed with ethanol twice and dried with nitrogen;

3. Reaction of the amino groups. The reaction is performed by passing the reagents through a Teflon tubing system, the same used in the LPG experiment see Fig. 5.5, where the part of the fiber with the gratings has been sealed. The reagents are loaded into a glass syringe and injected into the system at a fixed flow rate of 0.16 $\mu L/min$ by means of a syringe pump (KD Scientific 100 series). Following the reaction, the fiber is rinsed with *N,N*-dimethylformamide (DMF) for 2 h at a flow rate of 4 $\mu L/min$.

4. Activation of the carboxylic function, at a flow rate of 0.16 $\mu L/min$. The fiber is subsequently rinsed with DMF dry for 2 h at a flow rate of 4 $\mu L/min$;

5. PNA binding to the carboxylic functional groups by reaction of the activated ester to the PNA probe terminal amino group, at a flow rate of 0.16 $\mu L/min$;

6. Quenching of the excessive activated esters for 4 h at a flow rate of 1 $\mu L/min$.

Hybridization with solutions containing 1.2 nM, 12 nM, 120 nM, 1.2 μM and 12 μM DNA CA60Cy3 in PBS buffer (10 mM phosphate, 0.1 M NaCl, 0,1 mM EDTA in water, pH = 7), at room temperature with 1 $\mu L/min$ flow for 1-2 h in a Teflon tubing containing the part of the fiber with the LPG. Each hybridization was followed by

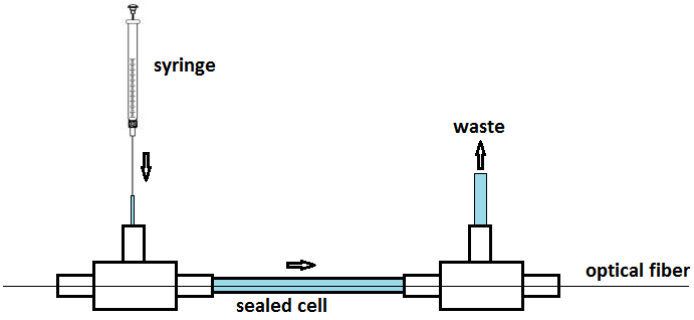

Figure 5.5: Scheme of the sealed cell set-up used.

washing with PBS (100 μL) and drying by flowing air into the tubing. Steps 1) and 2) were done by immersion of the part of the fiber, where the LPG is inscribed, in a bath of the reagent. The following steps, 3) - 6), were done using a sealed chamber composed of a 1.5 *mm* internal diameter Teflon tubing connected with a Hamilton 500 μm syringe operated by a KD Scientific 100 series infusion pump on one side and to a drain tubing on the other side. Fig. 5.5 shows a schematic draw of the set-up used. The DNA used was marked with Cy3 fluorophore in order to make fluorescence measurement at the end of the work, as a further proof of the fiber hybridization. The DNA and PNA sequences used in the experiment are reported in Table 5.3.

Table 5.3: PNA and DNA sequences used in the experiment. O in the PNA sequence is the 2-(2-aminoethoxy)ethoxyacetiyl group used as a spacer.

Oligo	**Sequence**
DNA cultivar Ogliarola (CA60)	3'- AATGAGTAAGTGG- 5'
PNA (A60)	H-O-O- TTACTCATTCACC - NH2

5.2.3 Results and discussion

The measurements were performed using a supercontinuum broadband laser source (NKT Photonics SuperK Compact), and an optical spectrum analyzer (ANDO AQ-6513A) as a receiver. The light has been coupled in air to the optical fiber through a x-y-z micropositioning system, and collected by a standard single mode patchcord, still through an air coupling. The air coupling of the light has been done in order to prevent reflections that may damage the supercontinuum source, since it is generated by a 1064 *nm* pulsed laser. The part of the optical fiber with the grating has been sealed in a closed cell, the one represented in Fig. 5.5(b), in which the reagents were flowing. While the DNA solutions were flowing in the sealed cell, the spectrum of the grating has been continually monitored, and data of the resonant wavelength have been kept. Measurements have been done for one hour.
DNA solutions of 1.2 nM, 12 nM, 120 nM, 1.2 μM and 12 μM concentrations, have been used for the experiment. For the first two concentrations only a slight shift of the resonant wavelength has been observed, while for the 120 nM concentration a shift of 1 *nm* of the resonant wavelength has been measured, as well as a clear spectrum modification of the grating. Fig. 5.6(a) reports the spectra of the grating at the beginning, and the end of the fiber hydridization. It is possible to observe that the binding between the PNA probes and the DNA strands induced a red shift of the resonant wavelength. The resonant wavelength shift during the measurement time is reported in Fig. 5.6(b). It is possible to see that the wavelength shift can be measured after 20 minutes. After about 35 minutes the wavelength tends to a constant value, this indicates that the hybridization process probably arrived to saturation. For the 1.2 μM and 12 μM DNA concentrations a significant wavelength shift has not been observed. This can be attributed to a saturation effect of the PNA active sites on the surface. At the end of the work, since the DNA was previously marked with a Cy3 fluorophore, fluorescence measurements were performed in order to assess the DNA capture process. The measurements were performed by means of a microarray fluorescence reader, the ScanArray Express by Perkin Elmer, which performs fluorescence scanning of the samples deposited on a glass slide, using two different laser sources for excitation of the fluorophores (543 *nm* for Cy3 channel and 633 *nm* for

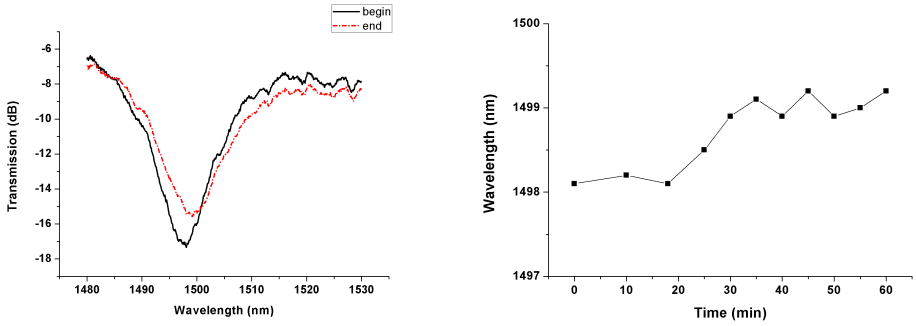

(a) (b)

Figure 5.6: (a) LPG spectra at the beginning, and at the end of the hybridization process. (b) Resonant wavelength shift monitored during the experiment.

Cy5 channel) and different filters for selecting the emitted fluorescence. The part of the fiber where the grating was inscribed has been placed on a glass slide, with a piece of the same fiber that has not been functionalized, as a negative proof. From Fig. 5.7 it is possible to observe how the fluorscence emitted by the fiber with the grating is higher than the one emitted by the negative fiber.

5.2.4 Summary

The feasibility of a DNA label-free biosensor based on a LPG has been demonstrated. After a proper fucionalization of the external fiber surface, which allows the immobilization of PNA.
A 120 *nM* DNA solution was detected, with a 1 *nm* shift of the resonant wavelength. Saturation was reached after about 35 *min*, time after that the wavelength reached a constant value. The wavelength shift has been monitored in real time during the whole hybridization phase, of the duration of 1 *h*. The functionalization of the fiber surface had a duration of five days.
As a further proof of the occurred hybridization, fluorescence measurements has been performed.

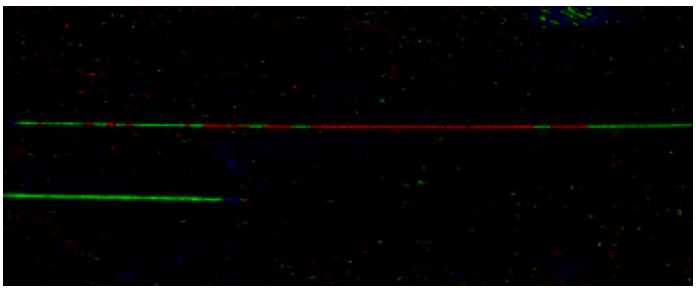

Figure 5.7: Image obtained from the microarray scanner. The fiber on the top is the one functionalized and hybridized, and it is possible to observe the high fluorescence signal, compared to the one of the negative fiber at the bottom.

5.3 Label-free DNA detection based on DTFBG

A new approach is presented to implement a DNA label-free sensor. Such technology is based on an optical fiber ring cavity sensor, utilizing a double TFBG (DTFBG) as a detector element. A specific functionalization of the external surface of the fiber has been performed, and a liquid handling system composed of Teflon tubing has been implemented for the packaging and functionalization of the fiber sensor. Significant spectral modulations in the visibility of the fringes have been measured after harmonic analysis and repeatability has been proved by making several tests. The experimental results are reported, demonstrating the feasibility of a DNA sensor based on a DTFBG for a variety of specific molarities exhibiting a wide dynamic range.

5.3.1 DTFBG

A DTFBG is composed by two identical blazed FBGs inscribed in the fiber core separated each other of a distance d. The two FBGs give origin to a Fabry-Perot cavity that creates two kind of interferences. One at the Bragg wavelength forming a Fabry-Perot resonance due to the radiation at the Bragg wavelength going back and forward between the two FBGs. The second kind of interference is due to the coupling between the core and the cladding, caused by the first blazed grating, at wavelengths

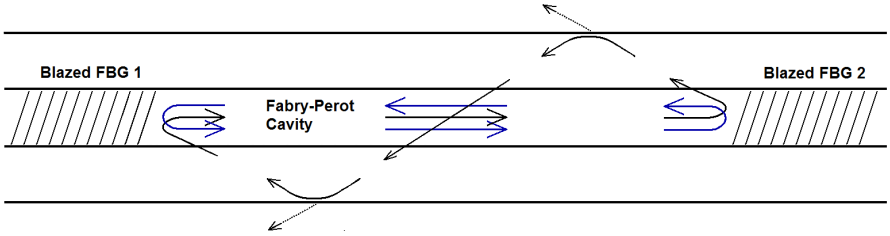

Figure 5.8: DTFBG structure. The blue line represents the Fabry-Perot resonance at the Bragg wavelength. The black line represents the ring cavity resonance.

lower than the Bragg one, and re-coupled again into the core giving rise to a cavity ring resonance. The cavity ring resonance is in contact with the cladding/external medium interface, see Fig. 5.8, and for this reason it is sensitive to external refractive index changes.

The interference in this structure can be modeled by the following equation:

$$T(\lambda) = E(\lambda)\,[1 + V cos(2\pi\sigma\lambda + \phi)] \tag{5.1}$$

where $T(\lambda)$ is the transmission spectrum of the sensor, $E(\lambda)$ is the envelope spectrum of the mode, V is the visibility of the fringes, σ is the frequency of the interference and ϕ is a phase offset.

Measurements of the external refractive index can be made exploiting the cavity ring resonance. The amount of interference is dependent on how much light is lost from the counter-propagating cladding mode at the cladding/external medium interface. In particular when the refractive index of the external medium, n_{ext}, is lower than the index of the cladding medium, n_{cl}, the structure is weakly guiding and then part of the light is re-coupled into the core. On the other hand if n_{ext} is equal or almost equal to n_{cl} this will cause the cladding modes to leach out, and V to approach zero. DTFBG devices have been used successfully as standard refractive index sensor [142] as well as a magnetic field sensor [143].

The visibility of the interference can be calculated in an approximate way by considering the Fourier transform of the transmission spectrum, $F(T)\{s\}$. The visibility

is the ratio between the average alternating component, caused by the ring cavity interference, and the average slowly-varying component, that describes essentially the DC component of the spectrum. The visibility can be expressed by the following equation:

$$V = \frac{\sigma_1 \Sigma_{s=\sigma-\sigma_2}^{\sigma+\sigma_2} |F(T)\{s\}|}{2\sigma_2 \Sigma_{s=0}^{\sigma_1} |F(T)\{s\}|} \tag{5.2}$$

where σ_1 and σ_2 are half widths of the triangles in the Fourier domain, given by the Fourier transform of the interference, to allow full windowing of the respective DC and first interference peaks without overlapping each other, a more clear explanation of the visibility will be given in section 5.3.3. The Fourier transform of the transmission spectrum and the calculation of the visibility have been performed by a specifically designed software [144].

One of the advantages of using this device for sensing is the relative insensitivity to strain and temperature effect, except the thermo-optic changes to the surrounding liquid. In fact, temperature and strain only cause a shift in the wavelength spectrum thus only altering the phase, not the magnitude, of the Fourier spectrum. Moreover since the Bragg wavelength is insensitive to changes of the external refractive index, can be used to compensate temperature changes. The sensitivity to strain can be overcome by fixing the fiber with magnets. This is extremely advantageous compared to other fiber optics techniques used for bio-sensing, such as LPGs that are highly sensitive to temperature changes [145].

5.3.2 Fiber surface functionalization and hybridization

The fiber has been functionalized following the same procedure for the LPG functionalization, described in section 5.2.2.

After the functionalization of the fiber, hybridization was performed with different concentrations of DNA solutions: 10 nM, 100 nM, and 1 μM diluted in a buffer solution. The system used to perform the hybridization is the same used for the surface modification.

During the hybridization the DNA solutions used flowed through the handling reagents

system at a flow rate of 1 $\mu L/min$ for about 1 h. The DNA used in the experiment were commercially available oligonucletides, provided by Thermo Fisher Scientific. The sequences of the strands were composed by 35 bases, while the PNA strands were composed by 13 bases. The DNA was coded for a sequence containing a Single Polymorphism Nucleotide (SNP), relevant for the recognition of different tomato varieties. Measurements with mis-matched DNA have been also taken in order to prove that the sensor is selective in the presence of a SNP. This could be very interesting in order to discriminate among different vegetables varieties. The PNA probes have been designed containing the part of the sequence with the SNP, thus enabling to prove the selectivity of the sensor with just a single base mis-match. The sequences of the DNA and PNA used in this work are reported in Table 5.4.

Table 5.4: PNA and DNA sequences used in the experiment.

Oligo	**Sequence**	**Role**
PNA	5'-CTTATC***C***GGTGCC-3'	Probe
DNA	5'-CTGAAAAAGAAGCTAAAGCAGA GGCACC***G***GATAAG-3'	Full-match
DNA	5'-CTGAAAAAGAAGCTAAAGCAGA GGCACC***A***GATAAG-3'	Mis-match

5.3.3 Results and discussion

Experimental set-up

The DTFBG used in the experiment was composed by two identical blazed FBGs of the length of 4 *mm* and separated of 30 *mm*, and with a tilt angle of 3.2°. They were inscribed in a photosensitive fiber (GF1B, Thorlabs) using 193 *nm* ultraviolet laser radiation and a phase mask.
The Measurements were taken in a clean room environment with a temperature controlled system. An Amplified Stimulated Emission (ASE) source (ASE 1600, NTT

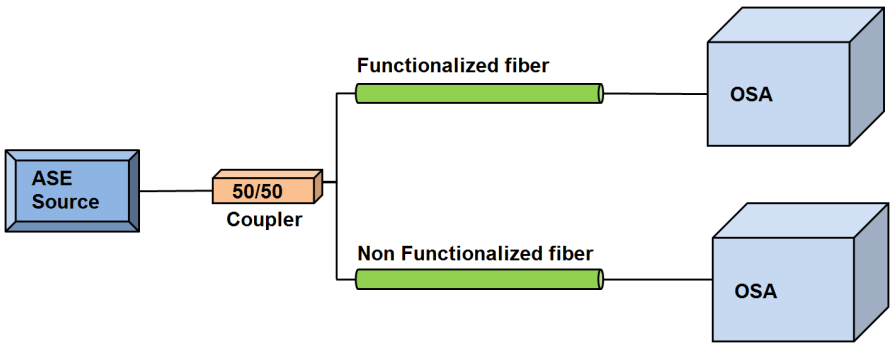

Figure 5.9: Schematic representation of the measurement set-up used in the experiment.

Electronics) has been used as broadband light source, and an Optical Spectrum Analyzer (OSA - Ando AQ6315A) has been used as the receiver. The transmission spectrum of the fiber has been continuously monitored and recorded every 5 minutes for the entire duration of the hybridization phase, about 1 h. The hybridization procedure was performed on the functionalized fiber and on a non functionalized fiber taken as a reference. The light was delivered to a 50/50 coupler, and the two outputs were connected to one of the two fiber respectively. The transmission spectra were taken for both fibers as described above. Both of them had a single mode patchcord as the output, and in order to collect the data the two patchcords were alternatively connected to the OSA. The set-up here described is schematically represented in Fig. 5.9.

The data were subsequently post processed, the visibility has been evaluated only in the ghost mode region (1553.9-1554.6 nm). In Fig. 5.10(a) the transmission spectrum of the functionalized fiber is reported, where the interference fringes are clearly visible. In Fig. 5.10(b) is represented the Fourier transform for two spectra recorded before and after the hybridization process. In this graph the definition of visibility given in eqn. 5.2 appears more clear, and from the graph it is also visible that there is no change in the continuous component of the spectrum, slow-varying component, while there is in the interference component.

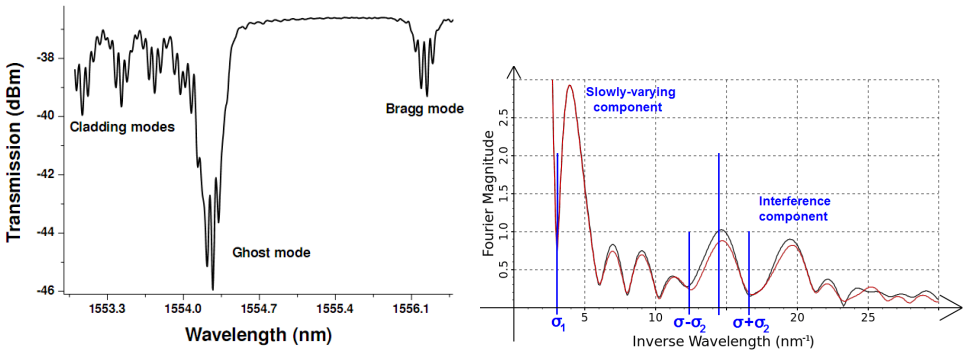

(a) (b)

Figure 5.10: (a) Transmission spectrum of the DTFBG after the functionalization. The interference fringes appear in the Bragg, ghost and cladding modes. In the graph the visibility of one particular interference fringe is reported. (b) Details of the transmission spectra in the inverse wavelength domain for the initial (black line) and final (red line) spectra of the experiment done with a 10 *nM* DNA solution.

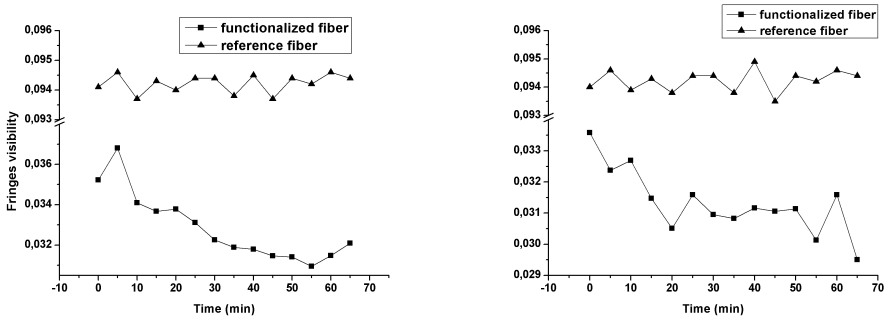

(a) (b)

Figure 5.11: (a) Visibility change obtained after a 10 nM DNA solution hybridization. (b) Visibility change obtained after a 100 nM DNA solution hybridization, and a 20 min washing with PBS.

Experimental results

At first a hybridization with a 10 *nM* concentration DNA in Phosphate Buffer Saline (PBS) solution has been carried on. Measurements show a clear modulation of the visibility for the functionalized fiber, there is net decrease in the visibility value in the first 50 *min*, while the non functionalized fiber shows no significant variation of the fringes visibility. The behavior of the visibility for both fibers is represented in the graphs in Fig. 5.11(a). The fact that there is basically no change in the visibility for the non functionalized fiber means that the change observed for the functionalized one must be attributed to the refractive index change due to the DNA-PNA binding, and not to phenomena like aspecific absorption of DNA molecules to the fiber surface.

After this first measurement other hybridizations with higher concentrations were carried on. After a washing with PBS solution, for about 20 *min*, the fibers have been re-hybridized with a 100 *nM* DNA solution. The measurements show, see Fig. 5.11(b), that the re-hybridization is possible. The graph shows a clear modulation of the visibility for the functionalized fiber, whilst there is no a significant change for the

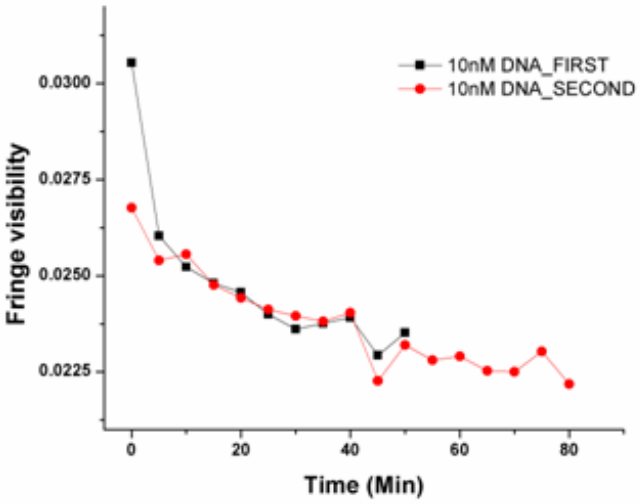

Figure 5.12: Fiber has been rehybridized twice after being washed for more than 24 *h* with the PBS solution. The trend of the fringe visibility modulation is similar for both experiments.

non functionalized fiber. The visibility modulation reaches almost the same value of the previous hybridization, suggesting that the fiber have already saturated. A second re-hybridization has been carried on with a 1 μM DNA solution, after a PBS washing of about 20 *min*, showing similar results, data not shown here.
In light of these results, the 10 *nM* solution has been used to verify the reproducibility of a single measurement. The recovery of the fringe visibility was improved by washing the fiber with PBS for a longer time, more than 24 *h*. The rehybridization process was implemented using the same conditions described earlier. Though the initial value of visibility was lower, a similar shift as that of Fig. 5.11(a) was observed, as shown in Fig. 5.12. A third washing with PBS followed by hybridization showed responsiveness of the fiber, with a smaller modulation, but showing the same trend. The different initial value of visibility can be caused by a memory effect of the

device, given by several factors. First, a different number of active sites occupied by DNA molecules after the washing process, washing reverses the hybridization process but not completely. Second, the high local sensitivity of such a device, which presents an optical response that is strongly dependent on the location of binding sites on the fiber surface. These parameters can be improved through optimization of the washing step in order to reduce time and to obtain the same initial conditions.
However, the experimental data suggest that the specific effect of the DNA on the fiber can still be visible for several hybridization steps. Analyzing the distribution of different experiments made on the same fibers using the 10 *nM* DNA solution, we can observe a clear difference in terms of visibility change between the tests made with the functionalized fiber and reference fiber. Considering the starting and ending points of each test, the functionalized fiber presents an average change of visibility μ = 0.006 with standard deviation σ = 0.001, which is more than one order of magnitude bigger with respect to the nonfunctionalized fiber, having μ = 0.0004 and σ = 0.0002, as shown in Fig. 5.13(a).

An additional control experiment was done using mismatched DNA strands, containing the SNP, to prove that this device is able to recognize a DNA sequence with just one SNP. Using the same procedure described earlier, a 10 *nM* mismatch DNA solution was infiltrated into the liquid handling system and spectral measurements were analyzed using the same parameters of the previous experiments. Two different tests done on the same fiber showed that the change in visibility for this additional test was of the same extent of the reference fiber, as shown in Fig. 5.13(b), proving the high sensor selectivity.

5.3.4 Summary

This study shows for the first time the application of DTFBG fibers for the direct label-free DNA detection. The system was shown to give a specific response only when the fiber was functionalized, with good sensitivity for a solution with a very low concentration of 10 *nM*, and lack of interference. Saturation was reached after about 50 *min*. The hybridization phase during which the data have been recorded

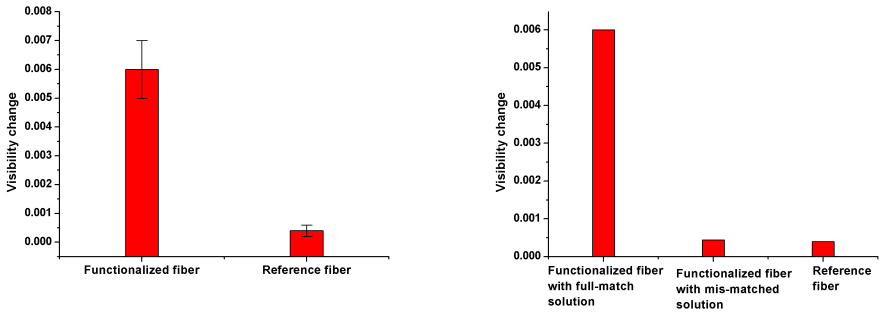

(a) (b)

Figure 5.13: (a) After four tests with a 10 nM DNA solution it is still possible to have a visibility change for the functionalized fiber higher than the reference one. (b) The visibility change observed for the functionalized fiber after the hybridization with a mis-matched DNA solution is comparable to the one of the reference fiber.

had a duration of 1 h, and the results have been obtained after the processing of the collected data. The functionalization, as for the two previous sensors presented, had a duration of five days.

Moreover, tests made using mismatched DNA strands showed that the sensor can discriminate an SNP of the DNA strand. This approach can be extended to other recognition elements and to other target analytes, such as proteins or contaminants, and can eventually be used in extremely narrow contexts, where large and less flexible platforms cannot easily operate.

Chapter 6

Refractive index sensor

Refractive index is a fundamental physical property of materials. Its correct measurement is crucial for some applications such as chemical, food beverage industries.
Different kinds of detection for refractive index measurement can be implemented exploiting fiber optics technology. Optical fiber devices as FBGs [146] and LPGs [147] can be employed as refractive index sensor, being the change in refractive index is detected by recording the shift in the resonant wavelength of the grating. The main drawback of these devices is that the wavelength shift is sensitive also to strain and temperature. It is possible to make insensitive the sensor to strain effects by a proper package. The insensitivity to temperature effects can be achived in a laboratory enviroment by using the sensor in a controlled temperature room, or by locally controlling the temperature in the grating area, e.g. by means of a peltier cell, but in some industrial production environments this can be quite challenging, and thus it would be impossible to use gratings for refractive index measurements.
Modal interferometric techniques can be exploited in order to make refractive index measurements [148]. Splicing a multimode fiber (MMF) to a SMF can lead to the formation of intermodal interference. This can be seen in transmission if a SMF is spliced both sides with MMFs, or in reflection if it is spliced from one side to a MMF, and on the other side a reflective coating is applied. This results in the generation of cladding modes that interfere with the SMF core mode forming spectral dips, which

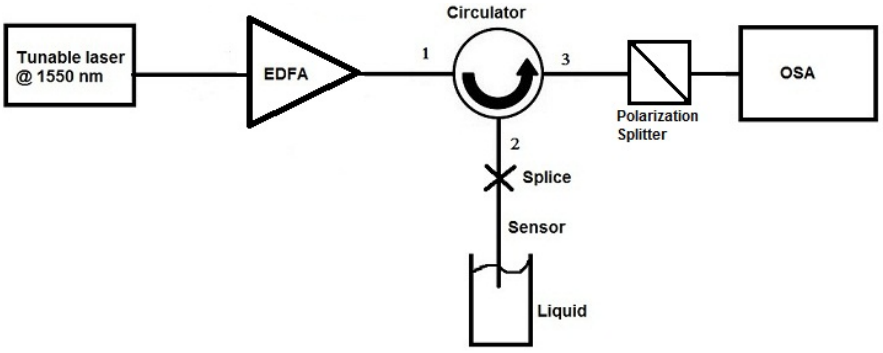

Figure 6.1: The set-up used for the refractive index measurements.

are sensitive to the change of the external refractive index.
Some in reflection PCF based refractive index sensors have been developed by using a large mode area PCF as the sensors head [149] or a Fabry-Perot sensing head fabricated through the splicing of a section of PCF between two SMFs [150].
Here a polarimetric refractive index sensor based on an in-reflection Highly Birefringent PCF (HB-PCF) sensing head is presented. Its operation principle exploits the back reflected light from the tip of a cleaved HB-PCF. An optical fiber with its end properly cleaved presents a 4 % back reflection of light (Fresnel reflection) . The amount of back reflected light will change with the refractive index of the material in contact with the sensor tip, making it possible to associate which refractive index corresponds to which material.

6.1 Experimental

The experimental set-up is represented in Fig. 6.1. It is composed by a tunable laser, emitting at the wavelength of 1550 *nm*, which is amplified by an Erbium Doped Fiber Amplifier (EDFA), in order to provide enough peak power. The input light is transmitted to the sensor tip through a circulator. The back reflected signal passes through

a polarization splitter and the peak power of each polarization state is acquired by an Optical Spectrum Analyzer (OSA) with a maximum resolution of 0.01 *nm*. Measurements were taken using first a SMF and then a HB-PCF as the sensing heads, for comparison. In the experiment six different volatile liquids, with different refractive index, were used, and are presented in Table 6.1.

Measurements were also made using an optical backscatter reflectometer (OBR)

Table 6.1: Liquids used in the experiments

Liquids	**Refractive index**
Methanol	1.329
Ethanol	1.362
2-Propanol	1.377
1-Butanol	1.397
1-Pentanol	1.409
1-Octanol	1.429

4600 developed by Luna Technologies, which provides a broadband illumination source and reads the back reflected signal (amplitude, phase, individual polarizations, etc). The set-up used for this series of measurements it is representend in Fig. 6.2.

During every measurement the fiber tip is immersed in the correspondent liquid and the peak power of each polarization is recorded. With the tip out of the liquid, the peak power recovers, moment after which the next measurement is taken.

6.2 Results and discussion

During the measurements it has been observed that the peak power decreases with the increase of the refractive index. At first the total reflected power has been measured, without using the polarization splitter in the set-up of Fig. 6.1. In the graph of Fig. 6.3(a) is represented the peak power behavior of HB-PCF and SMF. It is possbile to observe that the HB-PCF does not show a significant higher dynamic range than the

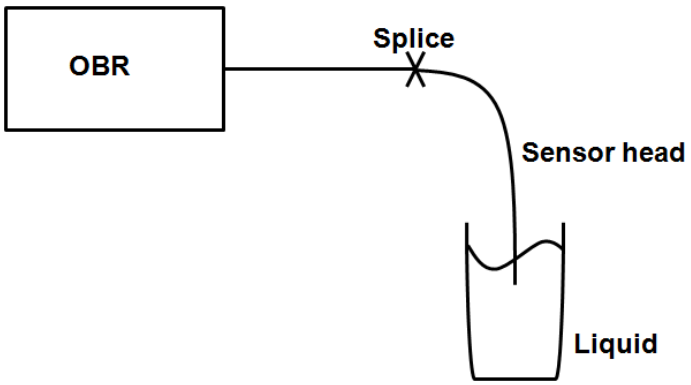

Figure 6.2: The set-up used for the measurements with the OBR.

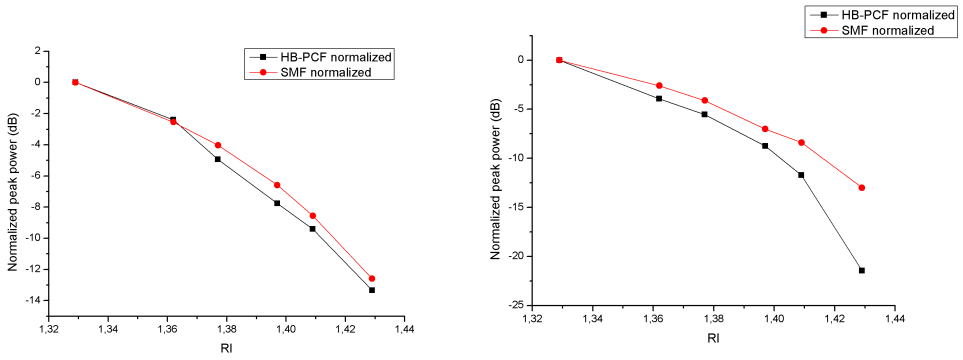

(a) (b)

Figure 6.3: (a) Peak power behavior of the SMF and the HB-PCF. (b) Peak power behavior of one of the two polarizations. The dynamic range of the HB-PCF is higher than the SMF one.

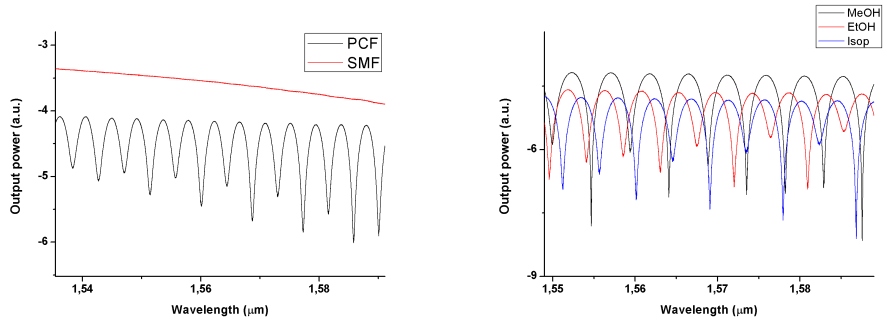

(a) (b)

Figure 6.4: (a) Comparison between the SMF and HB-PCF spectral response. The HB-PCF shows a well periodically defined spectrum. (b) Shift of the HB-PCF spectrum with the change of the refractive index.

SMF, this would not justify the use of the PCF instead of a SMF, due to its higher cost compared to a standard fiber. By separately considering the two states of polarization a similar behavior of the peak power is observed, but in this case the dynamic range of the HB-PCF is significantly better than the SMF one, as can be observed in the graph in Fig. 6.3, where the behavior of the reflected peak power referred to one state of polarization is represented.

The fact of having a polarization mantaining fiber can bring an advantage compared to a SMF. This was also demonstrated by measurements taken with the OBR. The HB-PCF has a well defined wavelength response of the two polarizations, considered separately. In Fig. 6.4(a) is represented the spectral response of one of the two polarizations, for both fibers. The SMF shows a basically flat behavior, while the HB-PCF shows a well defined periodic spectrum.

Further measurements showed also that the spectrum of the HB-PCF experienced a wavelength shift with the change of the refractive index. In Fig. 6.4(b) is represented the spectrum of one of the two polarizations shifting after measurements taken with methanol, ethanol, and 2-propanol. This behavior of the HB-PCF is an enourmous

advantage compared to the SMF. It can lead to the possibility of realizing a sensor with very high sensitivity and simple realization.

6.3 Summary

The feasibility of an in-reflection HB-PCF refractive index sensor was presented. The HB-PCF refractive index sensor proved to work using its variation in power with refractive index, as well as its wavelength variation with refractive index, leading to the possibility of finding different interrogation systems to improve its sensitivity. The device implemented has moreover the advantage of being simple, and future implementation with relatively low cost instrumentation is possible.

Conclusions

The use of optical devices for sensing can have the advantage of having a high sensitivity, and the possibility of reducing the costs and miniaturizing the device. Since they are frabicated with dielectric materials they are immune to electromagnetic interferences. They can also perform a fast and real-time detection. Among optical based sensors there are devices fabricated with optical fibers, these devices can add the advantage of performing a remote and *in situ* detection, due to the low signal attenuation of optical fibers. A remote detection can also give the possibility of measuring in harsh environments. Moreover a distributed detection is also possible by having more sensors in the same optical cable.

Optical fiber based sensors have been already employed in a standard way for monitoring physical quantities as temperature, pressure, and strain. Recently optical fiber sensors, and optical sensors in general, have been employed in a always growing number of applications in the bio-chemical field, with the realization of biosensors. From recent market analysis [2], [6] it is possible to recognize four main industry segments where the application of the biosensors technology is growing: medical diagnostics, enviormental monitoring, food, and military. In the medical diagnostics the employment of biosensors can be exploited to detect viruses or pathogen agents in general, in the medical industry the infection control is an area where biosensors are needed. In the food industry is fundamental to detect pathogen agents either in fresh and processed products, but in this sector they can also be employed for food traceability, and against food frauds. In the environmental monitoring biosensors can be employed for the detection of pathogen agents dangerous for large part of the pop-

ulation, for instance the monitoring of water supplies can be very critical because of the exposition to bacteria can affect large inhabited area with contaminated water. In military and homeland security specific tools are needed for the detection of pathogen agents in contaminated environments, that comes from the possibility of having a terroristic attack of bacterilogical nature. There is then a need of developing devices capable of providing a fast, reliable, and sensitive detection.

For this reason the research activity was focused on the realization of optical fiber based sensing platforms for bio-chemical sensing.

Part of the activity has been focused on the fabrication of FBGs in standard optical fibers and PCFs. Optical fiber gratings are devices that can be exploited for sensing operations. In the first instance FBGs in phosphate glass fibers have been inscribed. The exposure to high energy densities, lower than the damage threshold of the fiber, gave rise to a non monotonous refractive index change of the core, a characteristic typical of type IIA gratings, a kind of Bragg gratings inscribed exposing the fiber to very high energy densities. This was observed for the first time in such kind of fiber. The fabrication of a type IIA grating can lead to gratings that can withstand higher temperatures than the type I ones. Usually type IIA gratings can survive up to 800 $^{\circ}C$ [89], [90] while type I after 400 $^{\circ}C$ are already erased.

SR-FBGs have been inscribed in PCFs, in fibers with different designs. The exploitation of the LESAL technique, a technique that performs laser induced back side etching, made possible the etching of periodic structures inside the holes of PCFs, in particular from SEM scans high quality etching has been performed using toluene vapours as absorber. In samples of LMA10 and ESM12 fibers a reflection spectrum of the grating was also recorded, demonstrating the success of the method used. SR-FBGs compared to standard FBGs can survive to very high temperatures, teoretically till the melting temperature of silica, in literature mesurements has been made up to 1100 $^{\circ}C$ [129]. The methods proposed for the fabrication of SR-FBGs has the advantage of fabricating these kind of gratings in a simple way compared to the method so far used with D-shaped optical fibers [128], [129].

Different sensing platforms based on optical fibers have been used to realize sensors capable of detecting DNA molecules. All the sensors used PNA molecules as probes

for the target DNA, a functionalization of the silica surface was needed in order to strongly bind the probes to the fiber. At first the functionalization of inner surface of the holes of a SC-PCF was carried on. With this part of the work the feasibility of a DNA sensor through PNA surface functionalization was demontrated by fluorescence measurements. Tests were made with 100 *nM* DNA solution concentration, infiltrating the fibers with 34 μL of the solution, considering the fact that this is a large excess of the reagent used if compared to the internal volume of the fibers, around 23 *nL*. Moreover the selectivity of the probes was demonstrated by hybridizing the fiber with a single base mis matched DNA. These achievements open up a new path toward the development of biosensors with high accuracy and selectivity, despite the ultrasmall sample volume required to fill the fiber holes. The detection of proteins by fluorscence was already carried on in suspended core fibers made with soft glass [13], while here the DNA detection has been performed with a silicate fiber.

Optical fiber technology can be used for performing label-free DNA detection. The inscription of LPGs in standard fibers is suitable to this purpose. An LPG can couple the light from the core of the fiber to the cladding, forming in the transmission spectrum attenuation bands that are sensitive to the external refractive index. Since the fiber hybridization can be seen as a change in the external refractive index, a LPG can be exploited for DNA detection. Hybridizations with complementary DNA were carried on, and the DNA detection has been performed by continously observing the shift of the grating resonant wavelength. A 120 *nM* DNA solution was detected, with a 1 *nm* shift of the resonant wavelength. Saturation was reached after about 35 *min*, time after that the wavelength reached a constant value. The results obtained are consistent with other research groups that used LPGs inscribed in standard fibers to detect DNA [101], or proteins [102].

The coupling of the light from the core to the cladding can be achived also with tilted FBGs, and a ring cavity resonance can be generated with a DTFBG structure inscribed in the core of a standard fiber. As for the LPGs the transmission spectrum is affected by external refractive index change. In this case it was possible to detect the DNA by observing the change of the visibility fringes of the transmission spectrum by a Fourier analysis of the data. It was possible to detect a 10 *nM* DNA solution,

and saturation was reached after about 50 *min*. Moreover the reproducibility of the measurements, reuse of the probes, and selectivity of the sensor were demontrated. The use of such a device can also overcome some problems affecting the gratings like the wavelength shift due to temperature. In this work the measurements were made in a temperature controlled environment but it is woth to say that the temperature produces only a shift in the grating spectrum and it does not affect the fringe visibility. Single tilted FBGs have been used for the detection of proteins [36], and this is the first time that a DTFBG has been used to detect DNA molecules.

In the last period the reasearch activity focused on the realization of a refractive index sensor based on a HB-PCF. The refractive index detection was performed by monitoring the reflected power from the properly cleaved sensor head. The HB-PCF showed a better dynamic range compared to the SMF, another interesting feature of this fiber is the spectrum of each state of polarization which showed a well defined periodic behavior. The spectrum shifts with the change of the refractive index. This suggests that it is possible to realize a very sensitive sensor for chemical compounds, and the application can be extended also to biological molecules.

The future work will mainly focus on the realization of label-free biosensors. In the first instance the improving of the DTFBG sensor will be investigated. The detection of the 10 nM DNA solution showed a good dynamic range for the visibility change, this suggests that the sensor itself as it is can be sensitive to lower concentrations. Improvement can be made by using DTFBG with different distances between the two FBGs, to see which is the one which has the best performance in terms of sensitivity. One drawback of the DTFBG sensor, and the LPG one as well, is the reagents consumption. For every hybridization about 200 - 300 μL of DNA solution were used. One improvement can be reducing the flow rate during the hybridization, but this will not reduce the consumption under the dead volume of the reagents handling system of about 30 μL. Further improvements can be done by optimizing the system in order to minmize the reagents consumption, but it will be challenging to reach the consumption volumes reached for the suspended core fiber. An other way to pursue in the realization of a label-free biosensor is the possibility of having an FBG inscribed in a PCF. For having a sensitivity as highest as possible the evanescent field of the

propagating mode should be as highest as possible, then the suspended core fiber design is ideal for such a purpose. In this case it would be then possible to perform a label-free detection by infiltrating the PCF capillaries with the DNA solutions, and having very low reagents consumption. The future work will also move on this way, because realizing a biosensor with such a platform will give the possibility of having the waveguide and the microfluidics in the same device, when other platforms such as SPR based sensors or ring resonators [10], need the fabrication of microfluidics channels in order to perform the detection.

List of publications

A list of the publications on international journals, international and national conference proceedings, related to the work presented in this thesis is reported below.

Pubblications on international journals

E. Coscelli, M. Sozzi, F. Poli, D. Passaro, A. Cucinotta, S. Selleri, R. Corradini, R. Marchelli, *Toward A Highly Specific DNA Biosensor: PNA-Modified Suspended-Core Photonic Crystal Fibers*, IEEE Journal of Selected Topics in Quantum Electronics, vol. 16, pp. 967-972 , August 2010.

M. Sozzi, A. Rahman, and S. Pissadakis, *Non-monotonous refractive index changes recorded in a phosphate glass optical fibre using 248 nm, 500 fs laser radiation*, Optical Material Express, vol. 1, pp. 121-127, April 2011.

A. Candiani, M. Sozzi, A. Cucinotta, S. Selleri, R. Veneziano, R. Corradini, R. Marchelli, P. Childs, S. Pissadakis, *Optical fiber ring cavity sensor for label-free DNA detection*, IEEE Journal of Selected Topics in Quantum Electronics, doi: 10.1109/JSTQE.2011.2166110, August 2011.

International conferences proceedings

E. Coscelli, M. Sozzi, F. Poli, D. Passaro, A. Cucinotta, S. Selleri, R. Corradini, R. Marchelli, *Towards biosensing with suspended core photonic crystal fiber*, 3rd EOS Topical Meeting on Optical Microsystems (OμS'09), September 27-30, 2009, Capri,

Italy.

M. Sozzi, A. Cucinotta, R. Corradini, R. Marchelli, M. Konstantaki, S. Pissadakis, S. Selleri, *Modification of a long-period grating based fiber optic for DNA biosensing*, SPIE Photonics West 2011, January 22-27, 2011, San Francisco (CA), USA.

M. Sozzi, A. Cucinotta, R. Corradini, R. Marchelli, M. Konstantaki, S. Pissadakis, S. Selleri, *Label-free DNA detection with PNA modified long period fiber grating-based sensor*, The European Conference on Lasers and Electro-Optics - CLEO/Europe, May 22-26, 2011, Munich, Germany.

M. Sozzi, A. Rahman, S. Pissadakis, *Demonstration of negative refractive index photosensitivity mechanism in a phosphate glass optical fibre using 248 nm, 500 fs laser radiation*, The European Conference on Lasers and Electro-Optics - CLEO/Europe, May 22-26, 2011, Munich, Germany.

M. Sozzi, E. Coscelli, F. Poli, A. Cucinotta, R. Corradini, R. Marchelli, M. Konstantaki, S. Pissadakis, S. Selleri, *Long period grating-based fiber optic sensor for label-free DNA detection*, International Workshop on Biophotonics, June 8-10, 2011, Parma, Italy.

A. Candiani, P. Childs, S. Pissadakis, M. Sozzi, E. Coscelli, F. Poli, A. Cucinotta, S. Selleri, R. Veneziano, R. Corradini, R. Marchelli, *Double tilted fiber Bragg gratings for label-free DNA detection*, International Workshop on Biophotonics, June 8-10, 2011, Parma, Italy.

M. Sozzi, A. Candiani, A. Cucinotta, R. Veneziano, R. Corradini, R. Marchelli, P. Childs, S. Pissadakis, S. Selleri, *Label-free DNA sensor based on a Double Tilted Fiber Bragg Grating*, 4th International Workshop on Multianalyte Biosensing Devices, September 7-8, 2011, Athens, Greece.

A. Candiani, M. Sozzi, A. Cucinotta, S. Selleri, R. Veneziano, R. Corradini, R. Marchelli, P. Childs, S. Pissadakis, *Label-free DNA biosensor based on double tilted fiber Bragg grating*, SPIE Photonics West 2012, January 21-26, 2012, San Francisco (CA), USA.

National conferences proceedings

E. Coscelli , M. Sozzi, D. Passaro, F. Poli, A. Cucinotta, S. Selleri, C. Lantano, R. Corradini, R. Marchelli, *Sviluppo di un biosensore in fibra a cristallo fotonico per il riconoscimento di sequenze di DNA*, XVIII Riunione Nazionale di Elettromagnetismo, September 6-10, 2010, Benevento, Italy.

M. Sozzi, A. Cucinotta, S. Selleri, R. Corradini, R. Marchelli, M. Konstanki, S. Pissadakis, *Sensore in fibra ottica per DNA con reticoli a passo lungo*, FOTONICA 2011, May 9-11, 2011, Genoa, Italy.

A. Candiani, M. Sozzi, A. Cucinotta, S. Selleri, R. Veneziano, R. Corradini, R. Marchelli, P. Childs, S. Pissadakis, *Optical fiber sensor for DNA detection based on double-tilted Bragg grating*, Convegno Nazionale Sensori, February, 15-17, 2012, Rome, Italy.

M. Sozzi, S. Selleri, A. M. R. Pinto, M. Bravo, M. Lopez-Amo, *Polarimetric Hi-Bi PCF refractive index sensor for volatile liquids*, Convegno Nazionale Sensori, February 15-17, 2012, Rome, Italy.

Bibliography

[1] Daniel R. Thevenot, Klara Toth, Richard A. Durst, and George S. Wilson. Electrochemical biosensors: recommended definitions and classification. *Pure Appl. Chem.*, 71:2333–2348, 1999.

[2] Bansi D. Malhotra, Rahul Singhal, Asha Chaubey, Sandeep K. Sharma, and Ashok Kumar. Recent trends in biosensor. *Current Applied Physics*, 5:92–97, 2005.

[3] Leland C. Clark and Champ Lyons. Electrode systems for continous monitoring in cardiovascular surgery. *Ann NY Acad Sci*, 102:29–45, 1962.

[4] G. G. Guilbault, D. N. Kramer, and P. L. Cannon Jr. Electrochemical determination of organophosphorus compuonds. *Anal. Chem.*, 34:1437–1439, 1962.

[5] Georges G. Guilbault and Joseph G. Montalvo. A urea-specific enzyme electrode. *J. American Chem. Soc.*, 91:2164–2165, 1969.

[6] Evangelyn C. Alocilja and Stephen M. Radke. Market analysis of biosensor for food safety. *Biosensors and Bioelectronics*, 18:841–846, 2003.

[7] Leon A. Terry, Stephen F. White, and Linda J. Tigwell. The application of biosensors to fresh produce and the wider food industry. *J. Agric. Food Chem.*, 53:1309–1316, 2005.

[8] Miroslav Pohanka and Petr Skadal. Electrochemical biosensors - principles and applications. *J. Appl. Biomed.*, 6:57–64, 2008.

[9] Ye Fang. Label-free cell-based assays with optical biosensors in drug discovery. *Assays and Drug Development Technologies*, 4:583–595, 2006.

[10] Xudong Fan, Ian M. White, Siyka I. Shopova, Hongying Zhu, Jonathan D. Suter, and Yuze Sun. Sensitive optical biosensors for unlabeled targets: A review. *Analytica Chimica Acta*, 620:8–26, 2008.

[11] Andrea Germini, Stefano Rossi, Alessandro Zanetti, Roberto Corradini, Corrado Fogher, and Rosangela Marchelli. Development of a peptide nucleic acid array platform for the detection of genetically modified organisms in food. *J. Agric. Food Chem.*, 53:3958–3962, 2005.

[12] Stefano Rossi, Elena Scaravelli, Andrea Germini, Roberto Corradini, Corrado Fogher, and Rosangela Marchelli. A PNA-array platform for the detection of hidden allergenes in foodstuff. *Eur. Food Res. Technol.*, 223:1–6, 2006.

[13] Yinlan Ruan, Erik P. Schartner, Heike Ebendorff-Heidepriem, Peter Hoffmann, and Tanya M. Monro. Detection of quantum-dot labeled proteins using soft glass microstructured optical fibers. *Optics Express*, 15:17819–17826, 2007.

[14] W. E. Moerner. New directions in single-molecule imaging and analysis. *Proc. Natl. Acad. Sci.*, 104:12596–12602, 2007.

[15] Matthew A. Cooper. Optical biosensors: where next and how soon? *Drug Discovery Today*, 11:1061–1067, 2006.

[16] Bo Liedberg, Claes Nylander, and Ingemar Lunstrom. Surface plasmon resonance for gas detection and biosensing. *Sensors and Actuators*, 4:299–304, 1983.

[17] M. Manuel, B. Vidal, Raul Lopez, Salvador Alegret, Julian Alonso-Chamarro, Ignacio Garces, and Javier Mateo. Determination of probable alcohol yield in musts by means of an SPR optical sensor. *Sensors and Actuators B: Chemical*, 11:455–459, 1993.

[18] J. Dostalek, J. Ctyroky, J. Homola, E. Brynda, M. Skalsky, P. Nekvindova, J. Spirkova, J. Skvor, and J. Schrofel. Surface plasmon resonance biosensor based on integrated optical waveguide. *Sensors and Actuators B: Chemical*, 76:8–12, 2001.

[19] C. Mouvet, R. D. Harris, C. Maciag, B. J. Luff, J. S. Wilkinson, J. Piehler, A. Brecht, G. Gauglitz, R. Abuknesha, and G. Ismail. Determination of simazine in water samples by waveguide surface plasmon resonance. *Anal. Chimica Acta*, 338:109–117, 1997.

[20] Hyeon-Su Ro, Sun Ok Jung, Byung Hoon Kho, Hyung Pyo Hong, Jae Sung Lee, Yong-Beom Shin, Min Gon Kim, and Bong Hyun Chung. Surface plasmon resonance imaging-based protein array chip system for monitoring a hexahistidine-tagged protein during expression and purification. *Applied and Enviromental Microbiology*, 71:1089–1092, 2005.

[21] R. G. Heideman, R. P. H. Kooyman, and J. Greve. Performance of a highly sensitive optical waveguide Mach-Zehnder interferometer immunosensor. *Sensors and Actuators B*, 10:209–217, 1993.

[22] A. Brandenburg and R. Henninger. Integrated optical Young interferometer. *Applied Optics*, 33:5941–5947, 1994.

[23] Bernard H. Schneider, John G. Edwards, and Nile F. Hartman. Hartman interferometer: versatile integrated optic sensor for label-free, real-time quantification of nucleic acids, proteins, and pathogens. *Clinical Chemistry*, 43:1757–1763, 1997.

[24] Aurel Ymeti, Johannes S. Kanger, Jan Greve, Paul V. Lambeck, Robert Wijn, and Rene G. Heideman. Realization of a multichannel integrated Young interferometer chemical sensor. *Applied Optics*, 42:5649–5660, 2003.

[25] Victor S.-Y. Lin, Kianoush Motesharei, Keiki-Pua S. Dancil, Michael J. Sailor, and M. Reza Ghadiri. A porous silicon-based optical interferometric biosensor. *Science*, 278:840–843, 1997.

[26] H.J. Watts, C.R. Lowe, and D.V. Pollard-Knight. Optical biosensor for monitoring microbial cells. *Anal. Chem*, 66:2465–2470, 1994.

[27] Nicholas J. Goddard, Kirat Singh, Richard J. Holmes, and Behnam Bastani. Resonant grating sensors using frustrated total-internal reflection. *Sensors and Actuators B*, 51:131–136, 1998.

[28] N. Skivesen, R. Horvath, S. Thinggaard, N.B. Larsen, and H.C. Pedersen. Deep-probe metal-clad waveguide biosensors. *Biosensors and Bioelectronics*, 22:1282–1288, 2007.

[29] Robert Horvath, Henrik C. Pedersen, and Niels B. Larsen. Demonstration of reverse symmetry waveguide sensing in aqueous solutions. *Appl. Phys. Lett.*, 81:2166–2168, 2002.

[30] Andrea M. Armani, Rajan P. Kulkarni, Scott E. Fraser, Richard C. Flagan, and Kerry J. Vahala. Label-free, single-molecule detection with optical microcavities. *Science*, 317:783–787, 2007.

[31] A. Serpenguzel, S. Arnold, and G. Griffel. Excitation of resonances of microspheres on an optical fiber. *Optics Letters*, 20:654–656, 1995.

[32] Hongying Zhu, Jonathan D. Suter, Ian M. White, and Xudong Fan. Aptamer based microsphere biosensor for thrombin detection. *Sensors*, 6:785–795, 2006.

[33] Alan D. Kersey, Michael A. Davis, Heather J. Patrick, Michel LeBlanc, K. P. Koo, *Member, IEEE*, C. G. Askins, M. A. Putnam, and E. Joseph Friebele. Fiber grating sensors. *J. Lightwave Technol.*, 15:1442–1463, 1997.

[34] Kerstin Schroeder, Wolfgang Ecke, Rudolf Mueller, Reinhardt Willsch, and Andrey Andreev. A fibre Bragg grating refractometer. *Meas. Sci. Technol.*, 12:757, 2001.

[35] Wei Liang, Yanyi Huang, Yong Xu, Reginald K. Lee, and Amnon Yariv. Highly sensitive fiber Bragg grating refractive index sensors. *Applied Physics Lett.*, 86:151122–1 – 151122–3, 2005.

[36] Severine Maguis, Guillaume Laffont, Pierre Ferdinand, Benjamin Carbonnier, Khemara Kham, Tahar Mekhalif, and Marie-Claude Millot. Biofunctionalized tilted fiber Bragg gratings for label-free immunosensing. *Optics Express*, 16:19049–19062, 2008.

[37] S. A. Vasiliev, E. M. Dianov, D. Varelas, H. G. Limberger, and R. P. Salathe. Postfabrication resonance peak positioning of long-period cladding-mode-coupled gratings. *Optics Letters*, 21:1830–1832, 1996.

[38] Jaw-Luen Tang and Jien-Neng Wang. Chemical sensing sensitivity of long-period grating sensor enhanced by colloidal gold nanoparticles. *Sensors*, 8:171–184, 2008.

[39] Lars Rindorf and Ole Bang. Highly sensitive refractometer with a photonic crystal fiber long-period grating. *Optics Letters*, 33:563–565, 2008.

[40] Lars Rindorf, Jesper B. Jensen, Martin Dufva, Lars Hagsholm, Pedersen, Poul Erik Hoiby, and Ole Bang. Photonic crystal fiber long-period gratings for biochemical sensing. *Optics Express*, 14:8224–8231, 2006.

[41] Philip Russell. Photonic crystal fibers. *Science*, 299:358–362, 2003.

[42] Federica Poli, Annamaria Cucinotta, and Stefano Selleri. Photonic crystal fibers, properties and applications. *Springer-Verlag New York Inc.*, 2007.

[43] Limin Tong, Rafael R. Gattass, Jonathan B. Ashcom, Sailing He, Jingyi Lou, Mengyan Shen, Iva Maxwell, and Eric Mazur. Subwavelength-diameter silica wires for low-loss optical wave guiding. *Nature*, 426:816–819, 2003.

[44] Hidehisa Tazawa, Tomohiko Kanie, and Makoto Katayama. Fiber-optic coupler based refractive index sensor and its application to biosensing. *Applied Physics*, 91:113901–1 – 113901–3, 2007.

[45] J. Topol'ancik P. Bhattacharya, J. Sabarinathan, and P.-C. Yu. Fluid detection with photonic crystal-based multichannel waveguides. *Applied Physics Lett.*, 82:1143–1145, 2003.

[46] Marko Loncar, Axel Scherer, and Yueming Qiu. Photonic crystal laser sources for chemical detection. *Applied Physics Lett.*, 82:4648–4650, 2003.

[47] T. G. Euser, J. S. Y. Chen, M. Scharrer, P. St. J. Russell, N. J. Farrer, and P. J. Sadler. Quantitative broadband chemical sensing in air-suspended solid-core fibers. *J. App. Physics*, 103:103108–1 – 103108–3, 2008.

[48] Chao Shi, Chao Lu, Claire Gu, Lei Tian, Rebecca Newhouse, Shaowei Chen, and Jin Z. Zhang. Inner wall coated hollow core waveguide sensor based on double substrate surface enhanced Raman scattering. *Applied Physics Lett.*, 93:153101–1 – 153101–3, 2008.

[49] Daniel Colladon. On the reflections of a ray of light inside a parabolic liquid stream. *Comptes Rendus*, 15:800–802, 1842.

[50] John Tyndall. Notes of a course of nine lectures on light. 1870.

[51] Jeff Hecht. Illuminating the origin of light guiding. *Optics and Photonics News*, pages 26–30, 1999.

[52] John M. Dudley, Goery Genty, and Stephane Coen. Supercontinuum generation in photonic crystal fiber. *Reviews of Modern Physics*, 78:1135–1184, 2006.

[53] T. Schreiber, J. Limpert, H. Zellmer, A. Tunnermann, and K.P. Hansen. High average power supercontinuum generation in photonic crystal fibers. *Optics Communications*, 228:71–78, 2003.

[54] A. S. Webb, F. Poletti, D. J. Richardson, and J. K. Sahu. Suspended-core holey fiber for evanescent-field sensing. *OE Letters*, 46:010503–1 – 010503–3, 2006.

[55] Tanya M. Monro, Stephen Warren-Smith, Erik P. Schartner, Alexandre Francois, Sabrina Heng, Heike Ebendorff-Heidepriem, and Shahraam Afshar V. Sensing with suspended-core optical fibers. *Optical Fiber Technology*, 16:343–356, 2010.

[56] P. Di Vita, V. Lisi, M. Giaconi, and G. Vespasiano. Fibre ottiche per telecomunicazioni: propagazione. *Notiziario Tecnico SIP*, 2:11–25, 1993.

[57] URL: `http://www.corning.com/opticalfiber/products/SMF-28e+_fiber.aspx`.

[58] S. Selleri, E. Coscelli, M. Sozzi, A. Cucinotta, F. Poli, and D. Passaro. Air-suspended solid-core fibers for sensing. In *Proc. of SPIE - Optical Sensors 2009*, pages 7356–61, 2009.

[59] URL: `http://www.nktphotonics.com/nonlinearfibers`.

[60] Enrico Coscelli, Federica Poli, Thomas T. Alkeskjold, Davide Passaro, Annamaria Cucinotta, Lasse Leick, Jes Broeng, and Stefano Selleri. Single-mode analysis of yb-doped double-cladding distributed spectral filtering photonic crystal fibers. *Optics Express*, 18:27197–27204, 2010.

[61] Niels A. Mortensen, Jacob R. Folkenberg, Martin D. Nielsen, and Kim P. Hansen. Modal cutoff and the v parameter in photonic crystal fibers. *Optics Letters*, 28:1879–1881, 2003.

[62] Martin D. Nielsen and Niels A. Mortensen. Photonic crystal fiber design based on the V-parameter. *Optics Express*, 11:2762–2768, 2003.

[63] *Member, IEEE* Philip St.J. Russell. Photonic-crystal fibers. *J. Lightwave Technol.*, 24:4729–4749, 2006.

[64] P. J. Roberts, F. Couny, H. Sabert, B. J. Mangan, T. A. Birks, J. C. Knight, and P. St. J. Russell. Loss in solid-core photonic crystal fibers due to interface roughness scattering. *Optics Express*, 13:7779–7793, 2005.

[65] P. J. Roberts, F. Couny, H. Sabert, B. J. Mangan, D. P. Williams, L. Farr, M. W. Mason, A. Tomlinson, T. A. Birks, J. C. Knight, and P. St.J. Russell. Ultimate low loss of hollow-core photonic crystal fibres. *Optics Express*, 13:236–244, 2005.

[66] Enrico Coscelli, Federica Poli, Davide Passaro, Annamaria Cucinotta, Stefano Selleri, Christina B. Olausson, Lasse Leick, and Jes Broeng. Bending-induced single-mode behaviour of a polarizing double-clad yb-doped photonic crystal fiber. In *European Conference on Optical Communication - ECOC2010*, 2010.

[67] K. O. Hill, Y. Fujii, D. C. Johnson, and B. S. Kawasak. Photosensitivity in optical fiber waveguides: Application to reflection filter fabrication. *Appl. Phys. Lett.*, 32:647–649, 1978.

[68] Andreas Othonos. Fiber Bragg gratings. *Rev. Sci. Instrum.*, 68:4309–4341, 1997.

[69] G. Meltz, W. W. Morey, and W. H. Glenn. Formation of Bragg gratings in optical fibers by a transverse holographic method. *Optics Letters*, 14:823–825, 1989.

[70] D. P. Hand and P. St. J. Russell. Single-mode fibre grating written into sagnac loop using photosensitive fibre: transmission filters. In *7th International Conference of Integrated Optics and Optical Fiber Communication*, 1989.

[71] R. M. Atkins, V. Mizrahi, and T. Erdogan. 248 nm induced vacuum UV spectral changes in optical fibre preform cores: support for a colour centre model of photosensitivity. *Elect. Lett.*, 29:385–387, 1993.

[72] R. A. B. Devine and C. Fiori. Defect creation and photoablation in stoichiometric and sub-stoichiometric SiO_2. In *Mat. Res. Soc. Symp. Proc.*, 1986.

[73] F. Bilodeau, B. Malo, J. Albert, D. C. Johnson, K. 0. Hill, Y. Hibino, M. Abe, and M. Kawachi. Photosensitization of optical fiber and silica-on-silicon/silica waveguide. *Optics Letters*, 18:953–955, 1993.

[74] D. L. Williams, B. J. Ainslie, J. R. Armitage, R. Kashyap, and R. Campbell. Enhanced uv photosensitivity in boron codoped germanosilicate fibres. *Elect. Lett.*, 29:45–47, 1993.

[75] J. Albert, B. Malo, F. Bilodeau, D. C. Johnson, K. 0. Hill, Y. Hibino, and M. Kawachi. Photosensitivity in ge-doped silica optical waveguides and fibers with 193-nm light from an ArF excimer laser. *Optics Letters*, 19:387–389, 1994.

[76] Scott M. Norton, Turan Erdogan, and G. Michael Morris. Coupled-mode theory of resonant-grating filters. *J. Opt. Soc. Am. A*, 14:629–639, 1997.

[77] Turan Erdogan. Cladding-mode resonances in short- and long-period fiber grating filters. *J. Opt. Soc. Am. A*, 14:1760–1773, 1997.

[78] Benjamin J. Eggleton, Peter A. Krug, L. Poladian, K. A. Ahmed, and H.-F. Liu. Experimental demonstration of compression of dispersed optical pulses by reflection from self-chirped optical fiber Bragg grating. *Optics Letters*, 19:877–879, 1994.

[79] B. Malo, D. C. Johnson, F. Bilodeau, J. Albert, and K. 0. Hill. Single-excimer-pulse writing of fiber gratings by use of a zero-order nulled phase mask: grating spectral response and visualization of index perturbation. *Optics Letters*, 18:1277–1279, 1993.

[80] Michalis Livitziis and Stavros Pissadakis. Bragg grating recording in low-defect optical fibers using ultraviolet femtosecond radiation and a double-phase mask interferometer. *Optics Letters*, 33:1449–1451, 2008.

[81] B. Malo, K. 0. Hill, F. Bilodeau, D. C. Johnson, and J. Albert. Point-by-point fabrication of micro-Bragg gratings in photosensitive fibre using single excimer pulse refractive index modification techniques. *Elect. Lett.*, 29:1668–1669, 1993.

[82] S.J. Mihailov and M.C. Gower. Recording of efficient high-order Bragg reflectors in optical fibres by mask image projection and single pulse exposure with an excimer laser. *Elect. Lett.*, 30:707–709, 1994.

[83] Stephen W. James and Ralph P. Tatam. Optical fibre long-period grating sensors: characteristics and application. *Meas. Sci. Technol.*, 14:49–61, 2003.

[84] Alexey I. Kalachev, David N. Nikogosyan, and Gilberto Brambilla. Long-period fiber grating fabrication by high-intensity femtosecond pulses at 211 nm. *J. Light. Tech.*, 23:2568, 2005.

[85] K.P. Chen, P.R. Herman, R. Tam, and J . Zhang. Rapid long-period grating formation in hydrogen-loaded fibre with 157 nm F_2-laser radiation. *Elect. Lett.*, 36:2000–2001, 2000.

[86] L. Drozin, P.-Y. Fonjallaz, and L. Stensland. Long-period fibre gratings written by CO_2 exposure of H_2-loaded, standard fibre. *Elect. Lett.*, 36:742–743, 2000.

[87] Georges Humbert and Abdelrafik Malki. Electric-arc-induced gratings in non-hydrogenated fibres: fabrication and high-temperature characterization. *J. Opt. A: Pure Appl. Opt*, 4:194–198, 2002.

[88] Xiaojun Zhou, Shenghui Shi, Zhiyao Zhang, Jun Zou, and Yong Liu. Mechanically-induced π-shifted long-period fiber gratings. *Optics Express*, 19:6253–6259, 2011.

[89] Stavros Pissadakis, Michalis Livitziis, Georgios D. Tsibidis, Jens Kobelke, and Kay Schuster. Type IIA grating inscription in a highly nonlinear microstructured optical fiber. *Photonics Technology Letters*, 21:227–229, 2009.

[90] Nathaniel Groothoff and John Canning. Enhanced type IIA gratings for high-temperature operation. *Optics Letters*, 29:2360–2362, 2004.

[91] Y.F. Zhang, C.C. Chan, Y.M. Chan, and P. Zu. Tilted long period gratings pressure sesnsing in solid core photonic crystal fibers. *IEEE Sensors Journal*, DOI: 10.1109/JSEN.2011.2162945, 2011.

[92] Toru Mizunami, Hideo Kawashima, and Akihiko Hayashi. A flexible fabrication technique of long-period fiber gratings using a tilted amplitude mask. In *Proceedings of 2002 IEEE/LEOS Workshop on Fibre and Optical Passive Components, 2002.*, 2002.

[93] Ming Yan, Shouyu Luo, Li Zhan, Yilei Wang, Yuxing Xia, and Zhiming Zhang. Step-changed period chirped long-period fiber gratings fabricated by CO_2 laser. *Optics Communication*, 28:2784–2788, 2008.

[94] I. M. Jauncey, L. Reekie, R. J. Mears, and C. J. Rowe. Narrow-linewidth fiber laser operating at 1.55 μm. *Optics Letters*, 12:164–165, 1987.

[95] Andreas Othonos, Xavier Lee, and Din Ping Tsai. Spectrally broadband Bragg grating mirror for an erbium-doped fiber laser. *Opt. Eng.*, 35:1088–1092, 1996.

[96] Athanasios N. Chryssis, Sang M. Lee, Sang B. Lee, *Member, IEEE* Simarjeet S. Saini, and *Senior Member, IEEE* Mario Dagenais. High sensitivity evanescent field fiber Bragg grating sensor. *IEEE Photonics Tech. Lett.*, 17:1253–1255, 2005.

[97] *Member, IEEE* Geunmin Ryu, *Senior Member, IEEE* Mario Dagenais, Matthew T. Hurley, and Philip DeShong. High specificity binding of lectins to carbohydrate-functionalized fiber Bragg gratings: A new model for biosensing application. *IEEE J. Select. Topic Quantum Elect.*, 16:647–653, 2010.

[98] Ashish M. Vengsarkar, Paul J. Lemaire, Justin B. Judkins, Vikram Bhatia, Turan Erdogan, and John E. Sipe. Long-period fiber gratings as band-rejection filters. *J. Light. Tech.*, 14:58–65, 1996.

[99] Mini Das and K. Thyagarajan. Dispersion compensation in transmission using uniform long period fiber gratings. *Optics Communications*, 190:159–163, 2001.

[100] Mini Das and K. Thyagarajan. Wavelength-division multiplexing isolation filter using concatenated chirped long period gratings. *Optics Communications*, 197:67–71, 2001.

[101] Xianfeng Chen, Lin Zhang, Kaiming Zhou, Edward Davies, Kate Sugden, Ian Bennion, Marcus Hughes, and Anna Hine. Real-time detection of DNA interactions with longperiod fiber-grating-based biosensor. *Optics Letters*, 32:2541–2543, 2007.

[102] Matthew P. DeLisa, Zheng Zhang, Mira Shiloach, Saeed Pilevar, Christopher C. Davis, James S. Sirkis, and William E. Bentley. Evanescent wave long-period fiber bragg grating as an immobilized antybody biosensor. *Anal. Chem.*, 72:2895–2900, 2000.

[103] J. D. Watson and F. H. C. Crick. Molecular structure of nucleic acids: A structure for deoxyribose nucleic acid. *Nature*, 171:737–738, 1953.

[104] Peter J. Russell. Essential igenetics. *Pearson Education, Inc.*, 2003.

[105] J. D. Watson, T. A. Baker, S. P. Bell, A. Gann, M. Levine, and R. Losick. Molecular biology of the gene. *Pearson Education, Inc.*, 2004.

[106] P. E. Nielsen. Peptide nucleic acids: Protocols and applications. *Copenhagen, Denmark: Horizon Bioscience*, 2004.

[107] P. E. Nielsen. Peptide nucleic acid: A versatile tool in genetic diagnostics and molecular biology. *Curr. Opin. Biotechnol.*, 12:16–20, 2001.

[108] J. Cordek, X. Wang, and W. Tan. Direct immobilization of glutamate dehydrogenase on optical fiber probes for ultrasensitive glutamate detection. *Anal. Chem.*, 71:1529–1533, 1999.

[109] Monika S. Rutowska, Fatima C. Garcia Gunning, Francine Kivlehan, Eric Moore, Des Brennan, Paul Galvin, and Andrew D. Ellis. Integration of a 3D hydrogel matrix within a hollow core photonic crystal fibre for DNA probe immobilization. *Meas. Sci. Technol.*, 21:094016, 2010.

[110] S. Pissadakis, A. Ikiades, P. Hua, A. Sheridan, and J. Wilkinson. Photosensitivity of ion-exchanged Er-doped phosphate glass using 248 *nm* excimer laser radiation. *Opt. Express*, 14:3131–3136, 2004.

[111] S. Yliniemi, S. Honkanen, A. Ianoul, A. Laronche, and J. Albert. Photosensitivity and volume gratings in phosphate glasses for rare-earth-doped ion-exchanged optical waveguide lasers. *J. Opt. Soc. Am. B*, 23:2470–2478, 2006.

[112] C. Pappas and S. Pissadakis. Periodic nanostructuring of Er/Yb-codoped IOG1 phosphate glass by using ultraviolet laser-assisted selective chemical etching. *J. Appl. Phys.*, 100:114308, 2006.

[113] J. W. Chan, T. R. Huser, S. H. Risbud, J. S. Hayden, and D. M. Krol. Waveguide fabrication in phosphate glasses using femtosecond laser pulses. *Appl. Phys. Lett.*, 85:2371–2373, 2003.

[114] B. C. Hwang, S. Jiang, T. Luo, J. Watson, S. Honkanen, Y. Hu, F. Smektala, J. Lucas, and N. Peyghambarian. Erbium-doped phosphate glass fibre amplifiers with gain per unit length of 2.1 dB/cm. *Electron. Lett.*, 35:1007–1009, 1999.

[115] J. E. Shelby. *Introduction to Glass Science and Technology*. 2004.

[116] I. Michelakaki and S. Pissadakis. Atypical behaviour of the surface hardness and the elastic modulus of a phosphate glass matrix under 193 *nm* laser irradiation. *Appl. Phys., A Mater. Sci. Process.*, 95:453–456, 2009.

[117] J. Canning, M. G. Sceats, H. G. Inglis, and P. Hill. Transient and permanent gratings in phosphosilicate optical fibers produced by the flash condensation technique. *Opt. Lett.*, 20:2189–2191, 1995.

[118] J. Albert, A. Schulzgen, V. L. Temyanko, S. Honkanen, and N. Peyghambarian. Strong Bragg gratings in phosphate glass single mode fiber. *Appl. Phys. Lett.*, 89:101127, 2006.

[119] D. Grobnic, S. J. Mihailov, R. B. Walker, C. W. Smelser, C. Lafond, and A. Croteau. Bragg gratings made with a femtosecond laser in heavily doped Er-Yb phosphate glass fiber. *IEEE Photon. Technol. Lett.*, 19:943–945, 2007.

[120] M. Bernier, D. Faucher, R. Vallee, A. Saliminia, G. Androz, Y. Sheng, and S. L. Chin. Bragg gratings photoinduced in ZBLAN fibers by femtosecond pulses at 800 *nm*. *Opt. Lett.*, 32:454–456, 2007.

[121] J. Canning. Fibre gratings and devices for sensors and lasers. *Lasers Photonics Rev.*, 4:275–289, 2008.

[122] R. Matei Rogojan, A. Schulzgen, N. Peyghambarian, A. Laronche, and J. Albert. Photo-thermal gratings in Er^{3+}/Yb^{3+}-doped core phosphate glass single mode fibers. *Bragg Gratings, Photosensitivity, and Poling in Glass Waveguides*, OSA Technical Digest (Optical Society of America):paper BTuC3, 2007.

[123] S. Pissadakis and I. Michelakaki. Photosensitivity of the Er/Yb-codoped schott IOG1 phosphate glass using 248 *nm*, femtosecond and picosecond laser radiation. *Laser Chem.*, 2008:868767, 2008.

[124] D. B. Marshall, T. Noma, and A. G. Evans. A simple method for determining elastic-modulus-to-hardness ratios using knoop indentation technique. *J. Am. Ceram. Soc.*, 65:c175–c176, 1982.

[125] D. Ehrt, P. Ebeling, and U. Natura. UV transmission and radiation-induced defects in phosphate and fluoridephosphate glasses. *J. Non-Cryst. Solids*, 263-264:240–250, 2000.

[126] N. H. Ky, H. G. Limberger, R. P. Salathe, F. Cochet, and L. Dong. UV-irradiation induced stress and index changes during the growth of type-I and type-IIA fiber gratings. *Opt. Commun.*, 225:313–318, 2003.

[127] R. Aashia, K. V. Madhav, U. Ramamurty, and S. Asokan. Nanoindentation study on germania-doped silica glass preforms: evidence for the compaction-densification model of photosensitivity. *Opt. Lett.*, 34:2414–2416, 2009.

[128] Kevin H. Smith, Benjamin L. Ipson, Tyson L. Lowder, Aaron R. Hawkins, Richard H. Selfridge, and Stephen M. Schultz. Surface-relief fiber Bragg gratings for sensing applications. *Applied Optics*, 45:1669–1675, 2006.

[129] T. L. Lowder, K. H. Smith, B. L. Ipson, A. R. Hawkins, R. H. Selfridge, and S. M. Schultz. High-temperature sensing using surface relief fiber Bragg gratings. *IEEE Photonics Technology Letters*, 17:1926 – 1928, 2005.

[130] K. Zimmer and R. Bohme. Laser-induced backside wet etching of transparent materials with organic and metallic absorbers. *Laser Chemistry*, 2008:1–13, 2008.

[131] R. Bohme, D. Hirsch, and K. Zimmer. Laser etching of transparent materials at a backside surface adsorbed layer. *Applied Surface Science*, 252:4763–4767, 2006.

[132] R. Bohme and K. Zimmer. Low roughness laser etching of fused silica using an adsorbed layer. *Applied Surface Science*, 239:109–116, 2004.

[133] T. Smausz, T. Csizmadi, N. Kresz, Cs. Vass, Zs. Márton, and B. Hopp. Influence on the laser induced backside dry etching of thickness and material of the absorber, laser spot size and multipulse irradiation. *Applied Surface Science*, 254:1091–1095, 2007.

[134] M. N. Petrovich, A. van Brakel, F. Poletti, K. Mukasa, E. Austin, V. Finazzi, P. Petropoulos, E. O'Driscoll, M. Watson, T. DelMonte, T. M. Monro, J. P. Dakin, and D. J. Richardson. Microstructured fibres for sensing applications. *Proc. SPIE 6005*, Photonic Crystals and Photonic Crystal Fibers for Sensing Applications, 2005.

[135] D. Passaro, M. Foroni, F. Poli, A. Cucinotta, S. Selleri, J. Laesgaard, and A. O. Bjarklev. All-silica hollow-core microstructured Bragg fibers for biosensor application. *IEEE Sens. J.*, 8:1280–1286, 2008.

[136] F. M. Cox, A. Argyros, and M. C. J. Large. Liquid-filled hollow core microstructured polymer optical fiber. *Opt. Exp.*, 14:4135–4140, 2006.

[137] S. Smolka, M. Barth, and O. Benson. Highly efficient fluorescence sensing with hollow core photonic crystal fibers. *Opt. Exp.*, 15:12783–12791, 2007.

[138] F. M. Cox, R. Lwin, M. C. J. Large, and C. M. B. Cordeiro. Opening up optical fibres. *Opt. Exp.*, 15:11843–11848, 2007.

[139] Y. Han, D. Mayer, A. Offenhauser, and S. Ingebrandt. Surface activation of thin silicon oxides by wet cleaning and silanization. *Thin Solid Films*, 510:175–180, 2006.

[140] J. B. Jensen, G. Emiliyanov, O. Bang, P. E. Hoiby, L. H. Pedersen, T. P. Hansen, K. Nielsen, and A. Bjarklev. Microstructured polymer optical fiber biosensor for detection of DNA and antibodies. *OFS 2006*, OSA Tech. Dig.:23–27, Paper ThA2, 2006.

[141] R. D'Agata, R. Corradini, G. Grasso, R. Marchelli, and G. Spoto. Ultrasensitive detection of DNA by PNA and nanoparticle-enhanced surface plasmon resonance imaging. *Chem. Biochem.*, 9:2067–2070, 2008.

[142] P. Childs, A. C. L. Wong, I. Leung, G. D. Peng, and Y. B. Liao. An in-line in-fibre ring cavity sensor for localized multi-parameter sensing. *Meas. Sci. Technol.*, 19:065302, 2009.

[143] P. Childs and A. Candianiand S. Pissadakis. Optical fiber cladding ring magnetic field sensor. *IEEE Photonics Technology Letters*, 23:929 – 931, 2011.

[144] URL: `https://github.com/pchilds/Harmonic`.

[145] H. J. Patrick and A. D. Kerseyand F. Bucholtz. Analysis of the response of long period fiber gratings to external index of refraction. *J. Lightwav. Technol.*, 16:1606–1612, 1998.

[146] W. Liang, Y. Huang, Y. Xu, R. K. Lee, and A. Yariv. Highly sensitive fiber Bragg grating refractive index sensors. *Applied Physics Letters*, 86:151122, 2005.

[147] J.-L. Tang, T.-Y. Chiang, H.-P. Chang, and J.-N. Wang. Long-period grating-based sensor for chemical sensing applications. *Conference on Lasers and Electro-Optics, CLEO Pacific Rim 2005*, pages 975–976, 2005.

[148] Tian-Hao Xia, A. Ping Zhang, Bobo Gu, and Jing-Jing Zhu. Fiber-optic refractive-index sensors based on transmissive and reflective thin-core fiber modal interferometers. *Optics Communications*, 253:2136–2139, 2010.

[149] R. Jha, J. Villatoro, and G. Badenes. Ultrastable in reflection photonic crystal fiber modal interferometer for accurate refractive index sensing. *Applied Physics Letters*, 93:191106 – 191106–3, 2008.

[150] Y. J. Rao, M. Deng, D. W. Duan, and T. Zhu. In-line fiber Fabry-Perot refractive-index tip sensor based on endlessly photonic crystal fiber. *Sensors and Actuators A: Physical*, 148:33–38, 2008.

Acknowledgements

And now a few simple words to thank all the people that surrounded me during these years.
I'd like to start with my family, Mom, Dad, my brother Tommaso, that always supported me in what I've done, from Bachelor, through Master, and now with PhD. I also would like to spend a few words for my 94 years old (soon 95) Granpa, thanks to be still here.
Then I'd like to thank my two supervisors Prof. Stefano Selleri and Dr. Annamaria Cucinotta for the support they gave to my work during all this period. All my co-workers here in the lab at the University of Parma, Fede, Enrico, Ale, and Davide for the support and the help they gave me in the lab, mainly when results seemed to be miserables.
I'd like to thank Dr. Stavros Pissadakis and Dr. Mary Konstantaki that supervised my work at the photonics and material devices lab at the FORTH institute in Greece. Also my co-worker there, Ale (double thank), Jan Vanda (I'm still waiting your becherovka), and Aashia Rhaman (thanks for all the indian food recipes). And also thanks to Sir Apostolis Eglezis, laser technician at FORTH, to whom I owe a lot of USD for his help with excimer lasers, and together with him to Claudia, it was nice to travel through Crete with both of you.
Then I'd like to thank all my closest friends with whom I shared, and I'm still sharing many nice moments, travels, and adventures: Gigi, Aschio, Zilio&Marty, Pasce, Pucci, Lucio, Ba, Alessia, Zucco, Luca, Robbi, (S)Pam, Cirro, Gringo, e Faz. Thanks a lot guys.

A thanks to a special friend from Poland, thanks Aleksandra for your remote support and for being my tour guide in Poland, dziekuje bardzo Ola.
If I forgot someone I beg your pardon.